NUMERICAL SIMULATION OF MAGMATIC HYDROTHERMAL SYSTEMS

S. E. Ingebritsen,[1] S. Geiger,[2] S. Hurwitz,[1] and T. Driesner[3]

Received 16 March 2009; revised 7 July 2009; accepted 8 September 2009; published XX Month 2010.

[1] The dynamic behavior of magmatic hydrothermal systems entails coupled and nonlinear multiphase flow, heat and solute transport, and deformation in highly heterogeneous media. Thus, quantitative analysis of these systems depends mainly on numerical solution of coupled partial differential equations and complementary equations of state (EOS). The past 2 decades have seen steady growth of computational power and the development of numerical models that have eliminated or minimized the need for various simplifying assumptions. Considerable heuristic insight has been gained from process-oriented numerical modeling. Recent modeling efforts employing relatively complete EOS and accurate transport calculations have revealed dynamic behavior that was damped by linearized, less accurate models, including fluid property control of hydrothermal plume temperatures and three-dimensional geometries. Other recent modeling results have further elucidated the controlling role of permeability structure and revealed the potential for significant hydrothermally driven deformation. Key areas for future research include incorporation of accurate EOS for the complete H_2O-NaCl-CO_2 system, more realistic treatment of material heterogeneity in space and time, realistic description of large-scale relative permeability behavior, and intercode benchmarking comparisons.

Citation: Ingebritsen, S. E., S. Geiger, S. Hurwitz, and T. Driesner (2010), Numerical simulation of magmatic hydrothermal systems, *Rev. Geophys.*, *48*, XXXXXX, doi:10.1029/2009RG000287.

1. PURPOSE AND SCOPE

[2] This review emphasizes the application of numerical modeling to understand and quantify processes in magmatic hydrothermal systems. We assess the state of knowledge and describe advances that have emerged in the 2 decades since a similar review by *Lowell* [1991]. Though our ability to rigorously describe key hydrothermal processes is still imperfect, there have been substantial advances since *Lowell*'s [1991] review. These advances owe mainly to the steady growth of computational power and the concomitant development of numerical models that have gradually minimized various simplifying assumptions. They include incorporation of more accurate equations of state (EOS) for the fluid system, an increased ability to represent geometric complexity and heterogeneity, and faster and more accurate computational schemes. These advances have revealed dynamic behaviors that were entirely obscured in previous generations of models.

[3] For purposes of this paper we define "magmatic hydrothermal systems" as aqueous fluid systems that are influenced by magma bodies in the upper crust. We particularly emphasize multiphase, multicomponent phenomena, which can have both quantitative and qualitative effects on the behavior of hydrothermal systems [*Lu and Kieffer*, 2009]. Multiphase (liquid-vapor) hydrothermal phenomena of interest include phase separation at scales ranging from centimeters to kilometers, with concomitant geochemical effects; novel modes of heat transport such as boiling plumes and countercurrent liquid-vapor flow ("heat pipes") [*Hayba and Ingebritsen*, 1997]; profound retardation of pressure transmission [*Grant and Sorey*, 1979]; and boiling-related mineralization.

2. IMPORTANCE OF MAGMATIC HYDROTHERMAL SYSTEMS

[4] Magmatic hydrothermal systems have immense scientific and practical significance and have been the topic of many review papers [e.g., *Lister*, 1980; *Norton*, 1984; *Elderfield and Schultz*, 1996; *Kelley et al.*, 2002; *German and Von Damm*, 2003; *Pirajno and van Kranendonk*, 2005]. Nearly all of these reviews have focused on their essential physical, chemical, and biological characteristics. We will review those characteristics very briefly here, but

[1] U.S. Geological Survey, Menlo Park, California, USA.
[2] Institute of Petroleum Engineering, Heriot-Watt University, Edinburgh, UK.
[3] Institute of Isotope Geochemistry and Mineral Resources, ETH Zurich, Zurich, Switzerland.

8755-1209/10/2009RG000287$15.00
Paper number 2009RG000287

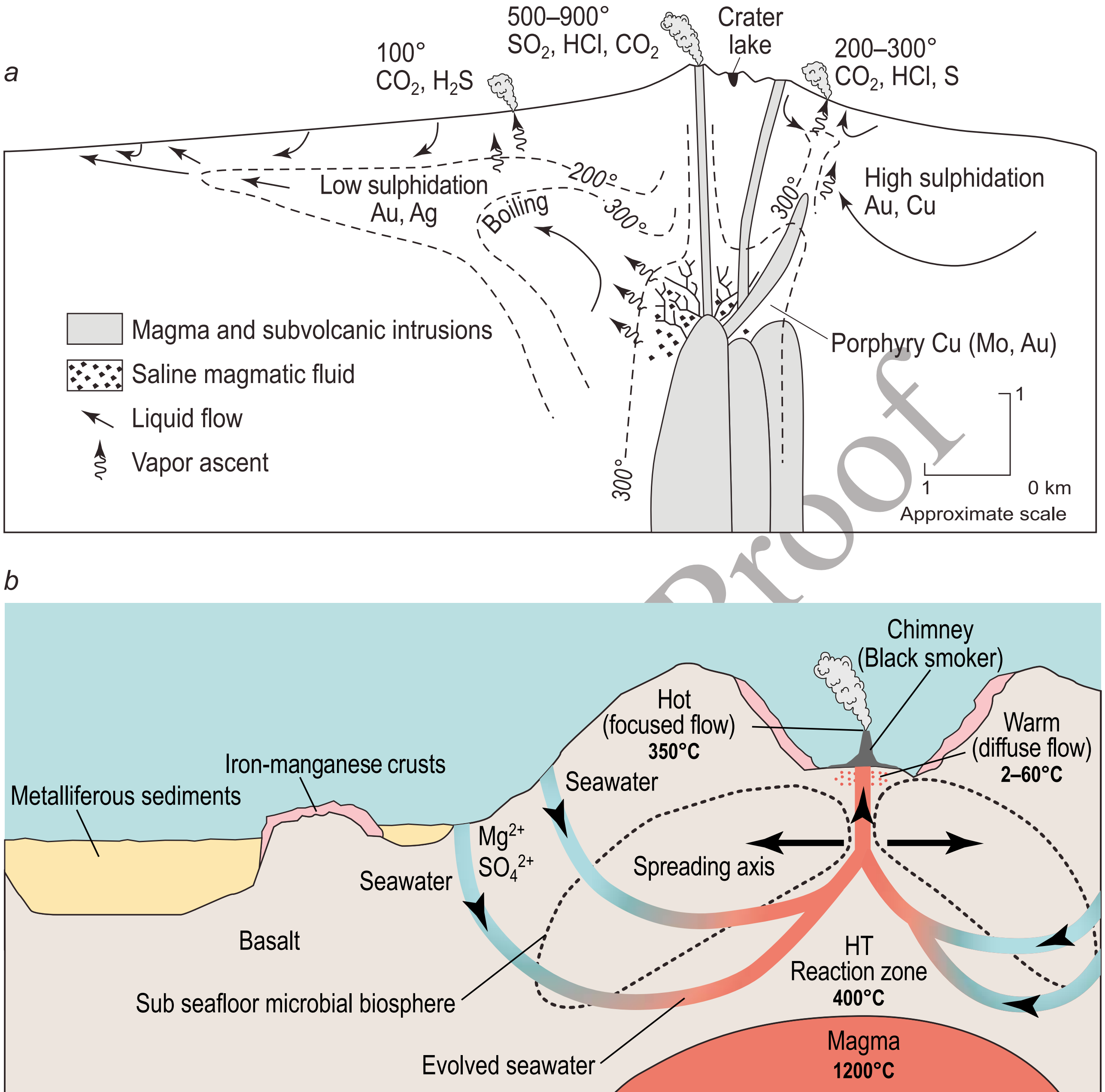

Figure 1. Conceptual models of (a) continental and (b) mid-ocean ridge (MOR) magmatic hydrothermal systems. Figure 1a after *Hedenquist and Lowenstern* [1994]. Note that on continents groundwater flow is mainly from topographic highs toward topographic lows, whereas in subsea environments flow is often from topographic lows toward topographic highs.

the remainder of this paper will focus specifically on quantitative analysis of magmatic hydrothermal systems and in particular the role of numerical modeling.

[5] Magmatic hydrothermal systems occur both on the continents, where they are concentrated near convergent plate boundaries, and on the ocean floor, where they are concentrated near the mid-ocean ridges (MOR) (Figure 1). Subsea hydrothermal activity near the MOR is critically important to the Earth's thermal budget and to global geochemical cycles. Heat flow studies consistently indicate that hydrothermal circulation near the MOR accounts for 20%–25% of the Earth's total heat loss [e.g., *Williams and Von Herzen*, 1974; *Sclater et al.*, 1980; *Stein and Stein*, 1994]. Without MOR hydrothermal sources and sinks of solutes, the oceans might be dominantly sodium bicarbonate with a pH near 10, rather than dominantly sodium chloride with a pH near 8 [*MacKenzie and Garrels*, 1966]. The discovery of MOR-associated ecosystems based on chemosynthetic bacteria [e.g., *Baross and Deming*, 1983; *Lutz and Kennish*, 1993] carries implications for the origins of life on Earth and other planetary bodies. Chemical energy, rather than solar (photosynthetic) energy, drives rich hydrothermal ecosystems with faunal biomass estimates that exceed even those for productive estuarine ecosystems.

[6] Magmatic hydrothermal systems on the continents are perhaps less fundamental to life on Earth than MOR hydrothermal systems and account for only ~1% of the Earth's heat loss [*Bodvarsson*, 1982]. However, they are of great interest because they are a primary source of economically important metals including copper, tungsten, tin, molybdenum, and gold [e.g., *Hedenquist and Lowenstern*, 1994; *Williams-Jones and Heinrich*, 2005]; constitute nearly all proven geothermal resources [e.g., *Muffler*, 1979; *Duffield and Sass*, 2004]; and, like MOR systems, support ecosystems that have only recently been discovered and begun to be understood [e.g., *Walker et al.*, 2005; *Windman et al.*, 2007]. Aqueous and gas-rich hydrothermal fluids in continental settings also contribute to volcanic hazards [*Newhall et al.*, 2001] by destabilizing volcanic edifices [*Lopez and Williams*, 1993; *Reid*, 2004], acting as propellant in steam-driven explosions [*Mastin*, 1991; *Germanovich and Lowell*, 1995; *Thiery and Mercury*, 2009], reducing effective stresses in mudflows [e.g., *Iverson*, 1997], and transporting potentially toxic gases [e.g., *Farrar et al.*, 1995; *Chiodini et al.*, 2007].

[7] From a conceptual point of view, continental (subaerial) and subsea hydrothermal systems differ in terms of their boundary conditions, permeability structures, and fluid properties. For instance, the expected upper boundary condition for flow in the shallow continental crust is a water table with some relief, often characterized as a subdued replica of the topography, so that flow in the shallow continental crust is mainly from topographic highs toward topographic lows (Figure 1a). Departures from this general pattern are due mainly to phase separation, magmatic heating, and magmatic volatile contributions (Figure 1a) or to fluid generation in relatively low permeability rocks [e.g., *Neuzil*, 1995]. In contrast, the upper boundary conditions for subsea circulation are the hydrostatic pressure and temperature at the ocean floor, and flow is often from topographic lows toward topographic highs, driven by density differences caused by magmatic heating (Figure 1b). Further, whereas on land sedimentary rocks are often more permeable than the underlying crystalline "basement," the oceanic crust is, in general, much more permeable than the overlying fine-grained oceanic sediments. Finally, the normal or expected circulating fluid in the upper continental crust is meteoric water, perhaps modified by the addition of salts or magmatic volatiles such as CO_2 (Figure 2, left), whereas the norm in a subsea environment is an H_2O-NaCl fluid (Figure 2, right) with salinity approximately that of seawater.

3. WHY NUMERICAL MODELING?

[8] Data from subaerial and subsea magmatic hydrothermal systems are typically sparse and expensive to acquire. Subaerial volcanoes are often remote, snow- and ice-covered, and steep. Access to active subseafloor volcanoes requires offshore drilling and dedicated submarine dives. In both environments, boreholes that penetrate deeply into magmatic hydrothermal systems and reach supercritical fluid conditions [e.g., *Doi et al.*, 1998; *Fridleifsson and Elders*, 2005] are rare and expensive, and extreme conditions (high temperatures and corrosive chemistry) in existing boreholes inhibit long-term data acquisition. Further, pertinent laboratory studies are rare and not fully representative. The spatial and temporal scales of natural hydrothermal systems exceed those that are experimentally accessible by orders of magnitude, and their typical pressure, temperature, and compositional ranges are difficult to deal with experimentally [e.g., *Elder*, 1967a; *Sondergeld and Turcotte*, 1977; *Menand et al.*, 2003; *Emmanuel and Berkowitz*, 2006, 2007].

[9] These hydrothermal systems are sufficiently complex that quantitative description of processes depends on coupled partial differential equations and complementary equations of state, equations that can be solved analytically only for a highly idealized set of boundary and initial conditions [e.g., *Pruess et al.*, 1987; *Woods*, 1999; *Bergins et al.*, 2005]. Thus, numerical simulation has played a pivotal role in elucidating the dynamic behavior of magmatic hydrothermal systems and for testing competing hypotheses in these complex, data-poor environments. To harness the power of this tool, modelers need to be aware of the assumptions they are invoking, the limitations of the numerical methods, and the range of plausible results that can be constrained by available data.

[10] The relevant theory includes equations of groundwater flow and descriptions of its couplings with heat transport, solute transport and reaction, and deformation. These couplings are inherently multiscale in nature; that is, their temporal and spatial scales vary by several orders of magnitude. Each of these couplings may be important to a given problem, potentially leading to emergent behavior that we cannot predict or quantify a priori.

[11] Let us consider hydrothermal circulation near MOR hydrothermal vents as an example. It is generally assumed that fluid flow is governed by some form of Darcy's law. Observed large gradients in salinity between MOR vents indicate active phase separation of modified seawater into a dense saline liquid and a buoyant vapor. Thus, we need to invoke a relatively complex, multiphase form of Darcy's law that might be written as

$$q_v = -\frac{k_{rv}k}{\mu_v}\left(\frac{\partial P}{\partial z} + \rho_v g\right) \quad (1)$$

$$q_l = -\frac{k_{rl}k}{\mu_l}\left(\frac{\partial P}{\partial z} + \rho_l g\right) \quad (2)$$

(volumetric flow rate equals fluid mobility multiplied by the driving force gradient) for a one-dimensional (vertical) flow of variable density water vapor (subscript v) and liquid water (subscript l), respectively (see the notation section for definitions of other parameters). There are large variations in salinity and temperature in MOR hydrothermal systems: ~0.1–7 wt % NaCl from venting salinities and up to >60 wt % NaCl from fluid inclusions and 2°C–400°C, respectively. These dictate that a realistic model of the system must account for material property variations as

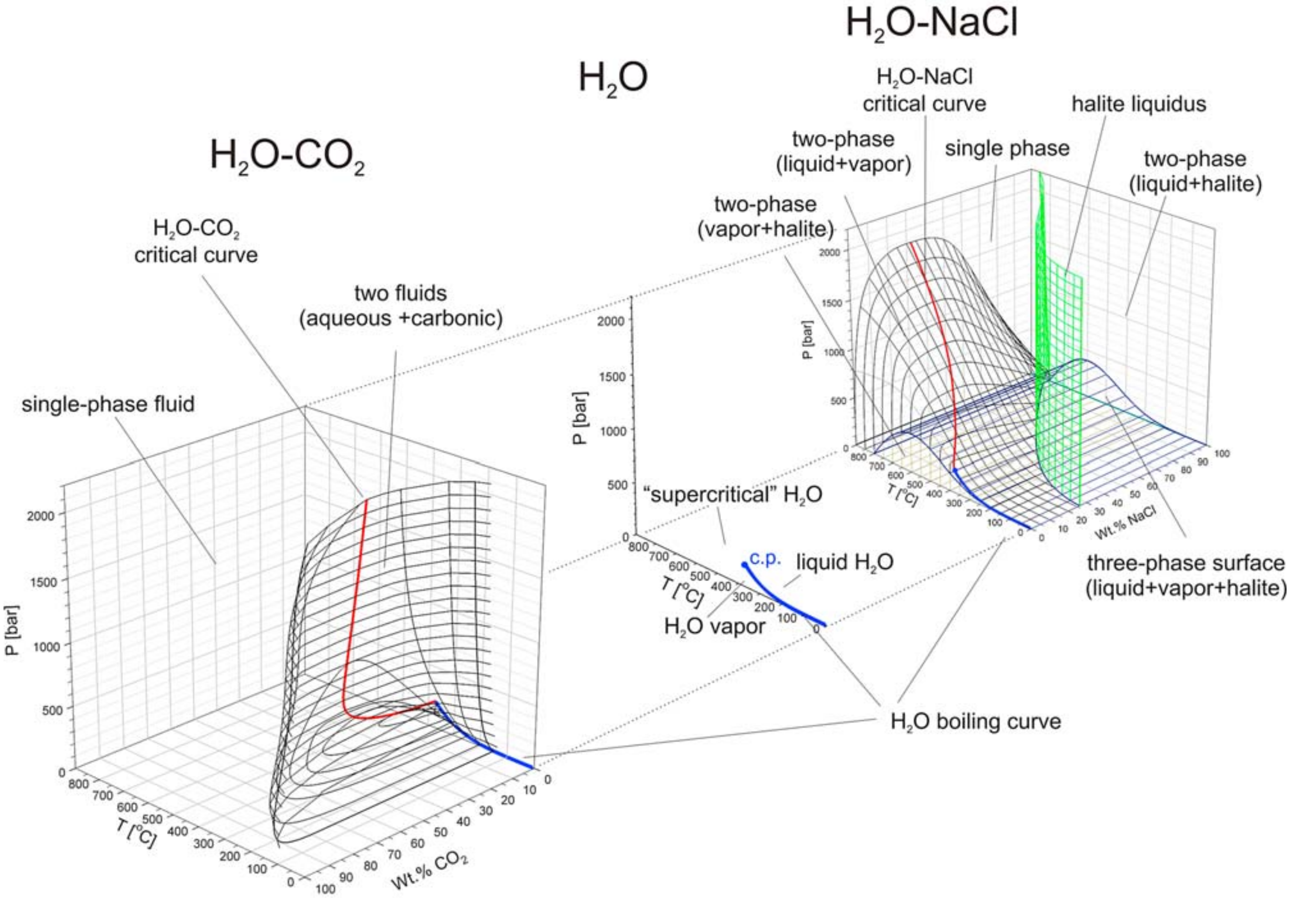

Figure 2. Phase diagrams for temperature-pressure-composition coordinates relevant to magmatic hydrothermal systems, showing relations between (middle) the pure H_2O system and the two most important binary systems, (left) H_2O-CO_2 and (right) H_2O-NaCl. The boiling curve of H_2O (blue) ends in the H_2O critical point (374°C, 220.6 bar) and separates liquid at high pressures from vapor at low pressures. At temperatures higher than the critical temperature, gradual transitions between liquid-like and vapor-like fluids occur as a response to changes in pressure. In the system H_2O-CO_2 (Figure 2, left), there is a large volume (rather than a single boiling curve) occupied by the coexistence region of an aqueous, liquid-like fluid with a carbonic fluid that may be vapor- or liquid-like, depending on pressure. This region closes toward higher temperatures, where only a single-phase fluid exists. In the system H_2O-NaCl (Figure 2, right), however, the region of two-phase liquid plus vapor coexistence becomes larger with increasing temperature. Magmatic hydrothermal systems may also encounter the vapor plus halite and liquid plus halite two-phase regions as well as the three-phase assemblage liquid plus vapor plus halite and liquid- or vapor-like single-phase fluids. H_2O diagram after *Haar et al.* [1984], H_2O-CO_2 after *Blencoe* [2004], and H_2O-NaCl after *Driesner and Heinrich* [2007].

functions of temperature, pressure, and composition and include heat transport, solute transport, and all phase relations between liquid, vapor, and salt. Further, we must anticipate that the flow systems are highly transient as the exceptionally high rates of heat discharge can only be explained as the result of rapid crystallization and cooling of large volumes of magma [e.g., *Lister*, 1974, 1983]. This implies that the intensity and spatial distribution of heat sources must vary with time. We would also expect that precipitation and dissolution of minerals cause continuous variations in porosity and permeability because the extreme variations in fluid composition and temperature make for a highly reactive chemical environment. As a result of these transient phenomena, deformation enters the picture: as permeability, flow rates, and temperatures wax and wane, rates of thermomechanical deformation are likely large enough to substantially affect permeability [*Germanovich and Lowell*, 1992]. MOR systems are also tectonically active, and faulting and fracturing will cause sudden changes in permeability. Tectonic plate movement away from the MOR itself (yet another mode of deformation) advects both fluid-saturated rock and heat. Finally, there may be mutual feedbacks between the fluid pressure and regional stress fields via fracture formation and/or reactivation.

[12] Although we can recognize the probable importance of each of these couplings we still do not know which

couplings affect the system behavior most and, almost invariably, neglect some of them in our analyses. Even the most sophisticated numerical model cannot yet fully describe MOR hydrothermal circulation or other complex, transient magmatic hydrothermal systems. We typically account, at most, for one or two of the couplings in each analysis, hoping to capture the essence of the system.

4. HISTORICAL DEVELOPMENT OF MODELING APPROACHES

[13] The earliest numerical modeling studies of hydrothermal flow in porous media were done circa 1960. They were aimed at determining the conditions for the onset of thermal convection and were motivated by efforts to understand the Wairakei geothermal system in the Taupo Volcanic Zone of New Zealand [*Wooding*, 1957; *Donaldson*, 1962]. They employed finite difference methods to solve fluid flow and heat transport equations posed in terms of dimensionless parameters for a two-dimensional domain with impermeable boundaries. They obtained approximate, steady state solutions, in which all partial time derivatives in the differential equations are equal to zero. These earliest studies also invoked the so-called "Boussinesq approximation," assuming that fluid density is constant except insofar as it affects the gravitational forces acting on the fluid. Thus, mass balance and volume balance are identical, and the velocity field is divergence-free, so that

$$\nabla \cdot q = 0, \tag{3}$$

where q is the volumetric flow rate per unit area. This particular simplification is still widely employed today (see section 6.7), though it can be significantly in error for cases of transient, variable density flow [e.g., *Furlong et al.*, 1991; *Hanson*, 1992; *Evans and Raffensperger*, 1992; *Jupp and Schultz*, 2000, 2004]. It allows convenient solution of the mathematical equations describing thermal convection via the stream function [*Slichter*, 1899; *de Josselin de Jong*, 1969], which can be contoured to represent fluid flow paths. The steady state approach and the stream function/Boussinesq approximation were adopted in the classic simulations of *Elder* [1967a], who compared numerical solutions with Hele-Shaw experiments, an analog for free convection in porous media. *Elder* [1967b] then modified the simulations to include transient effects in which temperature-dependent parameters changed with time.

[14] Work by *Norton and Knight* [1977] and *Cathles* [1977] represents the first significant numerical modeling study of fluid circulation near magma bodies. These pioneering studies, out of computational necessity, neglected every driving force for fluid flow except for lateral variations in fluid density, thereby forcing a convective pattern of fluid flow. They ignored or simplified two-phase (boiling) phenomena and assumed that fluid flow was quasi-steady over time. Nevertheless, they arrived at several important and robust conclusions that are consistent with the results of later, more sophisticated models. For instance, *Norton and Knight* [1977] showed that advective heat transport would be significant for host rock permeabilities $\geq 10^{-16}$ m^2 and demonstrated the feasibility of the large influxes of meteoric water indicated by oxygen isotope data [e.g., *Taylor*, 1971].

[15] Though many of the pioneering studies entailed high-temperature flow, they generally assumed a single-component (H_2O), single-phase fluid. The oil crisis of the 1970s led to a surge of interest in geothermal resources and simultaneous development of a handful of multiphase geothermal simulation tools [*Stanford Geothermal Program*, 1980]. Such simulators solve governing equations for steam-water two-phase flow, including boiling and condensation [e.g., *Faust and Mercer*, 1979a, 1979b; *Pruess et al.*, 1979; *Zyvoloski and O'Sullivan*, 1980; *Zyvoloski*, 1983; *Pruess*, 1988; *O'Sullivan et al.*, 2001]. Subsequent studies using multiphase simulators or single-phase research codes included effects such as thermal pressurization [*Delaney*, 1982; *Sammel et al.*, 1988; *Hanson*, 1992; *Dutrow and Norton*, 1995], magmatic fluid production [*Hanson*, 1995], temporal or spatial variations in permeability [*Norton and Taylor*, 1979; *Parmentier*, 1981; *Gerdes et al.*, 1995; *Dutrow and Norton*, 1995], and topographically driven flow [*Sammel et al.*, 1988; *Birch*, 1989; *Hanson*, 1996].

[16] Widely used multiphase simulators include Simultaneous Heat and Fluid Transport (SHAFT), Multicomponent Model (MULKOM) and its successors, the Transport of Unsaturated Groundwater and Heat (TOUGH) family of codes [*Pruess*, 1988, 1991, 2004; *Pruess et al.*, 1999], the Los Alamos National Laboratory Finite Element Heat and Mass Transfer (FEHM) code [*Zyvoloski et al.*, 1988, 1997; *Keating et al.*, 2002], and the U.S. Geological Survey code HYDROTHERM [*Hayba and Ingebritsen*, 1994; *Kipp et al.*, 2008]. TOUGH2 and FEHM are now both widely used simulators that have been adapted to a variety of applications including environmental issues, CO_2 sequestration, and geothermal studies. HYDROTHERM remains a hydrothermal modeling research tool.

[17] Most multiphase geothermal reservoir simulators are limited to subcritical temperatures (approximately <350°C), in part because of the inherent difficulty of simulating flow and transport near the critical point (~374°C and 22.06 MPa for pure water and 400°C and 30 MPa for seawater (see Figures 2 (middle) and 2 (right))). This difficulty is exacerbated by pressure-temperature formulations but minimized if the governing equation for heat transport is posed in terms of energy per unit mass (internal energy, enthalpy, or entropy), rather than temperature [*Faust and Mercer*, 1979a; *Ingebritsen and Hayba*, 1994; *Ingebritsen et al.*, 2006, pp. 125–129; *Coumou et al.*, 2008a; *Lu and Kieffer*, 2009]. There are still relatively few numerical modeling studies that include both two-phase and supercritical flow; examples include simulations of cooling plutons and dikes [e.g., *Hayba and Ingebritsen*, 1997; *Polyansky et al.*, 2002], stratovolcano hydrodynamics [e.g., *Hurwitz et al.*, 2003; *Fujimitsu et al.*, 2008], large-scale hydrothermal convection [e.g., *Kissling and Weir*, 2005], and cooling of ignimbrite sheets [*Hogeweg et al.*, 2005; *Keating*, 2005].

[18] Some multiphase simulators have incorporated more realistic equations of state for hydrothermal fluids

TABLE 1. Relative Capabilities of Selected Multiphase Numerical Codes Commonly Applied in Simulations of Magmatic Hydrothermal Systems[a]

Name	Reference	T_{max} (°C)	P_{max} (MPa)	Numerical Method	Reactive Transport	Deformation	CO_2	NaCl
CSMP++	*Matthäi et al.* [2007] and *Coumou* [2008]	1000	500	FE-FV				X
FEHM	*Zyvoloski et al.* [1988, 1997], *Bower and Zyvoloski* [1997], *Dutrow et al.* [2001], and *Keating et al.* [2002]	1500		FE	X	X	X	
FISHES[b]	*Lewis* [2007] and *Lewis and Lowell* [2009a]	800	1000	FV				X
HYDROTHERM	*Hayba and Ingebritsen* [1994] and *Kipp et al.* [2008]	1,00	1000	FD				
NaCl-TOUGH2	*Kissling* [2005b]	620	100	IFD				X
TOUGH2	*Pruess* [1991] and *Pruess et al.* [1999]	350	100	IFD			X	X
TOUGH2-BIOT	*Hurwitz et al.* [2007]	350	100	IFD-FE		X	X	
TOUGH-FLAC	*Rutqvist et al.* [2002]	350	100	IFD-FE		X	X	
TOUGHREACT	*Xu et al.* [2004b]	350	100	IFD	X		X	

[a]Numerical methods are as follows: FD, finite difference; IFD, integrated finite difference; FE, finite element; FE-FV, finite element–finite volume. The columns labeled CO_2 and NaCl indicate whether the equation of state formulations include those components. CSMP++, Complex Systems Platform; FEHM, Finite Element Heat and Mass Transfer; FISHES, Fully Implicit Seafloor Hydrothermal Event Simulator; TOUGH2, Transport of Unsaturated Groundwater and Heat; TOUGH2-BIOT, TOUGH With Poroelastic Deformation; TOUGH2-FLAC, TOUGH With Fast Lagrangian Analysis of Continua; TOUGHREACT, TOUGH With Reactions. Most of these codes have interactive websites: CSMP++, http://csmp.ese.imperial.ac.uk/wiki/Home; FEHM, http://fehm.lanl.gov/; HYDROTHERM, http://wwwbrr.cr.usgs.gov/projects/GW_Solute/hydrotherm/; TOUGH2, http://esd.lbl.gov/TOUGH2/. Crosses indicate the capability to model reactive transport, deformation, H_2O-CO_2 fluids, or H_2O-NaCl fluids.

[b]Successor model to Georgia Tech Hydrothermal Model (GTHM) [*Lowell and Xu*, 2000; *Bai et al.*, 2003].

[*Battistelli et al.*, 1997; *Kissling*, 2005a, 2005b; *Croucher and O'Sullivan*, 2008]. Two important new codes, Complex Systems Platform (CSMP++) and Fully Implicit Seafloor Hydrothermal Event Simulator (FISHES), have been developed specifically to allow simulation of high-temperature multiphase flow of NaCl-H_2O fluids [*Geiger et al.*, 2006a, 2006b; *Matthäi et al.*, 2007; *Coumou et al.*, 2009; *Lewis and Lowell*, 2009a, 2009b]. Other recent developments include higher-order accurate transport methods [*Oldenburg and Pruess*, 2000; *Geiger et al.*, 2004, 2006a; *Coumou et al.*, 2006; *Croucher and O'Sullivan*, 2008] and simulations of mineral precipitation and fluid-rock interactions [*Cline et al.*, 1992; *Steefel and Lasaga*, 1994; *Fontaine et al.*, 2001; *Xu and Pruess*, 2001; *Xu et al.*, 2001; *Giambalvo et al.*, 2002; *Geiger et al.*, 2002; *Xu et al.*, 2004a], coupling between hydrothermal flow and mechanical deformation [*Todesco et al.*, 2004; *Hurwitz et al.*, 2007; *Hutnak et al.*, 2009], and geometrically complex geological structures [*Zyvoloski et al.*, 1997; *Geiger et al.*, 2004, 2006a; *Paluszny et al.*, 2007]. The relative capabilities of selected multiphase simulators are summarized in Table 1.

5. GOVERNING EQUATIONS

[19] There are many ways of formulating the basic governing equations for the flow of multiphase, variable density fluids and its coupling with heat transport, solute transport, and deformation. One useful set of equations for multiphase, single-component fluid flow and heat transport is

$$\frac{\partial[\phi(S_l\rho_l + S_v\rho_v)]}{\partial t} - \nabla\cdot\left[\frac{\rho_l k_{rl} k}{\mu_l}(\nabla P + \rho_l g\nabla z)\right] - \nabla\cdot\left[\frac{\rho_v k_{rv} k}{\mu_v}(\nabla P + \rho_v g\nabla z)\right] - R_m = 0 \quad (4)$$

(change in mass stored minus mass flux of liquid minus mass flux of vapor minus mass sources equals 0) for fluid flow and

$$\frac{\partial[\phi(S_l\rho_l h_l + S_v\rho_v h_v) + (1-\phi)\rho_r h_r}{\partial t} - \nabla\cdot\left[\frac{\rho_l k_{rl} k h_l}{\mu_l}(\nabla P + \rho_l g\nabla z)\right] - \nabla\cdot\left[\frac{\rho_v k_{rv} k h_v}{\mu_v}(\nabla P + \rho_v g\nabla z)\right] - \nabla\cdot K_m\nabla T - R_h = 0 \quad (5)$$

(change in heat stored minus heat advected by liquid minus heat advected by vapor minus heat conducted minus heat sources equals 0) for heat transport. In these equations the gradient operator ∇ describes the gradient of a vector or scalar quantity in the x, y, and z directions; the R terms represent sources and sinks of fluid mass or heat; and the dependent variables for fluid flow and heat transport are pressure P and enthalpy h [*Faust and Mercer*, 1979a]. Although the permeability k is a second-rank tensor, numerical simulations often treat it as a scalar for practical purposes.

[20] In equation (5), the specific enthalpies h (J kg^{-1}) are used rather than the total enthalpy H (J). In publications on heat transport in a geologic context, enthalpy is often erroneously written as $h = cT$, whereas the correct relation is $dh = cdT$. However, the de facto implementation in (most) flow codes is the latter version; hence, the misrepresentation is not propagated into the simulation results. Though the pressure-entropy pair has certain advantages in representing multicomponent, multiphase H_2O systems [*Lu and Kieffer*, 2009], that approach has not yet been implemented in a hydrothermal simulator.

[21] Equations (4) and (5) are coupled and nonlinear. They are coupled by the appearance of both dependent variables (P and h) in the heat transport equation (equation (5)) and

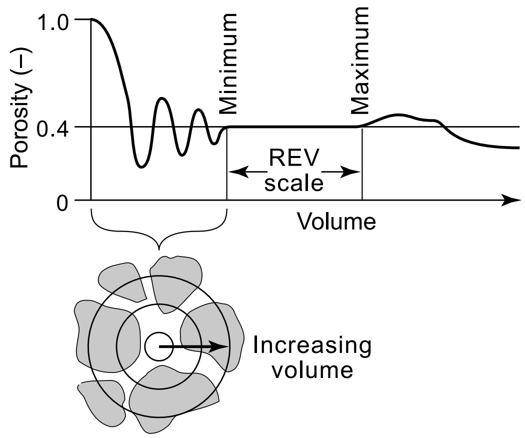

Figure 3. Porosity as a function of averaging volume. At a particular point within the porous medium (volume = 0), the value of porosity is either 0 or 1. The computed value of porosity stabilizes as it is averaged over progressively larger volumes. The value becomes essentially constant when a representative elementary volume (REV) is reached [*Bear*, 1972]. Averaging over larger volumes may incorporate geologic heterogeneities, leading to gradual changes in the averaged value. After *Hubbert* [1956].

are nonlinear because many of the coefficients (e.g., ρ_v, ρ_l, k_r, μ_v, and μ_l) are functions of the dependent variables.

[22] Formulations such as equations (4) and (5) were well established at the time of *Lowell*'s [1991] review. An ongoing challenge is the effective coupling of such equations with descriptions of multiphase, multicomponent solute transport and deformation.

[23] A general equation for solute transport of a single chemical component i in the vapor or liquid phase, denoted here as phase j, can be written

$$\frac{\partial(\phi\rho_j S_j C_i)}{\partial t} - \nabla\cdot(\rho_j \upsilon_j C_i) - \nabla\cdot(S_j\rho_j \overline{D}\nabla C_i) - R_i = 0 \qquad (6)$$

(change in solute mass stored minus solute advected minus solute transport by dispersion and diffusion minus solute sources equals 0), where C is aqueous concentration; $\overline{D}$ is hydrodynamic dispersion (also a second-order tensor); $\boldsymbol{\upsilon}$ is q/ϕ (see equations (1)–(3)), the average pore velocity; and R_i is a source (positive) or sink (negative) of the chemical component. Although such an equation is inadequate to represent the complexity of reactive solute transport in a multiphase, multicomponent, variable density fluid system, it does indicate the fundamental coupling with equations (4) and (5) for fluid flow and heat transport through porosity ϕ, density ρ, and the average pore velocity $\boldsymbol{\upsilon}$ (q/ϕ).

[24] Displacements (deformation) in porothermoelastic media subjected to changes in fluid pressure and temperature can be described by

$$G\nabla^2\mathbf{u} + \frac{G}{1-2\nu}\nabla(\nabla\cdot\mathbf{u}) = \alpha\nabla\hat{P} + G\frac{2(1+\nu)}{1-2\nu}\alpha_{\mathrm{T}}\nabla\hat{T}, \qquad (7)$$

where the circumflex above P and T is used to indicate an increase or decrease, rather than an absolute value; $\mathbf{u}$ is the displacement vector; and G is the shear modulus. This is an equation of mechanical equilibrium written in terms of displacements. Calculated pressure and temperature changes can be inserted into equation (7) to obtain the strain and the displacements experienced by the porous matrix. Typical displacements in magmatic hydrothermal systems range from mm yr^{-1} to m yr^{-1} (see section 8.2.7). Strain also affects fluid pressure and permeability, and thus, to represent poroelastic behavior, equation (7) must be coupled with a groundwater flow equation incorporating a volumetric strain term (which equation (4) lacks). In this context, "coupling" means that the equations are linked by incorporating the same strains and fluid pressures in their solutions. Problems in porothermoelasticity require coupling with equations of heat transport (such as equation (5)) as well. Unlike equations (4)–(6), the terms in equation (7) do not readily lend themselves to concise, intuitive definition; we refer interested readers to *Neuzil* [2003], *Wang* [2004], or *Ingebritsen et al.* [2006, pp. 39–61] for full developments.

6. COMMON ASSUMPTIONS AND SIMPLIFICATIONS

[25] In this section we review ten common assumptions and simplifications inherent in numerical modeling of hydrothermal systems via systems of equations such as (4)–(7). The first six of these assumptions are actually incorporated into equations (4)–(7), whereas the latter four are not.

[26] Assumptions are a key source of uncertainty in numerical model results and as such deserve careful examination. Most nonmodelers are probably unaware of these common assumptions, and they often go unmentioned, or are noted but not discussed, in modern modeling studies.

6.1. Representative Elementary Volume

[27] Equations for flow (e.g., equation (4)), transport (equations (5) and (6)), and deformation (equation (7)) are solved numerically over spatially discretized problem domains. The fundamental assumption is that a minimum spatial scale, termed the representative elementary volume (REV) [*Bear*, 1972], exists across which properties such as permeability, thermal conductivity, or porosity (Figure 3) can be treated as being constant. The model discretization scale must be large relative to the scale of microscopic heterogeneity (e.g., grain size in a granular porous medium) but small relative to the entire domain of interest. Some types of porous media, such as fractured rocks with poorly connected fracture networks or networks that do not have a characteristic fracture size limit, do not possess such a scaling behavior [*Berkowitz*, 2002]. Adequate representation of such systems in simulations is a topic of ongoing research.

6.2. Darcian Flow

[28] It is commonly assumed that groundwater flow is laminar, and hence, the momentum balance can be described by multiphase versions of Darcy's law (equations (1) and (2)). If flow rates exceed a certain threshold, flow becomes turbulent, and Darcy's law will overestimate the flow rate

associated with a particular pressure gradient. The upper limit for Darcy's law is usually estimated on the basis of the dimensionless Reynolds number *Re*,

$$Re = (\rho q L)/\mu, \tag{8}$$

where L is a characteristic length and ρ and μ are fluid density and dynamic viscosity, assumed constant in equation (8). The Reynolds number was developed for pipe flow [e.g., *Vennard and Street*, 1975, pp. 299–306], where L is the pipe diameter. Its application to flow in porous or fractured media is somewhat problematic, particularly in the context of variable density, multiphase systems. For single-phase flow in granular porous media, L can be related to median grain size (e.g., d_{50}) or sometimes to $k^{1/2}$ [*Ward*, 1964], and the transition from laminar to turbulent flow occurs at $Re \sim 1$–10 [*Bear*, 1979, pp. 65–66]. For fractured media, L can be related to fracture aperture, and q in equation (8) can be replaced by v, the average linear velocity; under these assumptions the transition may occur at $Re \sim 1000$ [*Ingebritsen et al.*, 2006, p. 5]. Flow rates sufficient to violate Darcy's law are not common in the subsurface but can occur in geyser conduits, near MOR vents, during phreatic eruptions, and, more generally, in open and well-connected fracture systems.

6.3. Local Thermal Equilibrium and Thermal Dispersion

[29] In hydrothermal modeling it is commonly assumed that fluid and rock are in local thermal equilibrium and that the effects of thermal dispersion are negligible. That is, in equation (5) steam and liquid water are permitted to have different specific enthalpies (h_v and h_l), but steam, liquid, and rock have the same temperature T at the REV scale (e.g., in the fourth term on the left-hand side of equation (5)); further, there is no provision for thermal dispersion in equation (5), though solute dispersion is explicitly represented in the solute transport equation (equation (6), third term on left-hand side). The assumptions of local thermal equilibrium and insignificant thermal dispersion are justified by the generally low rates of subsurface fluid flow and the relative efficiency of heat conduction in geologic media, which acts to homogenize the local temperature field. The "diffusive" transport of heat by conduction (the fourth term on the left-hand side of equation (5)) is much more effective than solute diffusion (the third term on the left-hand side of equation (6)) [*Bickle and McKenzie*, 1987], rendering thermal dispersion relatively insignificant. However, the assumption of thermal equilibrium may not be appropriate at the pore scale [*Wu and Hwang*, 1998] or in highly fractured media, given sufficiently high, transient flow rates.

6.4. Thermal Conduction and Radiative Heat Transfer

[30] Conduction of thermal energy is described by Fourier's law of heat conduction

$$\mathbf{q}_h = -K_m \nabla T, \tag{9}$$

where $\mathbf{q}_h$ is a vector and K_m is the thermal conductivity of the medium. The thermal conductivity of most common rocks decreases nonlinearly with increasing temperature to at least 250°C [*Sass et al.*, 1992; *Vosteen and Schellschmidt*, 2003]. A room temperature conductivity of 2.4 W m^{-1} K^{-1} is predicted to decrease to 1.6 W m^{-1} K^{-1} at 500°C [*Vosteen and Schellschmidt*, 2003]. Above ~600°C, radiative heat transfer becomes significant and can be approximated by a radiative thermal conductivity component which increases with increasing temperature [*Clauser*, 1988; *Hofmeister et al.*, 2007]. Both the temperature dependence of thermal conductivity and radiative heat transport are usually neglected in hydrothermal modeling. Instead, a "medium" thermal conductivity (K_m in equations (5) and (9)) is typically approximated by a single bulk conductivity of fluid and rock [*Bear*, 1972, pp. 648–650] or by a porosity-weighted (geometric mean) conductivity of fluid and rock [*Raffensperger*, 1997]. Such approximations may be significant in a conduction-dominated system and less so where advection is dominant. Temperature-dependent thermal conductivity is straightforward to implement in numerical solutions and is not computationally expensive in the context of modern computational resources.

6.5. Relative Permeabilities

[31] The concept of relative permeability (k_r in equations (1), (2), (4), and (5)) is invoked in multiphase flow problems to express the reduction in mobility of one fluid phase due to the interfering presence of one or more other phases. Relative permeability is treated as a scalar function of volumetric fluid saturation varying from 0 to 1 (Figure 4). The level of partial saturation below which a phase is disconnected and becomes immobile is called residual saturation. To paraphrase *Scheidegger* [1974, pp. 249–250], relative permeabilities are essentially "fudge factors" that allow Darcy's law to be applied to various empirical data on multiphase flows.

[32] Though relative permeability is an empirical construct, very few laboratory data are available for water-steam relative permeability curves [e.g., *Horne et al.*, 2000]. In porous rocks, steam-water relative permeabilities, like those for oil-water or gas-water flow, may be best described by nonlinear Corey-type relations [*Piquemal*, 1994]. However, steam-water functions for fracture-dominated media may be linear; that is, $k_r \sim S$, where S is the volumetric saturation of a particular phase, implying little phase interference and that relative permeabilities sum to 1 [e.g., *Gilman and Kazemi*, 1983; *Wang and Horne*, 2000]. Further, enthalpy data from well tests in geothermal reservoirs suggest Corey-type relative permeabilities for liquid water but with little phase interference [*Sorey et al.*, 1980], and some authors [e.g., *Cline et al.*, 1992] have introduced temperature-dependent relative permeability curves that reflect the decrease in surface tension toward the critical point of pure water. A possible physical explanation for less phase interference in steam-water flow (relative to immiscible fluids) is that steam can flow through water-filled pores by condensing on one side and boiling off on the other [*Verma*, 1990]. Regardless of the functional form of the relative

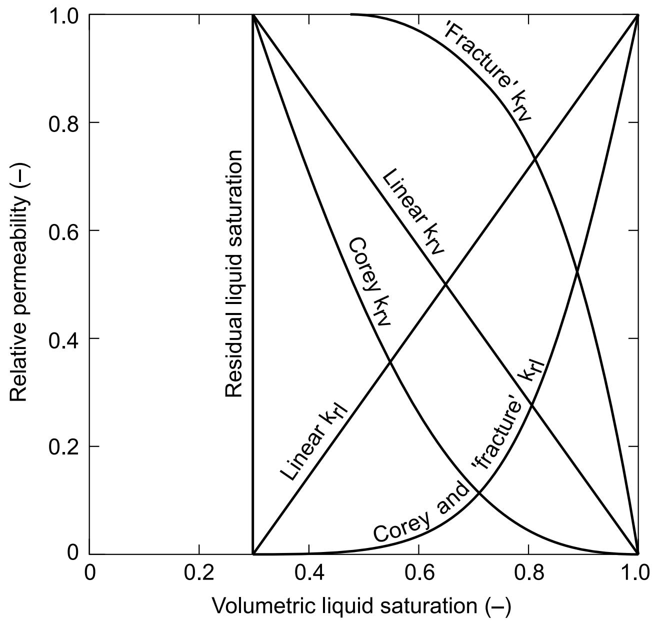

Figure 4. Linear, Corey-type [*Corey*, 1957], and "fracture flow" [*Sorey et al.*, 1980] relative permeability functions. These functions bracket the range of behavior that has been suggested for steam–liquid water systems. The Corey and "fracture flow" k_{rl} functions are identical, but their k_{rv} relations are very different. Whereas the Corey functions give $k_{rv} + k_{rl} \ll 1$ for a large range of saturations, the "fracture flow" functions give $k_{rv} + k_{rl} = 1$. Values of k_{rv} for the linear functions lie between the Corey and "fracture flow" values. In these examples, volumetric liquid saturation (S_l) is related to volumetric vapor saturation (S_v) by $S_l + S_v = 1$, and the residual vapor and liquid saturations are 0.0 and 0.3, respectively.

permeability curves, experimental data seem to indicate a near-zero residual saturation for the steam phase and 20%–30% residual saturation for the water phase.

[33] Realistic relative permeability functions should vary with pore and fracture geometry [*Helmig*, 1997], and therefore with scale, and should presumably include some hysteresis, which in this instance is the difference in flow behavior between when, for example, gas enters water-saturated media (gas imbibition) versus when gas leaves water-saturated media (gas drainage). However, hysteresis is often ignored in simulations of nonisothermal, multiphase flow [e.g., *Li and Horne*, 2006], and for modeling purposes, a single global relative permeability function is commonly invoked. The choice of relative permeability functions can have a large influence on the results of simulations [e.g., *Ingebritsen and Rojstaczer*, 1996, Figures 9, 10, and 13]. Relative permeability curves are also the largest potential source of nonlinearity in equations such as (4) and (5), greatly complicating numerical solution of any problem involving extensive multiphase flow.

6.6. Capillary Pressure

[34] Like relative permeability, capillary pressures (pressure differences between fluid phases) are usually computed as functions of saturation using empirical relations [*Helmig*, 1997] and do not account for dynamic effects such as hysteresis. Capillary pressure effects are often neglected in simulations of hydrothermal flow (for instance, equations (4) and (5) assume that a single value of pressure P applies to both phases). This omission is perhaps justified by the limited empirical data on steam–liquid water capillary behavior [*Li and Horne*, 2007]; the fact that relative permeability functions can incorporate some capillary effects, for instance, through residual liquid saturation (Figure 4); and the fact that the surface tension of water decreases with temperature and vanishes at the critical point, where the properties of steam and liquid water merge (Figure 2). However, simulations using plausible functional relations for capillary pressure have shown that capillary forces can increase the efficiency of heat transfer via countercurrent flow [*Udell*, 1985] and that in rocks with a porous matrix and a network of fractures (dual porosity), typical of hydrothermal systems, capillary pressures tend to keep the vapor phase in the fractures and the liquid in the matrix [*Urmeneta et al.*, 1998]. In low-permeability geothermal reservoirs, capillary forces can either extend or shrink two-phase zones, depending on the wettability of the media [*Tsypkin and Calore*, 2003].

6.7. Boussinesq Approximation

[35] The Boussinesq approximation assumes that transient variations in fluid density are negligibly small ($\partial\rho/\partial t = 0$), and density acts only on the buoyancy term (ρgz in equations (4) and (5)). This means that volume rather than fluid mass is conserved (equation (3)), and the approximation allows straightforward solution using a stream function approach, which is particularly useful to resolve boundary layers in convective hydrothermal systems. However, it is inappropriate in the general hydrothermal case even if a mass-based stream function [*Evans and Raffensperger*, 1992] is used because (1) the effects of fluid expansion and pressurization due to in situ heating are neglected [*Hanson*, 1992], (2) the compressibility of multiphase hydrothermal fluids can be extraordinarily high [*Grant and Sorey*, 1979], and (3) the stream function approach cannot describe the hydrodynamics of phase separation and two-phase flow. In some simulations using the stream function approach, two-phase flow has been crudely approximated by assuming that a computational cell is entirely filled by either steam or liquid water [*Cathles*, 1977; *Fehn and Cathles*, 1979, 1986; *Fehn et al.*, 1983], averaging the properties of the liquid and vapor phase [*Wilcock*, 1998; *Fontaine et al.*, 2007], or assigning identical fluid properties (except for density) for liquid and vapor [*Kawada et al.*, 2004]. All of these approaches are likely to generate significant errors. Another deficiency of the Boussinesq approximation/stream function approach is that because it assumes that $\partial\rho/\partial t = 0$, it is not strictly valid for transient flow simulations [*Evans and Raffensperger*, 1992]. Stream function solution of the governing equations for heat and mass transport is no longer necessary but remains quite common.

6.8. Fluid Composition

[36] The presence of salts (primarily NaCl) and noncondensible gas (primarily CO_2) in continental and submarine hydrothermal systems affects fluid phase relations, densities, and miscibilities. These effects are usually not represented in high-temperature, multiphase models. State-of-the-art modeling studies have typically employed realistic properties for pure water [e.g., *Ingebritsen and Hayba*, 1994; *Hayba and Ingebritsen*, 1997; *Jupp and Schultz*, 2000; *Hurwitz et al.*, 2003; *Coumou et al.*, 2006, 2008a, 2008b]. Studies incorporating accurate representations of the binary H_2O-CO_2 or H_2O-NaCl systems have only very recently become available [*Todesco et al.*, 2004; *Geiger et al.*, 2005; *Driesner and Geiger*, 2007; *Coumou et al.*, 2009; *Hutnak et al.*, 2009; *Lewis and Lowell*, 2009a, 2009b]. These first binary system studies have shown that the extended pressure-temperature range for phase separation can have a large impact on system behavior. Yet even the binary system studies have not captured the full complexity of crustal fluids that are usually better represented in terms of three major components, H_2O-NaCl-CO_2. Equation-of-state formulations for the ternary [*Bowers and Helgeson*, 1983; *Brown and Lamb*, 1989; *Duan et al.*, 1995; *Anovitz et al.*, 2004; *Duan and Li*, 2008] cover only limited parts of the pressure-temperature range encountered in hydrothermal systems and have been shown to be of limited accuracy in several regions of the phase diagram [e.g., *Schmidt and Bodnar*, 2000; *Blencoe*, 2004; *Gottschalk*, 2007]. Therefore, some level of approximation remains inevitable (see section 8.1.2). However, consideration of single-component end-member systems may lead to conclusions that exclude qualitatively and quantitatively important phenomena [*Lu and Kieffer*, 2009].

6.9. Nonreactive Fluid Flow

[37] The dynamic reality of hydrothermal geochemistry is not fully expressed by the solute transport equation presented as equation (6), in which chemical reactions are represented only by the "*R*" term. Laboratory experiments [e.g., *Seyfried*, 1987; *Bischoff and Rosenbauer*, 1988, 1996; *Bischoff et al.*, 1996; *Foustoukos and Seyfried*, 2007], observations of spring and vent chemistry [e.g., *Giggenbach*, 1984; *Von Damm*, 1990, 1995; *Shinohara*, 2008], and thermodynamic calculations [e.g., *Symonds et al.*, 2001] show that circulating hydrothermal fluids are highly reactive and that hydrothermal reactions have a strong feedback effect on the fluid flow field because they significantly alter both rock and fluid properties. For instance, laboratory experiments indicate that fluid flow under a temperature gradient can result in rapid mineral precipitation, decreasing permeability with time. During one experiment in which heated water was forced down a temperature gradient (300°C–92°C) through a cylindrical granite sample, the measured permeability dropped by a factor of ~25 in just 2 weeks [*Moore et al.*, 1983]. However, many laboratory studies involve strong chemical disequilibrium that may not be representative of natural systems. Further, it is yet unclear as to what degree the feedback between fluid pressure and rock mechanics may counteract the chemical reaction effect on permeability through creation of new fractures and/or reopening of existing fractures.

[38] The interactions that lead to precipitation and dissolution of minerals are commonly referred to as "reactive transport." Because reactive transport simulations of hydrothermal systems require a tremendous amount of computational power, they have been limited to one- or two-dimensional domains with relatively simple geometries. The limited numerical simulations of reactive transport under hydrothermal conditions have mainly been carried out with TOUGH With Reactions (TOUGHREACT) [e.g., *Xu and Pruess*, 2001; *Xu et al.*, 2001; *Dobson et al.*, 2004; *Todaka et al.*, 2004], CSMP++ [*Geiger et al.*, 2002], or specialized reactive transport codes [e.g., *Steefel and Lasaga*, 1994; *Alt-Epping and Smith*, 2001].

6.10. Simplified Descriptions of Permeability

[39] Intrinsic permeability (k in equations (1), (2), (4), and (5)) is probably the most influential, least constrained, and most variable parameter influencing fluid flow in magmatic hydrothermal systems. In the crystalline rocks typical of hydrothermal systems, fluid flow is focused in fractures and thus may vary by orders of magnitude when examined at different length scales [*Nehlig*, 1994; *Curewitz and Karson*, 1997]. Fluid flow in fractured rocks is fundamentally different from porous media flow and comprises a major research area in hydrogeology [*Berkowitz*, 2002; *Neuman*, 2005]. For practical purposes, numerical simulations of hydrothermal flow generally assume that an REV exists over which fracture permeability can be described by an equivalent porous media approximation.

[40] Although permeability varies by ~17 orders of magnitude in common geologic media, some systematic variation is suggested by various global and or crustal-scale studies [e.g., *Brace*, 1980, 1984; *Bjornsson and Bodvarsson*, 1990; *Fisher*, 1998; *Manning and Ingebritsen*, 1999; *Saar and Manga*, 2004; *Talwani et al.*, 2007; *Stober and Bucher*, 2007]. A global permeability-depth relation based on geothermal and metamorphic data suggests that mean crustal-scale permeability is approximated by

$$\log k \approx -3.2 \log z - 14, \tag{10}$$

where k is in m^2 and z is in km [*Manning and Ingebritsen*, 1999]. This relation suggests effectively constant permeability below 10–15 km, the approximate depth of the brittle-ductile transition in tectonically active crust, and the absence of a permeability discontinuity or barrier, implying that fluids produced by magmatism and metamorphism can be transmitted to the brittle crust and mix with meteoric fluids [*Ingebritsen and Manning*, 1999]. The brittle-ductile transition is probably much shallower than 10–15 km in the thin, hot crust associated with active magmatism.

[41] Proposed permeability-depth relations for the continental [*Manning and Ingebritsen*, 1999; *Shmonov et al.*, 2003; *Stober and Bucher*, 2007] and oceanic [*Fisher*, 1998] crust assume permeability to be isotropic. In many geologic

environments there is, in fact, large permeability anisotropy, which is conventionally defined as the ratio between the horizontal and vertical permeabilities but may also represent structural/tectonic features such as the axial rift/abyssal hill topography of the MOR. The relatively few hydrothermal modeling studies that have explored the effect of permeability anisotropy have found its effects to be significant [e.g., *Dutrow et al.*, 2001; *Hurwitz et al.*, 2002, 2003; *Saar and Manga*, 2004; *Fisher et al.*, 2008].

[42] Laboratory experiments involving hydrothermal flow under pressure, temperature, and chemistry gradients in crystalline rocks result in order-of-magnitude permeability decreases over daily to subannual time scales [e.g., *Summers et al.*, 1978; *Morrow et al.*, 1981, 2001; *Moore et al.*, 1983, 1994; *Vaughan et al.*, 1986; *Cox et al.*, 2001; *Polak et al.*, 2003; *Yasuhara et al.*, 2006]. Field observations of continuous, cyclic, and episodic hydrothermal flow transients at various time scales also suggest transient variations in permeability [e.g., *Baker et al.*, 1987, 1989; *Titley*, 1990; *Hill et al.*, 1993; *Urabe et al.*, 1995; *Haymon*, 1996; *Fornari et al.*, 1998; *Sohn et al.*, 1998; *Gillis and Roberts*, 1999; *Johnson et al.*, 2000; *Golden et al.*, 2003; *Hurwitz and Johnson*, 2003; *Husen et al.*, 2004; *Sohn*, 2007]. Despite these empirical observations, only a few modeling studies have invoked temperature- [*Hayba and Ingebritsen*, 1997; *Germanovich et al.*, 2000, 2001; *Driesner and Geiger*, 2007], pressure- [*Dutrow and Norton*, 1995; *Driesner and Geiger*, 2007; *Rojstaczer et al.*, 2008], or time-dependent permeability [e.g., *Hurwitz et al.*, 2002] or the effects of reactive transport on permeability [*Dutrow et al.*, 2001]. The widespread occurrence of active, long-lived (10^3–10^6 years) hydrothermal systems, despite the tendency for permeability to decrease with time, implies that other processes such as hydraulic fracturing and earthquakes regularly create new flow paths [e.g., *Rojstaczer et al.*, 1995]. In fact, there have been suggestions that crustal-scale permeability is a dynamically self-adjusting or even emergent property [e.g., *Rojstaczer et al.*, 2008].

7. NUMERICAL METHODS

[43] The fundamental idea of any numerical method is to represent the physical domain by a computational grid. This grid consists of a number of discrete points located on the intersections of lines that are orthogonal to each other ("structured grid") or in a nonorthogonal arrangement such that they optimize the representation of the geometrical features within the domain ("unstructured grid"). The number of grid points feasible or desirable in practical applications depends greatly on the computational efficiency of the numerical method, the complexity of the geological structures present in the physical domain, the nonlinearity of the flow and transport processes, and the degree of precision sought. At each grid point values of the parameters that describe the physical domain, for example, the porosity and permeability, are specified or calculated. The solution to the governing equations is then approximated numerically at these points. For magmatic hydrothermal systems the system of governing equations is coupled and highly nonlinear. Accurate, stable, and efficient solution of these equations is the subject of ongoing research.

[44] The first numerical methods used to simulate multiphase heat and mass transport were finite difference (FD) methods [*Faust and Mercer*, 1979a, 1979b]. They form the basis for the U.S. Geological Survey code HYDROTHERM [*Hayba and Ingebritsen*, 1994; *Kipp et al.*, 2008]. *Pruess et al.* [1979] used an integrated finite difference scheme (IFD) [*Narasimhan and Witherspoon*, 1976], formally equivalent to a finite volume (FV) method, that is the basis of the widely used TOUGH code family [*Pruess*, 2004]. The FV method is also used in the research code FISHES [*Lewis*, 2007; *Lewis and Lowell*, 2009a].

[45] Both FD and IFD methods are very intuitive because they approximate the spatial and temporal gradients of a given property in equations such as equations (4) and (5) as the difference in that property between two discrete points in x, y, and z directions or between two discrete points in time, respectively. The FD method is restricted to structured grids, which imposes restrictions in representing complex topography and stratigraphy or geological structures such as faults. The IFD method can be used for unstructured grids and hence provides more geometrical flexibility. However, it requires the interface between two grid points to be perpendicular to the line connecting them. If this is not the case, the locations of temperature, pressure, and saturation fronts will exhibit strong grid orientation effects unless the spatial gradients are approximated in a more complex manner [e.g., *Aavatsmark*, 2002; *Lee et al.*, 2002].

[46] To avoid numerical instabilities in situations where advective transport dominates over diffusive transport, FD and IFD methods commonly use upstream weighting. That is, certain parameters (e.g., ρ_v, ρ_l, k_r, μ_v, and μ_l), and thus the flow between two grid points, are weighted toward the grid point that lies in the upstream flow direction. Whereas upstream weighting stabilizes the numerical solution, it also overestimates diffusive flow between grid points. This causes artificial smearing of steep concentration fronts, also known as numerical dispersion. Numerical dispersion can be reduced by evaluating the flow between grid points at the interface between the points, rather than the upstream node. Such so-called "higher-order" flux approximations predict the locations of temperature, concentration, and saturation fronts more accurately [*Oldenburg and Pruess*, 2000; *Geiger et al.*, 2006a].

[47] The finite element (FE) method is a numerical method that allows truly unstructured grids and hence provides maximum geometric flexibility to represent complex geological structures. It was adapted for simulation of multiphase flow in magmatic hydrothermal systems by *Zyvoloski* [1983] and forms the basis of the Los Alamos National Laboratory code FEHM [*Zyvoloski et al.*, 1988, 1997; *Keating et al.*, 2002]. Standard FE methods also suffer from numerical instabilities if advection dominates over diffusion. Hence, the idea of upstream weighting was introduced here as well [*Dalen*, 1979]. However, upstream-weighted FE methods require special FE grids; otherwise, the upstream direction

cannot be identified uniquely, and nonphysical results can occur [*Forsyth*, 1991].

[48] More recently, a classical concept for modeling incompressible single- and two-phase flow and transport in porous media [e.g., *Baliga and Patankar*, 1980; *Durlofsky*, 1993] has been adapted to multiphase heat and mass transport simulations [*Geiger et al.*, 2006a; *Coumou*, 2008]. It combines the FE method to solve the diffusive parts of heat and mass transport equations with a higher-order FV method to solve the advective parts. This way, the numerical method that is best suited to solve a certain type of equation, FE for diffusion and FV for advection, can be used. At the same time, maximum geometric flexibility is provided, even for very complex three-dimensional structures such as fractured and faulted reservoirs [*Paluszny et al.*, 2007]. In the combined FE-FV approach, the mass balance equation (equation (4)) is reformulated as a pressure-diffusion equation. From its solution the velocity field can be computed, which is subsequently used in solution of the heat (equation (5)) and solute (equation (6)) transport equations [*Geiger et al.*, 2006a; *Coumou*, 2008].

[49] Regardless of the numerical method, the discretized form of the heat and mass transport equations results in a system of linear ordinary differential equations that can be written in matrix form as $\mathbf{A}x = b$. $\mathbf{A}$ is a sparse and diagonally dominant matrix containing the discretization of the governing equation. $\mathbf{A}$ is of size $n \times n$, where n is the number of unknowns. The vector x contains the solution variables (e.g., h_f and/or P) at each grid point, and the vector b contains the boundary and initial conditions. Both x and b are of length n. This implies that if there is only one solution variable, n is equal to the number of grid points. The system $\mathbf{A}x = b$ must be solved at least once for each time step and hence hundreds to thousands of times during a typical simulation. There are several ways to solve $\mathbf{A}x = b$. Common choices include (incomplete) decompositions of $\mathbf{A}$ into a lower and upper matrix (so-called LU and ILU methods), conjugate and biconjugate gradient (CG and BiCG) methods, and generalized minimum residual (GMRES) methods. Often, several methods are combined to accelerate the solution. For example, HYDROTHERM uses an ILU method to precondition a GMRES solver [*Kipp et al.*, 2008], whereas TOUGH2 uses an ILU solver with BiCG/GMRES acceleration [*Wu et al.*, 2002]. A problem with these methods is that the computing time for solving $\mathbf{A}x = b$ increases by a factor of $(n)^{1.5}$ to $(n)^3$; that is, if the number of unknowns doubles, the computing time increases by a factor of ~3–8. In practice, this scaling behavior imposes restrictions on the number of unknowns that can be solved for, thereby imposing limitations on how finely the grid can be resolved. However, a new generation of robust matrix solvers exists. They are based on algebraic multigrid methods, and their computing time scales linearly with the number of unknowns [*Stüben*, 2001]. Such a matrix solver is currently used in the CSMP++ code, which consequently can deal with much larger numbers of unknowns [*Matthäi et al.*, 2007].

[50] There are two fundamentally different ways that the system $\mathbf{A}x = b$ can be formulated, coupled and decoupled. In a fully coupled approach, one solves simultaneously for all unknowns such as enthalpy H_f and pressure P (equations (4) and (5)). Hence, the system $\mathbf{A}x = b$ contains the discretizations and boundary conditions of two equations. The number of unknowns (n) is now twice as large as the number of grid points. This approach can be expanded further to include concentration (equation (6)) or deformation (equation (7)). Such coupled systems must be solved using a nonlinear iteration, which is commonly achieved by a Newton-Raphson method. The advantage of fully coupled approaches is that the resulting pressure, temperature, and saturation fields are consistent and that relatively large time steps can be used as long as the iterations converge. Fully coupled approaches are most common to FD, IFD, and FE methods. Decoupled approaches solve the system $\mathbf{A}x = b$ for each governing equation sequentially. This introduces a numerical error which is on the order of the time step: if the time step is decreased by a factor of 2, the error decreases by the same factor. While this error leads to pressure, temperature, and saturation fields that may not be entirely consistent, decoupled approaches are numerically more stable because they do not require iteration. In practice, this often allows use of finer grid meshes and higher-order accurate transport schemes, which resolve the flow and transport processes more accurately in heterogeneous media than fully coupled approaches. Decoupled approaches are often used in conjunction with combined FE-FV methods.

[51] Currently, no single code solves the fully coupled equations for multiphase heat and mass transport and deformation in porous media. Instead, these equations are solved by coupling two different codes in sequence, one specialized code for fluid flow and transport and another specialized code for deformation [*Rutqvist et al.*, 2002; *Reid*, 2004; *Hurwitz et al.*, 2007]. Great care must be exercised because such "sequential coupling" can lead to nonphysical oscillations in the numerical solution [*Kim et al.*, 2009].

8. LESSONS LEARNED SINCE 1991

[52] We take *Lowell*'s [1991] review as the starting point for this part of our discussion. We divide this section into two parts, the first (section 8.1) emphasizing improvements in modeling capability and the second (section 8.2) focusing on the resulting insights into the physics of magmatic hydrothermal systems. Like *Lowell* [1991], we will emphasize "process-oriented" rather than site-specific modeling, though there are many recent, sophisticated modeling studies of producing geothermal fields [*O'Sullivan et al.*, 2001, 2009; *Mannington et al.*, 2004; *Kiryukhin and Yampolsky*, 2004; *Kiryukhin et al.*, 2008]. Numerical simulation is a powerful tool for testing competing hypotheses in data-poor environments where data acquisition is a major challenge (Figure 5).

[53] Parameter uncertainty and incomplete knowledge of initial conditions generally precludes site-specific, "predictive" forward modeling of subsurface hydrologic systems, even in shallow, low-temperature groundwater systems with relatively abundant data [e.g., *Konikow and Bredehoeft*,

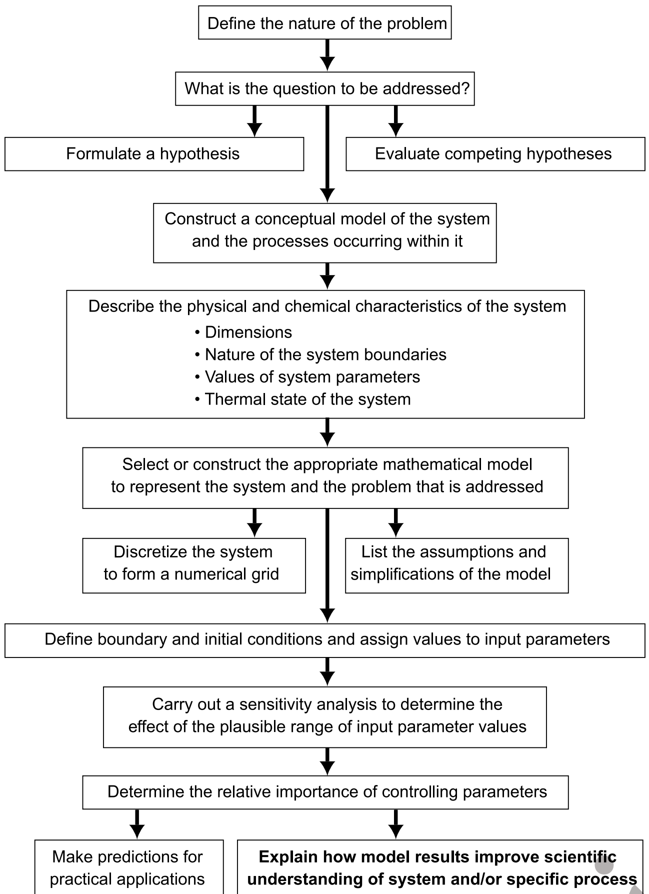

Figure 5. Flowchart showing steps in development of a numerical model suitable for hypothesis testing. The iterative nature of the modeling process could be represented by a variety of loops in this flowchart. For instance, exploration and reevaluation of boundary and initial conditions can be very important for understanding processes.

1992; *Oreskes et al.*, 1994; *Bethke*, 1994]. Data availability in magmatic hydrothermal systems is generally much more limited. Nevertheless, recent numerical modeling results suggest that high-temperature systems may in some respects be more "predictable" than shallow groundwater systems. This is because the properties of hydrothermal fluids themselves may exert considerable control on first-order behavior such as plume temperature (section 8.2.2) and circulation geometry (section 8.2.3). Numerical models that make such predictions can serve to guide expensive and complicated data acquisition efforts. Nearly 20 years later, we agree with *Lowell* [1991, p. 471] that "(m)odels of hydrothermal activity should be viewed as exploratory in nature."

8.1. Improvements in Modeling Capability

[54] Since 1991 there has been improvement in our ability to quantitatively describe hydrothermal fluids and simulate hydrothermal flow in porous and fractured media. As described in section 8.2, much of our current understanding is derived from models that can simulate multiphase, near-critical flow of realistic, non-Boussinesq fluids with an adequate degree of computational accuracy.

8.1.1. Descriptions of Fluid Thermodynamics

[55] Magmatic hydrothermal systems often operate at near-critical and/or boiling, two-phase conditions. Such conditions pose major computational challenges. For a one-component system such as H_2O (Figure 2, middle), the critical point is at the vertex of the vaporization curve in pressure-temperature coordinates and represents a singularity in the equations of state where the partial derivatives of fluid density and enthalpy ($\rho(P, T)$ and $h(P, T)$) diverge to $\pm\infty$ [*Johnson and Norton*, 1991]. In pressure-enthalpy coordinates, where two-phase conditions are represented as a region rather than a single curve (Figure 6a), the relevant properties of liquid water and steam merge smoothly to finite values at the critical point and do not show singularities. Consequently, many modern codes treat heat transport in terms of enthalpy or internal energy. This treatment naturally reflects the reality that phase separation is controlled by (usually large) latent heats and that there is partial to full mutual miscibility of the two phases. Multiphase phenomena in hydrothermal systems are fundamentally different in these respects from most low-temperature multiphase flows of immiscible fluids. For example, because water vapor can condense into liquid water in a boiling system upon pressurization, the compressibility of the mixture is extremely high, even higher than the pure vapor's gas-like compressibility [*Grant and Sorey*, 1979]. The thermodynamics of these effects have been incorporated in modern simulators (CSMP++, FEHM, FISHES, HYDROTHERM, and TOUGH2) since the mid-1990s, and these codes can now routinely be used to account for real properties in the pure water system.

[56] In binary water-salt systems such as H_2O-NaCl, the critical points of the two pure systems are usually connected by a line that forms the crest of the vapor plus liquid coexistence volume (e.g., in *T-P-X* or *H-P-X* coordinates (see Figure 2, right)). This line is called the critical curve (or critical line) and connects points that are often called critical points for fluids of the respective composition. However, these are not critical points of the same nature as the critical point of a one-component system, and there is no critical divergence to infinity of properties such as heat capacity, thermal expansion, and compressibility. Rather, at the "critical point" of a seawater equivalent in the H_2O-NaCl system (i.e., for 3.2 wt % NaCl at ~30 MPa and 400°C) all of these properties have finite values. The second component adds an additional degree of freedom to the system, eliminating singular behavior. Accordingly, phase proportions and two-phase compressibilities are no longer simple functions of bulk fluid enthalpy and the specific enthalpies of the two phases but are subject to additional constraints posed by mass balance of the chemical components. The thermodynamics of H_2O-NaCl have recently been incorporated into several codes, typically using an enthalpy-pressure-composition formulation: for subcritical temperatures to 350°C in TOUGH2 [*Battistelli et al.*, 1997] and for temperatures up to 650°C–1000°C in CSMP++ [*Coumou*, 2008; *Coumou et al.*, 2009], FISHES [*Lewis*, 2007; *Lewis and Lowell*, 2009a], and NaCl-TOUGH2 [*Kissling*, 2005a, 2005b] (Table 1). These codes use different numerical

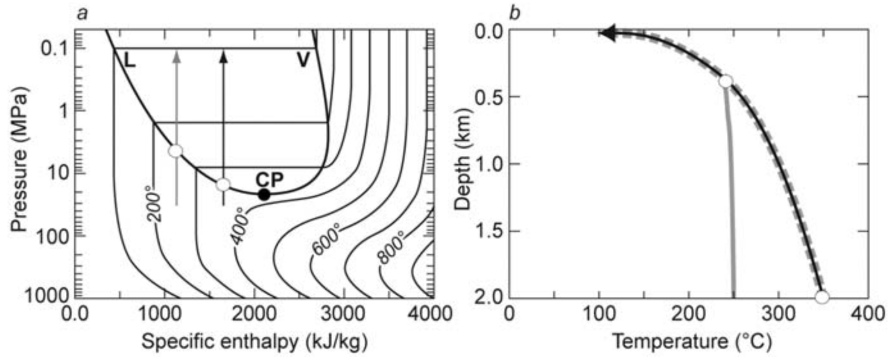

Figure 6. (a) Pressure-enthalpy diagram for pure water. The thick solid line represents the liquid (L) and vapor (V) branches of the boiling curve, joining at the critical point (CP). The area bounded by this curve is the coexistence region of a boiling liquid plus vapor mixture, within which phase proportions can be determined by the lever rule on a horizontal tie line. Arrows indicate adiabatic paths for a rising package of water that is initially 350°C (black) or 250°C (gray) at 30 MPa. In the 350°C case, the boiling curve is encountered at ~16.5 MPa, whereas in the 250°C case, boiling occurs at ~4 MPa. (b) In a temperature-depth context, this affords one explanation of why hydrothermal systems boil to various depths. The dashed gray curve in Figure 6b represents the boiling point curve, that is, the increase in boiling temperature with depth (pressure). The initially 350°C fluid (black curve with arrow) boils at ~2 km depth, and the initially 250°C fluid (gray curve) boils at ~0.4 km depth. The open circles in both Figures 6a and 6b indicate where the rising fluid intercepts the two-phase region (boils). Because of the large heat of vaporization of water, expressed as the width of the two-phase region in Figure 6a, rising hydrothermal plumes are unlikely to depart from the boiling point curve once they intercept it.

schemes and different equations of state: the EOS in CSMP++ are from *Driesner and Heinrich* [2007] and *Driesner* [2007]; those in FISHES are a synthesis of data and extrapolations from *Archer* [1992], *Anderko and Pitzer* [1993], and *Tanger and Pitzer* [1989]; and those in NaCl-TOUGH2 are from *Palliser and McKibbin* [1998a, 1998b, 1998c]. Systematic comparisons among these several codes have yet to be done.

[57] The system H_2O-CO_2 (Figure 2, left) is fundamentally different from H_2O-NaCl in that the critical line for this system limits the two-phase region to temperatures lower than the critical temperature of pure water, and only a single-phase fluid exists at temperatures above those indicated by the two-fluid surface. Knowledge of the topology of this two-phase region has recently been improved by high-accuracy experimental studies, but available equations of state only approximate current understanding (see *Blencoe* [2004] for a summary). Complicated phase relations at low temperatures [*Diamond*, 2001] are not usually relevant to hydrothermal studies. Currently, only TOUGH2 and to some degree the FEHM simulator have implemented hydrothermal H_2O-CO_2 thermodynamics.

8.1.2. Accurate Representation of Fluid Properties

[58] Recent work has demonstrated that approximation of the temperature-pressure-composition dependence of fluid properties in equations (1), (2), (4), and (5) can actually suppress behavior that is revealed when fluid properties are rendered more accurately (see sections 8.2.2, 8.2.3, 8.2.6, and 8.2.7). An increasing number of high-temperature (to >350°C) studies have employed realistic properties for pure water as a function of temperature (or enthalpy) and pressure [cf. *Ingebritsen and Hayba*, 1994; *Hayba and Ingebritsen*, 1997; *Jupp and Schultz*, 2000, 2004; *Hurwitz et al.*, 2003; *Coumou et al.*, 2006, 2008a, 2008b]. However, the presence of salts (primarily NaCl) and noncondensible gas (primarily CO_2) adds composition as another factor that affects fluid phase relations, densities, enthalpies, and viscosities. The binary H_2O-NaCl system (Figure 2, right) is of particular interest as a reasonable first-order proxy for MOR fluids. Complete and accurate representations for this system recently became available for conditions to 1000°C, 500 MPa, and 0–1 X_{NaCl} [*Driesner and Heinrich*, 2007; *Driesner*, 2007] and have begun to be employed in numerical models [*Geiger et al.*, 2005, 2006a; *Coumou*, 2008; *Coumou et al.*, 2009]. Previous descriptions of the H_2O-NaCl system at high temperature either contained errors in the thermodynamic formulation [*Palliser and McKibbin*, 1998a, 1998b, 1998c] or were published only as preliminary studies.

[59] In spite of these advances, some level of approximation of fluid properties remains ubiquitous in hydrothermal modeling. For instance, in essentially all hydrothermal applications, the composition dependence of viscosity in the binary systems is represented by approximations. Further, the complexity of crustal fluids would be better represented in terms of the three major components (H_2O-NaCl-CO_2), but data and thermodynamic models for this ternary remain incomplete. To be useful in numerical modeling studies, equation-of-state descriptions must be accurate over an extended range of pressure, temperature, and composition; be coherent across potential discontinuities such as phase boundaries; and be amenable to efficient numerical evaluation. Incorporation of H_2O-NaCl-CO_2 equations of state is not yet feasible, and incorporation of other salts such as

TABLE 2. Dimensionless Parameters

Parameter	Equation
Buoyancy ratio	$Rb = \frac{\gamma \Delta X}{\alpha_T \Delta T}$
Dimensionless porosity[a]	$\phi^* = \frac{\phi}{\sigma}$, where $\sigma = \frac{(1-\phi)c_r\rho_r + \phi(c_f\rho_f)}{c_f\rho_f}$
Lewis number	$Le = \frac{\kappa}{D}$, where $\kappa = \frac{K}{(1-\phi)c_r\rho_r + \phi(c_f\rho_f)}$
Nusselt number[b]	$Nu = \frac{h_f q_f T + \frac{K_m(T_L - T_U)}{L}}{\frac{K_m(T_L - T_U)}{L}}$
	or $Nu = -\int_0^1 \frac{\partial \overline{T}}{\partial \overline{z}}\Big\vert_{\overline{z}=0} d\overline{x}$[c]
Peclet number	$Pe = \frac{q_f L}{D}$
Thermal Peclet number	$Pe_T = \frac{q_f L}{\sigma \kappa}$
Rayleigh number[d]	$Ra = \frac{\rho_f k \alpha_T \Delta T g z}{\kappa \mu_f}$
	$Ra_T = \frac{k_z k_{rl}(\rho_l - \rho_v) g Z}{\kappa_l \mu_l} + \frac{k_z k_{rv}(\rho_l - \rho_v) g Z}{\kappa_v \mu_v}$
	$Ra_L = \left\vert \frac{\nabla \cdot (\rho_l h_l q_l)}{\nabla \cdot (K_m \nabla T)} \right\vert + \left\vert \frac{\nabla \cdot (\rho_v h_v q_v)}{\nabla \cdot (K_m \nabla T)} \right\vert$
Reynolds number	$Re = \frac{\rho_f q_f L}{\mu_f}$

[a]Describes how much heat advection is retarded compared to solute advection due to the heat exchange between fluid and rock; applies only to single-phase conditions.
[b]The overbar above the variables means that dimension, concentration, and temperature are nondimensionalized by the maximum dimension, concentration, or temperature, respectively.
[c]An analogous number (C replaces T) can be derived for solute transport and is called the Sherwood number.
[d]Ra_T is the general extension of Ra to two-phase conditions; Ra_L is the local Rayleigh number.

H_2O-KCl [*Anderko and Pitzer*, 1993] or H_2O-$CaCl_2$ [*Bischoff et al.*, 1996], which can shift phase boundaries and enhance the reactivity of the fluid, is limited by the pressure-temperature range of available experimental data.

8.1.3. Role of Dimensionless Numbers

[60] The Boussinesq approximation and the assumption that fluid density, viscosity, and heat capacity vary linearly as functions of temperature or composition allows definition of a set of dimensionless parameters to characterize convection (Table 2). These parameters are the Rayleigh number Ra, which describes the vigor of convection; the Nusselt number Nu, which describes the ratio of the total heat flux to the heat flux transported by conduction alone; the Lewis number Le, which describes the ratio between thermal and chemical diffusivity; the buoyancy ratio Rb, which is a ratio of fluid density contributions from salinity and temperature variations; and the dimensionless porosity ϕ^*, which describes the degree to which advective heat transport is retarded with respect to advective solute transport [e.g., *Nield and Bejan*, 1992].

[61] For realistic fluids with strongly nonlinear fluid properties and two-phase flow, nearly identical dimensionless parameters can describe vastly different convective systems [*Geiger et al.*, 2005]. For instance, when the results of many numerical simulations are parameterized in terms of Ra, Rb, and ϕ^*, no clearly defined parameter spaces exist in which a certain type of convection pattern occurs (Figure 7). These parameters also cannot predict whether phase separation occurs.

[62] A more accurate, physically based parameterization is given by the local Rayleigh number Ra_L [*Jupp and Schultz*, 2000], a ratio that measures the influence of fluid flow on the evolution of the local temperature field, rather than the entire domain. The local Rayleigh number Ra_L (Table 2) describes the accumulation of energy due to advection and diffusion and can readily be extended to two-phase conditions [*Geiger et al.*, 2005]. For $Ra_L < 1$, local thermal disturbances decay by diffusion, and convection does not occur. For $Ra_L > 1$, advection is dominant over diffusion, and convection cells form locally where Ra_L is largest.

8.1.4. Numerical Accuracy

[63] Although the important and sometimes dominant role of fluid properties appears to be a first-order physical effect in a number of geological settings, there is no guarantee that these effects are correctly captured in simulations. The first generation of multiphase geothermal reservoir simulators [e.g., *Stanford Geothermal Program*, 1980] employed numerical techniques that were designed to enhance numerical stability and thereby permit stable solutions to certain steam-liquid water flow problems. Applied mathematicians have long recognized that traditional numerical approaches

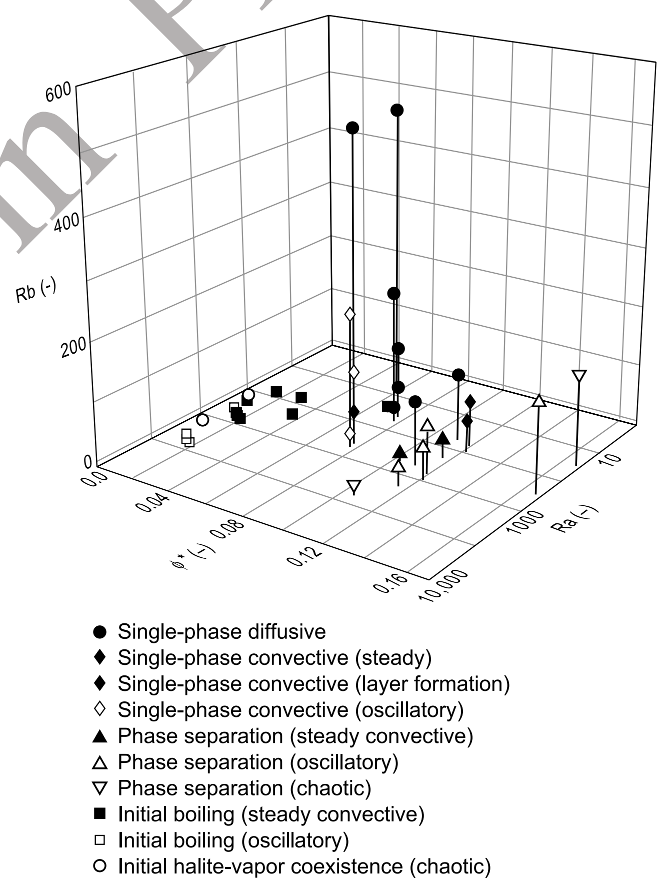

Figure 7. Diagram summarizing numerous simulations of convecting NaCl-H_2O fluids spanning a wide temperature, pressure, and salinity space. The simulated systems were quantified using traditional dimensionless parameters: the Rayleigh number Ra, the buoyancy ratio Rb, and the dimensionless porosity ϕ^*. Fundamentally different flow patterns were associated with nearly identical parameters. After *Geiger et al.* [2005].

involving coarse spatial discretization and lower-order numerical accuracy can artificially damp perturbations [e.g., *Harten*, 1983; *Sweby*, 1984]. However, limited computational resources have necessitated coarse discretization of simulated magmatic hydrothermal systems. Only recently have more accurate high-resolution discretization techniques been adopted [*Oldenburg and Pruess*, 2000; *Geiger et al.*, 2006a] (see also section 7), and it has been shown that they can actually reveal hidden dynamic behavior that is physically "real" (i.e., nonnumerical), such as hydrothermal plume splitting and fluctuations in vent temperature [*Coumou et al.*, 2006].

8.2. Recent Insights Into the Physics of Magmatic Hydrothermal Systems

8.2.1. Nature of the Magma Hydrothermal Interface

[64] In some hydrothermal flow models, the lower boundary is defined so as to approximately coincide with the brittle-ductile transition, which may be viewed as separating ductile and hence very low permeability rocks (and near-lithostatic pressures) below the transition from brittle, higher-permeability rocks (and near-hydrostatic pressures) above the transition [*Fournier*, 1999]. The transition may roughly coincide with a thin, heat-conducting boundary layer (sometimes referred to as "carapace") that has long been inferred to exist between cooling magma (certainly ductile) and the overlying hydrothermal system [e.g., *Lister*, 1974, 1983]. A relatively thin conductive boundary layer seems necessary to maintain the power output (~100–1000 MW) typical of large magmatic hydrothermal systems [*Schultz et al.*, 1992; *Lowell and Germanovich*, 1994]. As the magma in the underlying reservoir cools, the conductive boundary layer will migrate downward, allowing progressively deeper penetration of hydrothermal fluids [*Kelley and Delaney*, 1987; *Fournier*, 1999]. The transition from brittle to ductile conditions is traditionally assumed to occur in a temperature range of 350°C–400°C [*Fournier*, 1999], which coincides with the maximum temperature of 405°C measured in hydrothermal vents along the MOR [*Von Damm et al.*, 2003] and with maximum temperatures measured in deep geothermal wells worldwide [*Fournier*, 1991]. However, experimental studies have shown that under realistic geological strain rates, the temperatures at which different rock types undergo transition from brittle to ductile rheology can range from 260°C for wet quartz to ~700°C for dry orthopyroxene [*Carter and Tsenn*, 1987; *Hirth et al.*, 1998; *Simpson*, 2001].

[65] Recent high-resolution, three-dimensional numerical simulations using temperature-dependent permeability suggest that the brittle-ductile transition temperature in mid-ocean ridge settings is probably not lower than 650°C [*Coumou*, 2008]. These simulations assume that permeability is negligibly low at temperatures above the brittle-ductile transition. If the brittle-ductile transition is set at temperatures less than ~650°C, the hydrothermal convection system cannot effectively mine heat from the underlying magma. A broad hot zone develops at depth, and relatively low-temperature discharge ($\ll$400°C) occurs on and off axis. A brittle-ductile transition defined at 650°C–750°C results in simulated near-axial discharge at ~400°C in a domain with homogeneous and isotropic permeability.

8.2.2. Maximum Hydrothermal Plume Temperatures and "Superconvection"

[66] There are a number of possible explanations for the observation that maximum MOR fluid temperatures appear to be limited to ~400°C, much less than the temperature of basaltic magma. Analytical solutions for conductive heat transport show that temperatures at the surface of a single, instantaneous intrusion will not exceed $0.5T_{\max}$ [e.g., *Lachenbruch et al.*, 1976], or ~600°C in the case of basalt. Further, for typical hydrothermal pressures there is a maximum in silica solubility at 350°C–400°C such that at higher temperatures fluid circulation may be inhibited by deposition of silica [*Fournier and Potter*, 1982]. Finally, it has been suggested that vent temperatures are linked to the temperature of the brittle-ductile transition (section 8.2.1).

[67] Each of these explanations for MOR vent temperatures seems plausible, but none of them are required. Simulations of free convection above an arbitrarily hot base show that the temperatures of upwelling plumes are effectively buffered by the properties of water itself. Pure water will tend to rise from an arbitrarily hot boundary layer at temperatures of 350°C–400°C (Figure 8), the temperature range associated with convection cells operating at maximum energy transport [*Jupp and Schultz*, 2000]. This result has recently been supported by chemical geothermometry of MOR fluids [*Fontaine et al.*, 2009].

[68] This self-organizing effect is not evident in a "Boussinesq" fluid, for which the upflow temperature scales linearly with the basal temperature (Figure 9). The plateauing of upflow temperature at ~400°C for non-Boussinesq water (see again Figure 9) can be understood in terms of a quantity termed "fluxibility" F [*Jupp and Schultz*, 2000], which measures the ability of buoyancy-driven water to transport heat:

$$F = (\rho_0 - \rho)\rho h/\mu, \tag{11}$$

where ρ_0 is the density of cold water. For pure water, this locally defined quantity is weakly pressure-dependent and shows clear peaks in $\partial F/\partial T$ at temperatures ranging from 384°C at 25 MPa to 412°C at 35 MPa. These are thus the temperatures at which pure water will tend to rise at a given pressure. The fluxibility peaks shift to somewhat higher temperatures in a seawater system (Figure 10).

[69] The fluxibility peaks at near-critical temperatures are related to an empirically observed phenomenon named "superconvection" [*Dunn and Hardee*, 1981]. Numerical experiments involving a two-dimensional vertical slab with fixed temperature top and bottom boundaries showed that near-critical heat transfer enhancements result from dramatic increases in the gradients in fluid enthalpy ($h_{\mathrm{bot}} - h_{\mathrm{top}}$, or Δh) and density ($\rho_{\max} - \rho_{\min}$, or $\Delta\rho$) across the slab that occur as its temperature approaches the critical temperature [*Ingebritsen and Hayba*, 1994]. Maximum enhancements in simulated heat transfer rates for a rectangular

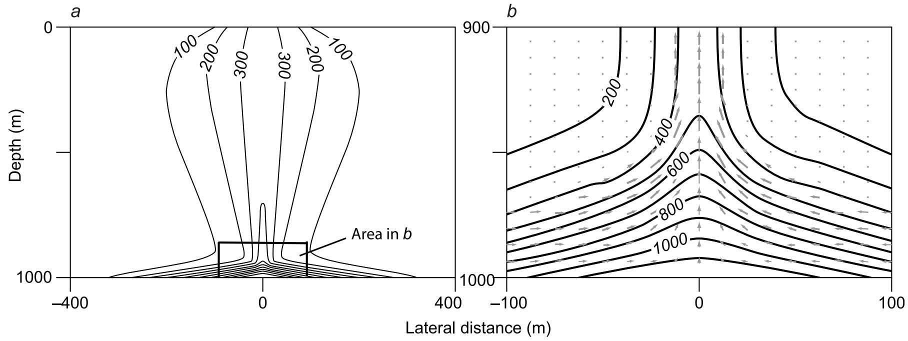

Figure 8. Simulated temperature distribution in a subsea convection cell. The top boundary is maintained at a pressure and temperature representing the seafloor and is permeable; a Gaussian (bell-shaped) temperature profile is imposed along the bottom boundary, with a maximum temperature of 1200°C representing magmatic temperatures. The lateral boundaries for the simulation are at distances of 1700 m, well beyond the range of these Figures. (a) Overall temperature structure of the convection cell, showing the distinction between the basal boundary layer and the plume, and (b) close-up view of the flow regime and temperature structure inside the boundary layer, showing only the bottom 100 m of the simulation domain. Vectors in Figure 8b indicate volumetric fluid flow rates per unit area. Adapted by permission from Macmillan Publishers Ltd [*Jupp and Schultz*, 2000], copyright 2000.

(10 m × 10 m) slab ($Nu > 100$) exceeded the maximum enhancement ($Nu \sim 80$) observed by *Dunn and Hardee* [1981] in their much smaller experimental cylinder. However, other simulations showed that subcritical two-phase processes ("heat pipes") afford equally viable or superior heat transfer mechanisms. This result has been confirmed by more recent simulations [*Coumou et al.*, 2008a] and makes sense on an intuitive level because ΔH (in this case H_v–H_l, the heat of vaporization) and $\Delta\rho$ ($\rho_{\max} - \rho_{\min}$) are both larger under two-phase conditions than they can be at or above the critical point itself.

8.2.3. Self-Organizing Geometries of Convection Cells

[70] Numerical simulations that incorporate more accurate water properties and dense computational grids can also help to explain the three-dimensional geometry of MOR hydrothermal circulation (Figure 11) [*Coumou et al.*, 2008b]. The concept of fluxibility (equation (11)) can be extended to include both upflow (subscript *u*) and downflow (subscript *d*) zones of a hydrothermal convection cell,

$$F = \frac{\rho_u(h_u - h_d)(\rho_d - \rho_u)}{\mu_u(1 + \varepsilon B)}, \tag{12}$$

where ε represents the ratio $A_u/k_u/A_dk_d$; A_u and A_d are the horizontal cross-sectional areas of the upflow and downflow zones, respectively; and B is the ratio of the fluid properties $\mu_d\rho_u/\mu_u\rho_d$. This version of F expresses the ability of a multidimensional, single-phase system to transport energy by buoyancy-driven convection. When evaluated, it indicates that in a uniform permeability medium, optimum energy transport occurs when convection cells self-organize into pipelike upflow zones (~380°C) that are surrounded by narrow zones of focused, hot recharge (100°C–300°C). This implies that recharge in MOR systems is much more focused than depicted in Figure 1b.

[71] Though the system depicted in Figure 11 has uniform intrinsic permeability k, the hydraulic conductivity

$$K = \frac{k\rho_f g}{\mu_f} \tag{13}$$

of both upflow and downflow zones is enhanced relative to surrounding regions by the presence of hot fluids with lower viscosity μ_f. Once established, this geometry seems to be fairly robust. The hydraulic conductivity contrast caused by differences in fluid viscosity has the same stabilizing effect as a contrast in intrinsic permeability. The hot, areally restricted flow geometry dictated by water properties implies short fluid residence times. It has important implications for proposed MOR tracer tests and the formation of massive sulfide ore deposits [*Coumou et al.*, 2008b, 2009].

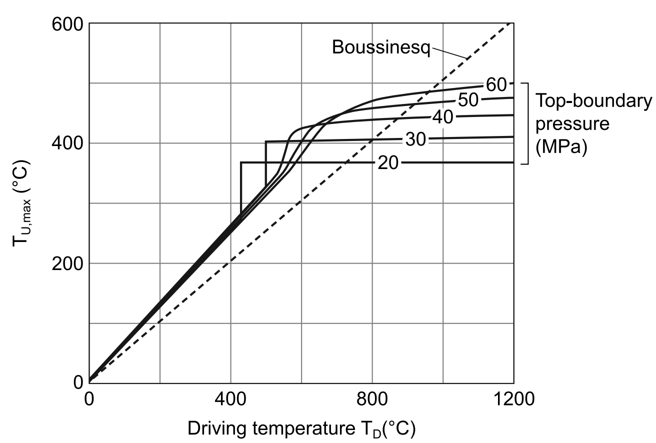

Figure 9. Temperature of upwelling fluid in a porous convection cell as a function of temperature at the base of the model domain, showing results for pure water at various top boundary pressures (solid lines) and a Boussinesq fluid (dashed line). After *Jupp and Schultz* [2004].

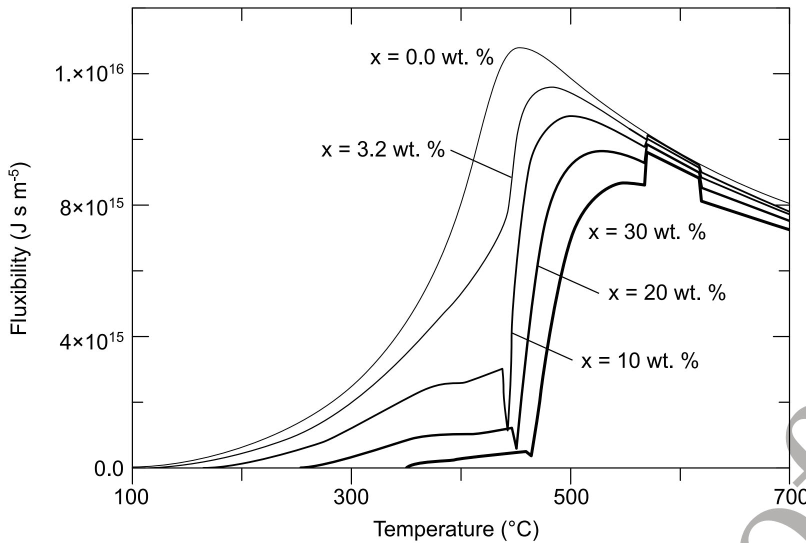

Figure 10. The "fluxibility" F (the ability of a buoyancy-driven fluid to carry energy) as a function of temperature, evaluated at 388 bars and several different salinities. Heat transport in a convecting system is maximized when the fluxibility is highest. Fluxibility peaks shift to progressively higher temperatures with increasing salinity. The discontinuity in fluxibility at ~600°C is due to the coexistence of halite and vapor at this temperature. After *Geiger et al.* [2005].

[72] In addition to the gross geometry of hydrothermal circulation (Figure 11), numerical simulation has elucidated finer-scale behavior. For instance, plume splitting (viscous fingering) can potentially explain spatial and temporal variations in hydrothermal venting, including the sudden extinction of black smokers [*Coumou et al.*, 2006]. Plume splitting occurs in relatively high-permeability systems when a less viscous fluid displaces a more viscous one. It can only be resolved numerically when hydrothermal convection is modeled using a high-resolution grid and a second-order accurate transport scheme and therefore has not been observed in less accurate simulations. This is because plume splitting occurs only when the thermal front (the contact between low- and high-viscosity fluids) is sufficiently sharp. Less accurate numerical approaches do not preserve sharp thermal fronts.

[73] Each of these geometrical insights depends on unrestricted flow geometries. The classic single-pass or U-tube models of hydrothermal convection [e.g., *Lowell and Germanovich*, 1995] assume fixed flow geometries and therefore preclude these self-organizing phenomena.

8.2.4. Evolving Conceptual Models of Hydrothermal Convection

[74] The pioneering studies of *Elder* [1967a, 1967b], *Cathles* [1977], and *Norton and Knight* [1977] manifested the concept that convection in magmatic hydrothermal systems occurs in large, stationary, roughly circular cells (Figure 1) of essentially two-dimensional character. Although it has long been known that heat and salt advect and diffuse at different rates, leading to so-called double-diffusive systems [*Nield*, 1968; *Fournier*, 1990], only since the early 1990s have numerical simulations begun to demonstrate that convection of hot and saline fluids in hydrothermal systems is nonstationary and can lead to periodic

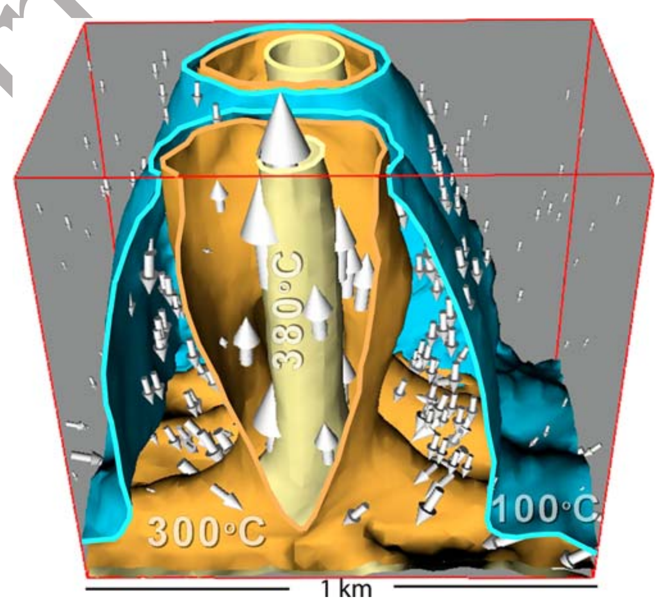

Figure 11. Thermal and fluid flow structure of one of nine plumes along a 4 km segment of MOR axis after a simulation time of 100 years. The plume cross section shows 100°C (blue), 300°C (brown), and 380°C (yellow) isotherms as well as mass fluxes (arrows). Figure 11 represents a 1 km × 1 km × 1 km portion of a 4 km × 3 km × 1 km model domain with a uniform permeability of 5×10^{-14} m^2 and closed lateral boundaries. The upper boundary is maintained at a constant pressure of 25 MPa with a "mixed" thermal boundary condition [*Jupp and Schultz*, 2000]. A spatially variable (Gaussian) heat flux is imposed along the lower boundary, representing estimated MOR conditions of 350 MW per km of ridge length. After *Coumou et al.* [2008b].

oscillations or even chaotic changes in the effluent composition and temperature of hydrothermal fluids [e.g., *Rosenberg and Spera*, 1992; *Schoofs et al.*, 1999; *Schoofs and Spera*, 2003]. Subsequent numerical simulations and Hele-Shaw cell experiments showed that oscillatory, chaotic, and very narrow convection cells can form if the Rayleigh number is sufficiently large [*Cherkaoui and Wilcock*, 1999, 2001]. Other convective instabilities are triggered by the convecting fluid itself: hot, rising plumes can split during hydrothermal convection due to viscous fingering effects [*Coumou et al.*, 2006]. Numerical simulations suggest that the frequently observed variations in black smoker salinities can be caused by plume splitting, by the dynamic effects of phase separation during multiphase NaCl-H_2O convection [*Coumou et al.*, 2009], or by chemical reactions that trigger rapid changes in permeability [*Steefel and Lasaga*, 1994].

[75] Permeability anisotropy and heterogeneity also influence hydrothermal convection. There is widespread evidence that regional stress patterns in the oceanic crust lead to regional fracture patterns, which cause azimuthal anisotropy in permeability in MOR systems with ratios of 100:1 or 1000:1 [*Wilcock and Fisher*, 2004; *Fisher et al.*, 2008], yet the effect of anisotropic permeability on convection is rarely studied (see section 6.10). Most simulations of hydrothermal convection at MOR systems have assumed uniform and isotropic permeability and simple box-shaped geometries. *Wilcock* [1998] and *Fontaine et al.* [2007] showed that horizontal layering can influence the temperature of black smokers; shallow high-permeability layers cause lower effluent temperatures. A vertically extensive impermeable zone, representing a mineralized region between the upflow and downflow zones of a hydrothermal convection cell, can increase effluent temperatures and salinities to values consistent with MOR observations [*Fontaine et al.*, 2007]. High-permeability faults can accelerate hydrothermal convection and allow discharge velocities of up to ~4 m s^{-1} and effluent temperatures of up to ~450°C [*Schardt et al.*, 2006]. Elongated convection cells can form if the along-axis lithospheric thickness increases from segment center to segment end, consistent with heat flow observations at slow spreading MOR systems [*Fontaine et al.*, 2008]. Topography can have a significant impact on hydrothermal convection, concentrating hydrothermal activity on topographic highs [*Harris et al.*, 2004; *Schardt et al.*, 2006].

[76] Because numerical simulations of hydrothermal convection are computationally intensive, most studies have considered two-dimensional systems, consistent with the long-standing view that convection is essentially two-dimensional. *Rabinowicz et al.* [1998, 1999] presented the first three-dimensional analysis of the influence of permeability on convection patterns, based on streamline solutions that employ the Boussinesq approximation. They demonstrated unsteady convection in three-dimensional systems, either as high-temperature (~300°C), high-flow rate (~2.5 m yr^{-1}) "jets" if the permeability is uniformly high or as tall and narrow cells (~270°C) if convection is confined to a narrow, highly permeable slot representing the fissure zone of a MOR. *Coumou et al.* [2008b] performed high-resolution three-dimensional simulations of MOR hydrothermal convection that included accurate thermodynamic properties of H_2O and realistic heat flow rates representing a magma chamber at depth. As discussed in section 8.2.3, they showed that the nonlinear fluid properties lead to self-organization of the convection cells. Hot and narrow upflow zones are directly surrounded by warm and narrow downflow zones, which are also nonstationary given reasonable permeability values ($\geq 5 \times 10^{-14}$ m^2). The flow rates in these convection cells were high, suggesting that residence times are low and that massive sulfide deposits can form at the seafloor within 100–1000 years.

[77] All of this numerical evidence implies that our conceptual model of hydrothermal convection must be revised. Convection does not occur in large, symmetric, stationary and quasi-two-dimensional cells that draw in cold fluid over large distances. At MOR systems may entail very narrow and confined convection cells that permit fast fluid flow.

8.2.5. Controlling Influence of Permeability

[78] The paramount influence of permeability on the behavior of hydrothermal systems was well recognized by the time of *Lowell*'s [1991] review. In fact, much of Lowell's discussion section was devoted to what he termed "permeability control." Significant new insights have emerged since then. Here we will focus mainly on what might be termed "process-limiting" values of permeability.

[79] The limiting permeability value for significant heat advection of ~10^{-16} m^2 that was inferred by *Norton and Knight* [1977] has been confirmed in many subsequent analyses of magmatic hydrothermal systems [e.g., *Manning et al.*, 1993; *Ingebritsen and Hayba*, 1994; *Hayba and Ingebritsen*, 1997]. *Hurwitz et al.* [2003] invoked relatively complex geometries and permeability structures in a modeling study of hydrothermal circulation in subaerial stratovolcanoes. They found that several conditions facilitate the ascent of a hydrothermal plume into a steep volcanic edifice, including a sufficient source of heat and magmatic volatiles at depth, strong buoyancy forces, and a relatively weak gravity-driven flow system. A further prerequisite is that the plume must be connected to a deep heat source through a pathway with a time-averaged effective permeability $\geq 1 \times 10^{-16}$ m^2.

[80] The hottest and most vapor-rich hydrothermal plumes are associated with somewhat higher permeabilities. When magma intrudes and heats host rock, uniformly "high" host rock permeabilities (approximately $\geq 10^{-14}$ m^2) lead to relatively low hydrothermal temperatures because heat advects rapidly away from the magma reservoir. "Low" permeabilities (approximately $\leq 10^{-16}$ m^2) also lead to lower hydrothermal temperatures, in this case because the thermal regime is conduction-dominated. Intermediate permeabilities (~10^{-15} m^2) lead to the hottest hydrothermal systems and the largest two-phase zones. This emergent behavior was first identified in modeling studies by *Hayba and Ingebritsen* [1997]. The key permeability value of 10^{-15} m^2 has been used to explain fluid inclusion homog-

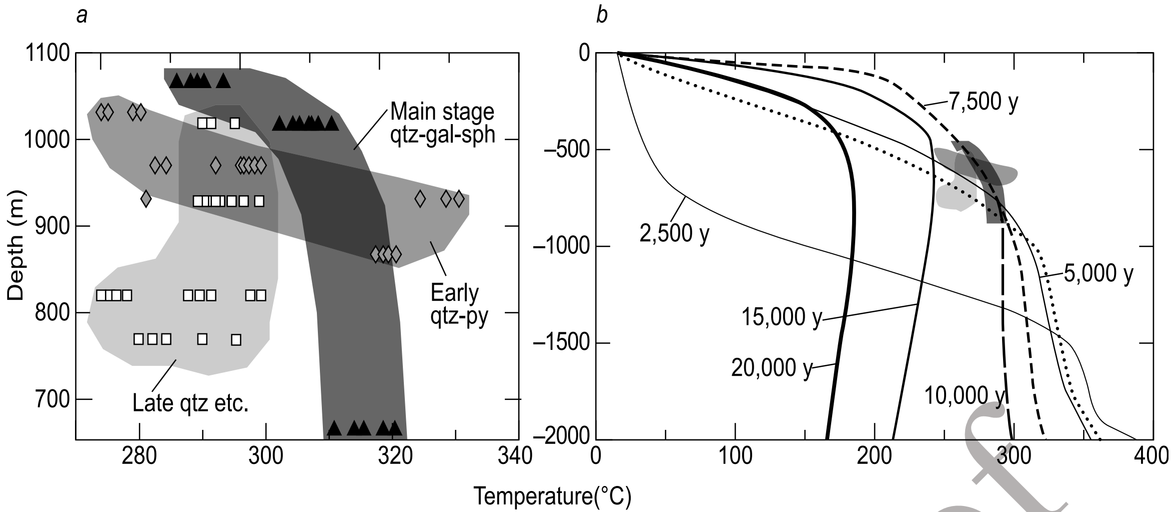

Figure 12. (a) Fluid inclusion homogenization temperatures from three different paragenetic stages in Pb-Zn epithermal veins of the Madan (Bulgaria) ore deposit as a function of present-day topographic elevation and (b) the same temperature data fields plotted relative to temperature-depth curves from a simulation of hydrothermal circulation above a cooling pluton intruded in host rock with a uniform permeability of 10^{-15} m^2 [*Hayba and Ingebritsen*, 1997]. The early quartz-pyrite stage apparently formed in a very strong thermal gradient during early heating of the system (~5000 years simulation time). Main stage quartz-galena-sphalerite deposition evidently formed during an extended period of boiling to depths of ~1 km (~7500–10,000 years simulation time). The zone of economic mineralization may be related to the pronounced curvature of the boiling-point-with-depth curve (Figure 3) beginning at ~1 km depth. After *Kostova et al.* [2004] and *Driesner and Geiger* [2007].

enization temperatures in epithermal Pb-Zn veins [*Kostova et al.*, 2004] (Figure 12).

[81] Permeability is also the major determinant of the magnitude and extent of thermal pressurization resulting from magma intrusion [*Delaney*, 1982]. For low values of host rock permeability, in situ changes in fluid density and magmatic volatile release can be the dominant postintrusion driving forces for fluid flow for times of up to ~10^4 years [*Sammel et al.*, 1988]. This "expulsive" fluid flux can temporarily dominate the convective fluid flux for permeabilities as large as 10^{-16} m^2 [*Hanson*, 1992]. *Reid* [2004] performed a thorough hydrothermal modeling study of the hydraulic controls on thermal pressurization, motivated by the deep-seated volcanic edifice collapses that sometimes occur in the absence of magmatic eruption. Far-field pressurization can occur only for a certain range of host rock hydraulic properties, but this range of hydraulic properties appears to be consistent with observations from geothermal reservoirs or hydrothermal systems (Figure 13). Given parameters typical of Earth materials, fluid pressure effects travel much faster than thermal effects, and the rapid movement of the fluid pressure front effectively decouples the pressure and temperature fields over the time scale of interest.

[82] In addition to absolute values of permeability, permeability contrasts exert significant control on the behavior of hydrothermal systems. Underpressured (subhydrostatic) vapor-dominated zones are often surrounded by low-permeability barriers that shield the relatively permeable vapor-dominated zones from surrounding, normally pressured flow systems [*Straus and Schubert*, 1981; *Ingebritsen and Sorey*, 1988]. Simulations of periodic geysering show that permeability contrasts on the order of 10^3 between geyser conduit and surrounding matrix are required for geyser-like behavior, whereas smaller contrasts lead to steady upflow [*Ingebritsen and Rojstaczer*, 1996]. When flow in fractures is simulated, the fracture (k_f)-matrix (k_m) permeability contrast is a determinant of whether the fractures dominate flow, which is usually the case for $k_f/k_m > 10^2$–10^4, with the actual value depending on fracture spacing and aperture [*Matthäi and Belayneh*, 2004].

8.2.6. Cooling Plutons: Time Scales, Geothermal Resources, and Ore Deposits

[83] The fundamental role of fluid circulation in cooling of plutons was demonstrated by the earliest numerical modeling studies. Fluid circulation can remove heat much more efficiently than conduction alone and thereby can accelerate cooling. Active fluid circulation associated with cooling plutons can generate very high, geologically transient heat flows, exploitable geothermal fields, and hydrothermal ore deposits. As pointed out by *Cathles* [1977], cooling by conduction alone will not create high-enthalpy geothermal resources and will not necessarily cause substantial near-surface heat flow anomalies.

[84] More recent modeling work has explored the dynamic interplay between pluton cooling, hydrothermal plume development, and boiling and phase separation. Figure 12b depicts the evolution of the temperature field above a 2 × 1 km planar pluton emplaced at 2 km depth. At early times there is a steep temperature gradient directly above the pluton. Gradually, the steepest part of the thermal gradient migrates toward shallow levels. At 7500 years, the

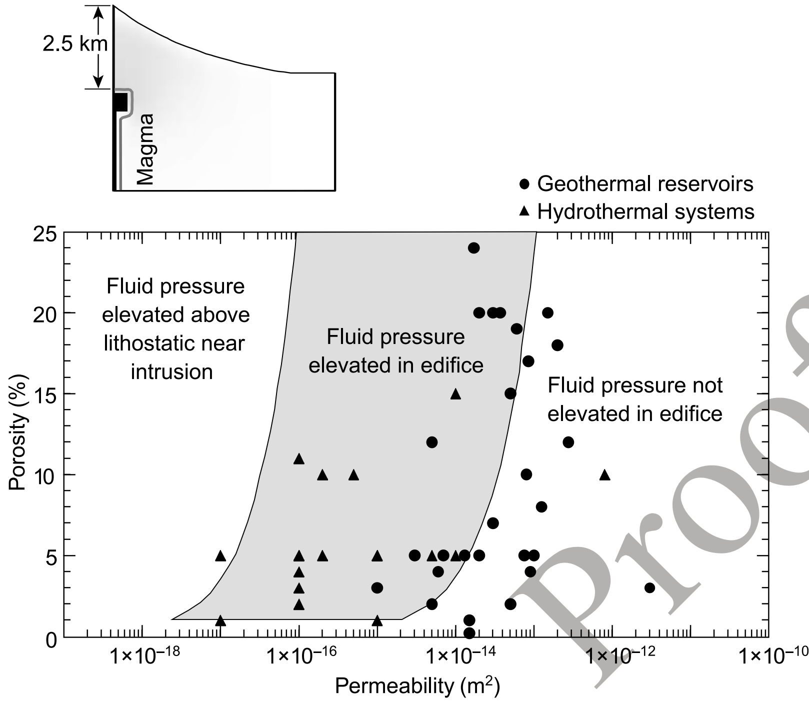

Figure 13. Fluid pressure response to intrusion of 900°C magma at 2.5 km depth below a stratovolcano as a function of host rock permeability and porosity. Intermediate values of permeability lead to significantly elevated fluid pressures within the edifice, lower values lead to fluid pressures in excess of lithostatic near the top of the intrusion, and higher values lead to minimal (<5%) disturbance of preintrusion pressures. The variably shaded regions bounded by curves were determined by numerical modeling. The solid symbols represent permeability/porosity data points determined from geothermal reservoirs [*Bjornsson and Bodvarsson*, 1990] or inferred from hydrothermal systems [*Manning and Ingebritsen*, 1999]. These data show that the permeability/porosity conditions required for thermal pressurization are not unusual. After *Reid* [2004].

steepest gradient occurs near the surface, and temperatures follow the boiling point–depth curve to depths of more than 1 km. The system begins to wane by 15,000 years, at which time temperatures in the hydrothermal plume actually decrease with depth. The result depicted in Figure 12 is for a host rock permeability of 10^{-15} m^2, which produces the hottest, most steam-rich systems (see section 8.2.5). An analogous conduction-dominated system (10^{-17} m^2) would achieve maximum temperatures at a time of ~30,000 years and entail no boiling. An analogous system with 10 times higher permeability would persist for only ~5000 years; have a maximum temperature of ~250°C; and entail very limited, near-surface boiling.

[85] Though cooling rates depend strongly on pluton and host rock permeability, it is evident that small, shallow plutons cool over a time scale on the order of ~10^4 years. This geologically short lifetime tends to focus exploration for shallow, high-enthalpy geothermal resources on areas of very recent magmatic activity.

[86] For the "optimal" permeability of order 10^{-15} m^2 (Figure 12), temperatures at the base of the hydrothermal plume during its hottest phases (~2500–7500 years) are close to the temperatures predicted to be most energy efficient by the "fluxibility" argument of *Jupp and Schultz* [2000] (section 8.2.3). Boiling persists for ~10,000 years over depth ranges of up to 1.5 km. The development of such vertically extensive boiling zones is yet another consequence of fluid rather than rock properties. In the pressure-enthalpy diagram of Figure 6, the pressure axis has been inverted to illustrate the paths that ascending hot water might take. Because of the large heats of vaporization (represented by the width of the vapor plus liquid coexistence region), an ascending hydrothermal fluid that enters the vapor plus liquid field is unlikely to leave it as it continues to rise. Hence, vertically extensive two-phase/boiling zones can develop above the first level of boiling [*Hayba and Ingebritsen*, 1997]. Where this level is reached depends largely on the heat content of the ascending fluid and the system-scale permeability [*Driesner and Geiger*, 2007].

[87] The occurrence, persistence, and spatial distribution of boiling are significant to economic geologists because of their implications for certain types of ore deposits [*Williams-Jones and Heinrich*, 2005]. The main stage quartz-galena-sphalerite deposition depicted in Figure 12a

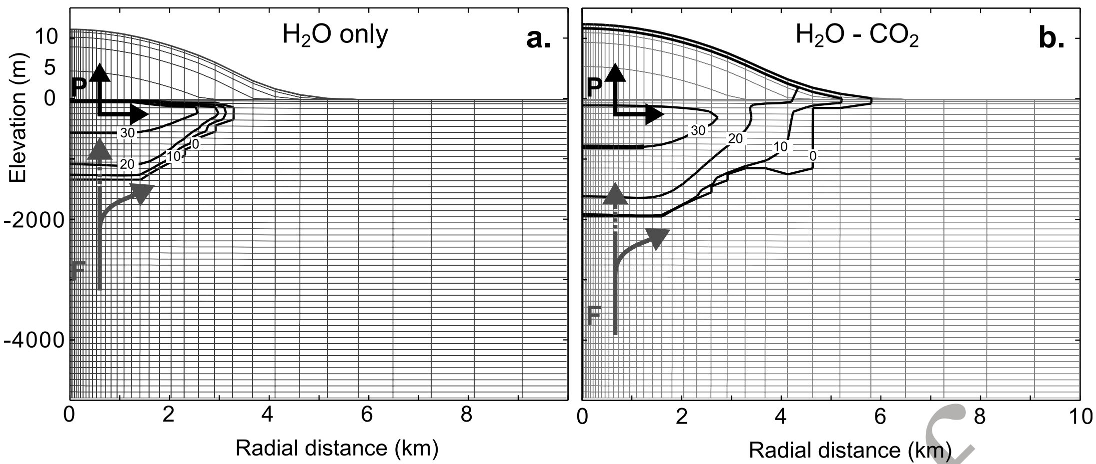

Figure 14. Cross section of a simulated caldera at a time of 20,000 years for host rock permeability of 10^{-15} m^2, showing contours of vapor saturation (%) resulting from basal injection of (a) single-component fluid (21 kt/d H_2O) and (b) multicomponent fluid (20 kt/d H_2O and 1 kt/d CO_2) at 350°C. Vertical deformation ranges up to ~12 m at the center of the model (a radial distance of 0); note the break in vertical scale at 0 m elevation. The multicomponent simulation has a much larger region of multiphase flow. Vapor formation reduces relative permeability, impeding vertical aqueous fluid flow (F), increasing pressure gradients (P), and deflecting warm fluids radially outward. The magnitude of vertical deformation and the radial extent of deformation are slightly larger in the multicomponent system (by 10% and 15%, respectively). From *Hutnak et al.* [2009].

is one example of boiling-related mineralization. Low-sulfidation epithermal gold is another example. In epithermal systems, gold may be transported as bisulfide complexes in the liquid phase and precipitate where the liquid starts to boil because the boiling partitions H_2S into the vapor phase and leads to decomplexation [e.g., *Hedenquist and Henley*, 1985].

8.2.7. Hydrothermally Driven Deformation

[88] Numerical modeling studies of the coupling between high-temperature, multiphase fluid flow and deformation were pioneered by *Bonafede* [1991] but are still in their infancy. The few modeling studies performed to date are intriguing because they suggest that the rates and patterns of ground surface deformation (GSD) measured in some large calderas could be induced by poroelastic transients in the hydrothermal system [*Todesco et al.*, 2004; *Hurwitz et al.*, 2007; *Hutnak et al.*, 2009; *Todesco*, 2009]. Traditionally, interpretations of GSD invoke volume change of a discrete source (often assumed to be a magma chamber) with a specified geometry in a homogeneous, isotropic, and elastic [e.g., *Mogi*, 1958; *Fialko et al.*, 2001] or viscoelastic [*Newman et al.*, 2001] half-space. The calculated depth, shape, and volume change of the source in these models are derived from inversion of the measured GSD. However, these traditional models cannot readily explain episodes of subsidence or the spatial and temporal variability revealed by modern geodetic methods [e.g., *Dzurisin*, 2007]. *Todesco et al.* [2004] simulated multiphase, multicomponent (H_2O-CO_2) fluid flow to explain recent deformation in the Campi Flegrei (Italy) caldera. *Hurwitz et al.* [2007] simulated a single-component (H_2O) fluid to assess the range of conditions under which poroelastically induced deformation might occur. Most recently, *Hutnak et al.* [2009] explored the effects of a multiphase (liquid-gas), multicomponent (H_2O-CO_2) hydrothermal fluid and found that the addition of noncondensible gas enhanced deformation relative to pure water systems (Figure 14). Such studies typically invoke a "one-way" coupling between fluid flow and heat transport and poroelastic deformation. That is, the strains determined by equations analogous to equation (7) are not fed back into equations such as equations (4) and (5) so that the stress dependence of permeability and other material properties is not considered.

9. SUGGESTIONS FOR FUTURE WORK

[89] In the past 2 decades, and particularly the past few years, significant advances have been made in development and application of numerical models to simulate magma hydrothermal systems. Faster computers, sophisticated software, and improved observational and experimental data enable more rigorous modeling studies that can reduce many of the assumptions discussed in this review. Continued progress will require the following.

9.1. Accurate Fluid Equation-of-State Formulations

[90] In light of the immense influence of EOS descriptions on system behavior (see sections 8.2.2–8.2.4), additional work is needed to develop and incorporate usable EOS formulations for multicomponent systems, particularly the complete H_2O-NaCl-CO_2 system. The availability of documented, open source multiphase simulators (Table 1) has eliminated the need for ad hoc approximations of multiphase behavior, and the use of best available EOS formulations should become standard in this era of widespread access to adequate computational resources.

9.2. More Realistic Treatment of Material Heterogeneity in Space and Time

[91] There is clear field and laboratory evidence for extreme heterogeneity and dynamic variation in permeability in hydrothermal systems. Attempts to represent this variability in numerical models are limited. More sophisticated representations of heterogeneity at the fault zone [*Lopez and Smith*, 1995] or system-wide [*Matthäi et al.*, 2004] scales generally do not involve high-temperature, multiphase, multicomponent flow. Attempts to represent dynamic variations in permeability in a hydrothermal context have been ad hoc rather than physically rigorous [e.g., *Rojstaczer et al.*, 2008]. Realistic representations of heterogeneity could also benefit from the calculation of effective permeabilities and multiphase properties (e.g., relative permeabilities). So-called "upscaling" is a standard procedure in reservoir engineering, helping to capture the essential heterogeneity of a geological model while reducing the number of grid points in the numerical model, ultimately reducing computing time [e.g., *Christie*, 2001].

9.3. Improved Description of Relative Permeability and Capillary Pressure Effects

[92] We have noted that the choice of relative permeability functions (section 6.5 and Figure 4) can have a large influence on the results of numerical simulations, particularly if the simulations involve highly transient behavior [e.g., *Ingebritsen and Rojstaczer*, 1996]. The role of capillary pressure effects may be equally important but is generally neglected (section 6.6). It requires a leap of faith to extrapolate relative permeability and capillary pressure relations determined from lab-scale experiments to REV-scale behavior in numerical models. We suggest renewed efforts to estimate field-scale relative permeability and capillary pressure behavior from observations in producing geothermal fields [e.g., *Sorey et al.*, 1980]. Such efforts should include mapping of subsurface fluid saturations in active hydrothermal systems using state-of-the-art geophysical imaging techniques [*Finizola et al.*, 2006; *Revil et al.*, 2008]. Pore network modeling techniques, which are routinely used to obtain consistent relative permeability and capillary pressure curves for oil-gas-water systems [e.g., *Blunt*, 2001], could complement such studies. In addition to potentially elucidating magmatic hydrothermal phenomena, research in this area is highly pertinent to practical geothermal reservoir engineering issues.

9.4. Focus on "Process-Based" Simulations Conditioned on Field Data

[93] Laboratory experimentation relevant to hydrothermal systems peaked in the 1980s and 1990s and has decreased substantially in the past decade, as has deep drilling in magmatic provinces. Given the current level of data availability, "system-based" numerical modeling studies are likely to yield nonunique results and may be of limited predictive ability, with the important exception of focused reservoir engineering applications constrained by borehole data from producing geothermal fields. In the broader context of magmatic hydrothermal systems, most system-specific models will remain overparameterized (underconstrained). Research studies that attempt to characterize specific systems should include sensitivity analyses in order to explore the full range of conditions that can explain observed phenomena. Formal sensitivity analysis can help identify the appropriate degree of generality for system-specific modeling and will typically reveal, for instance, that only one to two values of system permeability can be legitimately constrained [e.g., *Deming*, 1993]. More geometrically complex and heterogeneous models can be useful for heuristic purposes but are generally nonunique. Given the paucity of data from most individual systems, it can be useful to aggregate data from several systems in order to explore and constrain process behavior [e.g., *Lewis and Lowell*, 2009b].

9.5. Continued Attention to Numerical Accuracy

[94] Recent simulations with high-resolution discretization techniques [*Oldenburg and Pruess*, 2000; *Geiger et al.*, 2006a] have revealed hidden dynamic behavior that is "real" (i.e., nonnumerical), such as hydrothermal plume splitting and fluctuations in vent temperature [*Coumou et al.*, 2006]. Fine spatial discretization and second-order accurate transport descriptions seem indicated for problems involving highly transient and/or heterogeneous systems.

9.6. Continued Improvement of Solvers and Use of Parallel Processing Methods

[95] Multiphase simulations with refined spatial discretization require substantial computational power, particularly when phase changes are widespread and frequent or when reactive transport is considered. Simulations of even simple geometries can still require days of computational time. Thus, methods to reduce run time are required. Parallelization is attractive because fast, multiprocessor clusters have become more available. Such capability was recently added to the TOUGH2 [*Wu et al.*, 2002; *Zhang et al.*, 2008] and CSMP++ codes [*Coumou et al.*, 2008c; *Geiger et al.*, 2009]. Additional significant gains can be realized by improving solver efficiency. Because the computing time of algebraic multigrid solvers scales linearly with the number of unknowns [*Stüben*, 2001] and because the system $\mathbf{A}x = b$ is computed hundreds to thousands of times during a typical simulations, these solvers are key to simulating multiphase and multicomponent fluid flow in more complex two- and three-dimensional geologic structures. Another advantage of algebraic multigrid solvers is that they do not need any information on the geometry of the domain, which is useful in light of the structural complexity of magmatic hydrothermal systems. Parallelization and algebraic multigrid approaches can be linked to make best use of both methods [*Coumou et al.*, 2008c; *Geiger et al.*, 2009].

9.7. Benchmarking and Intercode Comparisons

[96] It is not possible to fully test multiphase, multicomponent simulators against analytical solutions or empirical results. Analytical solutions are limited, and experimental data have to be developed for each specific application [e.g.,

Woods, 1999; *Bergins et al.*, 2005; *Benard et al.*, 2005]. Thus, systematic intercomparison of independently developed simulators can be an important way of building confidence in their performance. An ensemble of state-of-the-art codes should be exercised on a common problem set. Such intercode comparison projects have been conducted in many other subsurface modeling areas and have led to significant improvements. Previous efforts include the U.S. Department of Energy–Stanford code comparison project [*Stanford Geothermal Program*, 1980], which exercised the first generation of multiphase geothermal simulators; the Hydrologic Code Intercomparison (HYDROCOIN) [*Larsson*, 1992], Development of Coupled Models and Their Validation Against Experiments (DECOVALEX, http://www.decovalex.com), and Benchmark Tests and Guidance on Coupled Processes for Performance Assessment of Nuclear Waste Repositories (BENCHPAR) [*Stephansson and Min*, 2004] projects, which focused on modeling coupled flow and transport processes; and, most recently, comparisons of subsurface CO_2 storage simulators [*Pruess et al.*, 2004; *Ebigbo et al.*, 2007].

10. CONCLUDING STATEMENT

[97] We expect that numerical modeling exercises in coming years will continue to increase our conceptual understanding of basic processes in magma hydrothermal systems and, in turn, provide guidance for expensive exploration efforts. Fundamental questions remain to be addressed by the next generation of numerical models: For instance, how is 25% of the Earth's heat crust transmitted from cooling magma to overlying hydrothermal systems at the MOR? What is the expected near-surface hydrogeochemical expression of magmatic unrest at several kilometers depth? How does hydrothermal circulation transport microbes, their food, and their respiration products within the subsurface biosphere? What is the nature of hydrothermal circulation on extraterrestrial bodies such as Mars? Credible efforts to attack such problems require continued improvements in our ability to simulate coupled hydrothermal flow and deformation and reactive transport in multiphase systems and, particularly in the case of extraterrestrial systems, formal consideration of the third water phase, ice.

NOTATION

- c specific heat capacity (usually isobaric heat capacity) ($E\ M^{-1}\ T^{-1}$).
- c_b bulk compressibility ($L\ t^2\ M^{-1}$).
- c_s bulk compressibility of nonporous solids ($L\ t^2\ M^{-1}$).
- C aqueous concentration ($M\ L^{-3}$).
- D hydrodynamic dispersion ($L^2\ t^{-1}$).
- F fluxibility ($M\ L^{-3}\ t^{-1}$).
- g gravitational acceleration ($L\ t^{-2}$).
- G shear modulus, $E/2(1-\nu)$ ($M\ L^{-1}\ t^{-2}$).
- h specific enthalpy ($E\ M^{-1}$).
- H enthalpy (E).
- k intrinsic permeability (L^2).
- k_r relative permeability (dimensionless).
- K hydraulic conductivity ($L\ t^{-1}$).
- K_m medium thermal conductivity ($E\ t^{-1}\ L^{-1}\ T^{-1}$).
- L characteristic length or distance (L).
- P pressure ($M\ L^{-1}\ t^{-2}$).
- q volumetric flow rate per unit area (volume flux, specific discharge, or Darcy velocity) ($L\ t^{-1}$).
- q_h conductive heat flux per unit area ($E\ L^{-2}\ t^{-1}$).
- R general source/sink term for mass (with subscript m), heat (subscript h), or chemical reactions.
- S volumetric saturation ($L^3\ L^{-3}$, dimensionless).
- t time (t).
- T temperature (T).
- $\mathbf{u}$ displacement vector (L).
- v average linear velocity (seepage velocity) ($L\ t^{-1}$).
- X mass fraction H_2O, NaCl, or CO_2 in an H_2O-NaCl-CO_2 mixture (dimensionless).
- z elevation above a datum, vertical Cartesian coordinate, or depth (L).
- α effective stress coefficient, 1 (c_s/c_b) (dimensionless).
- α_T porous medium linear thermal expansivity (T^{-1}).
- γ chemical expansivity (dimensionless).
- ϕ porosity ($L^3\ L^{-3}$, dimensionless).
- μ dynamic viscosity ($M\ L^{-1}\ t^{-1}$).
- ν Poisson's ratio (dimensionless).
- ρ density ($M\ L^{-3}$).
- $(\hat{\ })$ increase or decrease in a quantity.
- $(\bar{\ })$ a nondimensionalized quantity.

Subscripts

Unless otherwise locally redefined, subscripts have the following meanings:

- f fluid mixture in place (either a single phase or a two-phase mixture).
- l liquid.
- m porous medium.
- r rock.
- v vapor (steam).
- 0 an initial state.

[98] **ACKNOWLEDGMENTS.** We thank Barbara Dutrow, Hedeff Essaid, Andy Fisher, Mark Reid, Philipp Weis, an anonymous reviewer, and Editor Michael Manga for their careful reviews of earlier versions of this manuscript, which greatly improved the final product. S. Geiger thanks the Edinburgh Collaborative of Subsurface Science and Engineering, a joint research institute of the Edinburgh Research Partnership in Engineering and Mathematics, for financial support. This study was also partly supported by the U. S. Geological Survey Volcano Hazards Program.

[99] The Editor responsible for this paper was Michael Manga. He thanks Barbara Dutrow, Andrew Fisher, and an additional anonymous technical reviewer.

REFERENCES

Aavatsmark, I. I. (2002), An introduction to multipoint flux approximations for quadrilateral grids, *Computat. Geosci.*, *6*, 405–432, doi:10.1023/A:1021291114475.

Alt-Epping, P., and L. Smith (2001), Computing geochemical mass transfer and water/rock ratios in submarine hydrothermal systems: Implications for estimating the vigour of convection, *Geofluids*, *1*, 163–181, doi:10.1046/j.1468-8123.2001.00014.x.

Anderko, A., and K. S. Pitzer (1993), Phase equilibria and volumetric properties of the systems KCl-H_2O and $NaCl$-KCl-H_2O above 573 K: Equation of state representation, *Geochim. Cosmochim. Acta*, *57*, 4885–4897.

Anovitz, L. M., T. C. Labotka, J. G. Blencoe, and J. Horita (2004), Experimental determination of the activity-composition relations and phase equilibria of H_2O-CO_2-$NaCl$ fluids at 500°C, 500 bars, *Geochim. Cosmochim. Acta*, *68*, 3557–3567.

Archer, D. G. (1992), Thermodynamic properties of the $NaCl$ + H_2O system. II. Thermodynamic properties of $NaCl$ (aq), $NaCl.2H_2O$ (cr), and phase equilibria, *J. Phys. Chem. Ref. Data*, *21*, 793–829.

Bai, W., W. Xu, and R. P. Lowell (2003), The dynamics of submarine geothermal heat pipes, *Geophys. Res. Lett.*, *30*(3), 1108, doi:10.1029/2002GL016176.

Baker, E. T., G. J. Massoth, and R. A. Feely (1987), Cataclysmic hydrothermal venting on the Juan de Fuca Ridge, *Nature*, *329*, 149–151, doi:10.1038/329149a0.

Baker, E. T., J. W. Lavelle, R. A. Feely, G. J. Massoth, S. L. Walker, and J. E. Lupton (1989), Episodic venting of hydrothermal fluids from the Juan de Fuca Ridge, *J. Geophys. Res.*, *94*(9), 9237–9250.

Baliga, B. R., and S. V. Patankar (1980), A new finite-element formulation for convection-diffusion problems, *Numer. Heat Transfer*, *3*, 393–409, doi:10.1080/01495728008961767.

Baross, J. A., and J. W. Deming (1983), Growth of 'black smoker' bacteria at temperatures of at least 250°C, *Nature*, *303*, 423–426, doi:10.1038/303423a0.

Battistelli, A., C. Calore, and K. Pruess (1997), The simulator TOUGH2/EWASG for modeling geothermal reservoirs with brines and non-condensible gas, *Geothermics*, *26*, 437–464, doi:10.1016/S0375-6505(97)00007-2.

Bear, J. (1972), *Dynamics of Fluids in Porous Media*, Elsevier, New York.

Bear, J. (1979), *Hydraulics of Groundwater*, McGraw-Hill, New York.

Benard, J., R. Eymard, X. Nicolas, and C. Chavant (2005), Boiling in porous media: Model and simulations, *Transp. Porous Media*, *60*, 1–31, doi:10.1007/s11242-004-2594-9.

Bergins, C., S. Crone, and K. Strauss (2005), Multiphase flow in porous media with phase change. Part II: Analytical solutions and experimental verification for constant pressure steam injection, *Transp. Porous Media*, *60*, 275–300, doi:10.1007/s11242-004-5740-5.

Berkowitz, B. (2002), Characterizing flow and transport in fractured geological media: A review, *Adv. Water Resour.*, *25*, 861–884, doi:10.1016/S0309-1708(02)00042-8.

Bethke, C. M. (1994), The question of uniqueness in geochemical modeling, *Geochim. Cosmochim. Acta*, *56*, 4315–4320.

Bickle, M. J., and D. McKenzie (1987), The transport of heat and matter by fluids during metamorphism, *Contrib. Mineral. Petrol.*, *95*, 384–392, doi:10.1007/BF00371852.

Birch, M. U. (1989), Groundwater flow systems and thermal regimes near cooling igneous plutons: Influence of surface topography, M.S. thesis, Utah State Univ., Logan.

Bischoff, J. L., and R. J. Rosenbauer (1988), Liquid-vapor relations in the critical region of the system $NaCl$-H_2O from 380 to 415°C: A refined determination of the critical point and two-phase boundary of seawater, *Geochim. Cosmochim. Acta*, *52*(2), 2121–2126.

Bischoff, J. L., and R. J. Rosenbauer (1996), The alteration of rhyolite in CO_2 charged water at 200 and 350°C: The unreactivity of CO_2 at higher temperature, *Geochim. Cosmochim. Acta*, *60*, 3859–3867.

Bischoff, J. L., R. J. Rosenbauer, and R. O. Fournier (1996), The generation of HCl in the system $CaCl_2$-H_2O: Vapor-liquid relations from 380–500°C, *Geochim. Cosmochim. Acta*, *60*, 7–16, doi:10.1016/0016-7037(95)00365-7.

Bjornsson, G., and G. Bodvarsson (1990), A survey of geothermal reservoir properties, *Geothermics*, *19*, 17–27, doi:10.1016/0375-6505(90)90063-H.

Blencoe, J. G. (2004), The CO_2-H_2O system, IV. Empirical, isothermal equations for representing vapor-liquid equilibria at 110–350°C, $P < 150$ MPa, *Am. Mineral.*, *89*, 1447–1455.

Blunt, M. J. (2001), Flow in porous media—Pore-network models and multiphase flow, *Curr. Opin. Colloid Interface Sci.*, *6*, 197–207, doi:10.1016/S1359-0294(01)00084-X.

Bodvarsson, G. (1982), Terrestrial energy currents and transfer in Iceland, in *Continental and Oceanic Rifts*, *Geodyn. Ser.*, vol. 8, edited by G. Palmason, pp. 271–282, AGU, Washington, D. C.

Bonafede, M. (1991), Hot fluid migration: An efficient source of ground deformation: Application to the 1982–1985 crisis at Campi Flegrei-Italy, *J. Volcanol. Geotherm. Res.*, *48*, 187–198, doi:10.1016/0377-0273(91)90042-X.

Bower, K. M., and G. Zyvoloski (1997), A numerical model for thermo-hydro-mechanical coupling in fractured rock, *Int. J. Rock Mech. Min. Sci.*, *34*, 1,201–1,211.

Bowers, T. S., and H. C. Helgeson (1983), Calculation of the thermodynamic and geochemical consequences of nonideal mixing in the system H_2O-CO_2-$NaCl$ on phase relations in geologic systems: Equation of state for H_2O-CO_2-$NaCl$ fluids at high pressures and temperatures, *Geochim. Cosmochim. Acta*, *47*, 1247–1275.

Brace, W. F. (1980), Permeability of crystalline and argillaceous rocks, *Int. J. Mech. Min. Sci. Geomech. Abstr.*, *17*, 241–251, doi:10.1016/0148-9062(80)90807-4.

Brace, W. F. (1984), Permeability of crystalline rocks: New in situ measurements, *J. Geophys. Res.*, *89*, 4327–4330.

Brown, P. E., and W. M. Lamb (1989), P-V-T properties of fluids in the system $H_2O + CO_2 + NaCl$: New graphical presentations and implications for fluid inclusion studies, *Geochim. Cosmochim. Acta*, *53*, 1209–1221.

Carter, N. L., and M. C. Tsenn (1987), Flow properties of continental lithosphere, *Tectonophysics*, *136*, 27–63, doi:10.1016/0040-1951(87)90333-7.

Cathles, L. M. (1977), An analysis of the cooling of intrusives by ground-water convection which includes boiling, *Econ. Geol.*, *72*, 804–826, doi:10.2113/gsecongeo.72.5.804.

Cherkaoui, A. S. M., and W. S. D. Wilcock (1999), Characteristics of high Rayleigh number two-dimensional convection in an open-top porous layer heated from below, *J. Fluid Mech.*, *394*, 241–260, doi:10.1017/S0022112099005716.

Cherkaoui, A. S. M., and W. S. D. Wilcock (2001), Laboratory studies of high Rayleigh number circulation in an open-top Hele-Shaw cell: An analog to mid-ocean ridge hydrothermal systems, *J. Geophys. Res.*, *106*, 10,983–11,000, doi:10.1029/2000JB900470.

Chiodini, G., A. Baldini, F. Barberi, M. L. Carapezza, C. Cardellini, F. Frondini, D. Granieri, and M. Ranaldi (2007), Carbon dioxide degassing at Latera caldera (Italy): Evidence of geothermal reservoir and evaluation of its potential energy, *J. Geophys. Res.*, *112*, B12204, doi:10.1029/2006JB004896.

Christie, M. A. (2001), Flow in porous media—Scale up of multiphase flow, *Curr. Opin. Colloid Interface Sci.*, *6*, 236–241, doi:10.1016/S1359-0294(01)00087-5.

Clauser, C. (1988), Opacity—The concept of radiative thermal conductivity, in *Handbook of Terrestrial Heat-Flow Density Determinations*, edited by R. Haenel, L. Rybach, and L. Stegena, pp. 143–165, Kluwer Acad., Dordrecht, Netherlands.

Cline, J. S., R. J. Bodnar, and J. D. Rimstidt (1992), Numerical simulation of fluid flow and silica transport and deposition in boiling hydrothermal solutions: Application to epithermal gold deposits, *J. Geophys. Res.*, *97*, 9085–9103.

Corey, A. T. (1957), Measurement of water and air permeabilities in unsaturated soil, *Soil Sci. Soc. Am. Proc.*, *21*, 7–10.

Coumou, D. (2008), Numerical simulation of fluid flow in mid-ocean ridge hydrothermal systems, Ph.D. thesis, ETH Zurich, Zurich, Switzerland.

Coumou, D., T. Driesner, S. Geiger, C. A. Heinrich, and S. Matthäi (2006), The dynamics of mid-ocean ridge hydrothermal systems: Splitting plumes and fluctuating vent temperatures, *Earth Planet. Sci. Lett.*, *245*, 218–235, doi:10.1016/j.epsl.2006.02.044.

Coumou, D., T. Driesner, and C. A. Heinrich (2008a), Heat transport at boiling, near-critical conditions, *Geofluids*, *8*, 208–215, doi:10.1111/j.1468-8123.2008.00218.x.

Coumou, D., T. Driesner, and C. A. Heinrich (2008b), The structure and dynamics of mid-ocean ridge hydrothermal systems, *Science*, *321*, 1825–1828.

Coumou, D., S. Matthäi, S. Geiger, and T. Driesner (2008c), A parallel FE-FV scheme to solve fluid flow in complex geologic media, *Comput. Geosci.*, *34*, 1697–1707.

Coumou, D., P. Weiss, T. Driesner, and C. A. Heinrich (2009), Phase separation, brine formation, and salinity variation at Black Smoker hydrothermal systems, *J. Geophys. Res.*, *114*, B03212, doi:10.1029/2008JB005764.

Cox, S. F., M. A. Knackstedt, and J. Braun (2001), Principles of structural control on permeability and fluid flow in hydrothermal systems, *Rev. Econ. Geol.*, *14*, 1–24.

Croucher, A. E., and M. J. O'Sullivan (2008), Application of the computer code TOUGH2 to the simulation of supercritical conditions in geothermal systems, *Geothermics*, *37*, 622–634, doi:10.1016/j.geothermics.2008.03.005.

Curewitz, D., and J. A. Karson (1997), Structural settings of hydrothermal outflow: Fracture permeability maintained by fault propagation and interaction, *J. Volcanol. Geotherm. Res.*, *79*, 149–168, doi:10.1016/S0377-0273(97)00027-9.

Dalen, V. (1979), Simplified finite-element methods for reservoir flow problems, *Soc. Pet. Eng. J.*, *19*, 333–343, doi:10.2118/7196-PA.

de Josselin de Jong, G. (1969), Generating functions in the theory of flow through porous media, in *Flow Through Porous Media*, edited by R. J. M. De Wiest, pp. 377–400, Academic, San Diego, Calif.

Delaney, P. T. (1982), Rapid intrusion of magma into hot rock: Groundwater flow due to pore pressure increases, *J. Geophys. Res.*, *87*, 7739–7756.

Deming, D. (1993), Regional permeability estimates from investigations of coupled heat and groundwater flow, North Slope of Alaska, *J. Geophys. Res.*, *98*, 16,271–16,286, doi:10.1029/93JB01427.

Diamond, L. W. (2001), Review of the systematics of CO_2-H_2O fluid inclusions, *Lithos*, *55*, 69–99, doi:10.1016/S0024-4937(00)00039-6.

Dobson, P. F., S. Salah, N. Spycher, and E. L. Sonnenthal (2004), Simulation of water-rock interaction in the Yellowstone geothermal system using TOUGHREACT, *Geothermics*, *33*, 493–502, doi:10.1016/j.geothermics.2003.10.002.

Doi, N., O. Kato, K. Ikeuchi, R. Komatsu, S.-I. Miyazaki, K. Akaku, and T. Uchida (1998), Genesis of the plutonic-hydrothermal system around Quaternary granite in the Kakkonda geothermal system, Japan, *Geothermics*, *27*, 663–690, doi:10.1016/S0375-6505(98)00039-X.

Donaldson, I. (1962), Temperature gradients in the upper layers of the Earth's crust due to convective water flows, *J. Geophys. Res.*, *67*, 3449–3459.

Driesner, T. (2007), The system H_2O-NaCl. Part II: Correlations for molar volume, enthalpy, and isobaric heat capacity from 0 to 1000°C, 1 to 5000 bar, and 0 to 1 X_{NaCl}, *Geochim. Cosmochim. Acta*, *71*(4), 4902–4919.

Driesner, T., and S. Geiger (2007), Numerical simulation of multiphase fluid flow in hydrothermal systems, in *Fluid-Fluid Interactions in the Earth's Lithosphere*, *Rev. in Mineral. and Geochem.*, vol. 65, edited by A. Liebscher and C. A. Heinrich, pp. 187–212, Mineral. Soc. of Am., Washington, D. C.

Driesner, T., and C. A. Heinrich (2007), The system H_2O-NaCl. Part I: Correlation formulae for phase relations in temperature-pressure-composition space from 0 to 1000°C, 0 to 5000 bar, and 0 to 1 X_{NaCl}, *Geochim. Cosmochim. Acta*, *71*(4), 4880–4901.

Duan, Z., and D. Li (2008), Coupled phase and aqueous species equilibrium of the H_2O-CO_2-NaCl-$CaCO_3$ system from 0 to 250°C, 1 to 1000 bar with NaCl concentrations up to saturation of halite, *Geochim. Cosmochim. Acta*, *72*, 5128–5145.

Duan, Z., N. Møller, and J. H. Weare (1995), Equation of state for the NaCl-H_2O-CO_2 system: Prediction of phase equilibria and volumetric properties, *Geochim. Cosmochim. Acta*, *59*, 2869–2882.

Duffield, W. A., and J. H. Sass (2004), Geothermal energy—Clean power from the Earth's heat, *U.S. Geol. Surv. Circ., 1249*.

Dunn, J. C., and H. C. Hardee (1981), Superconvecting geothermal zones, *J. Volcanol. Geotherm. Res.*, *11*, 189–201, doi:10.1016/0377-0273(81)90022-6.

Durlofsky, L. J. (1993), A triangle based mixed finite element–finite volume technique for modeling two phase flow through porous media, *J. Comput. Phys.*, *105*, 252–266, doi:10.1006/jcph.1993.1072.

Dutrow, B., and D. Norton (1995), Evolution of fluid pressure and fracture propagation during contact metamorphism, *J. Metamorph. Geol.*, *13*, 677–686, doi:10.1111/j.1525-1314.1995.tb00251.x.

Dutrow, B. L., B. J. Travis, C. W. Gable, and D. J. Henry (2001), Coupled heat and silica transport associated with dike intrusion into sedimentary rock: Effects on isotherm location and permeability evolution, *Geochim. Cosmochim. Acta*, *65*, 3749–3767.

Dzurisin, D. (2007), *Volcano Deformation*, Springer, London.

Ebigbo, A., H. Class, and R. Helmig (2007), CO_2 leakage through an abandoned well: Problem oriented benchmarks, *Comput. Geosci.*, *11*, 103–115, doi:10.1007/s10596-006-9033-7.

Elder, J. W. (1967a), Steady free convection in a porous medium heated from below, *J. Fluid Mech.*, *27*, 29–84, doi:10.1017/S0022112067000023.

Elder, J. W. (1967b), Transient convection in a porous medium, *J. Fluid Mech.*, *27*, 609–623, doi:10.1017/S0022112067000576.

Elderfield, H., and A. Schultz (1996), Mid-ocean ridge hydrothermal fluxes and the chemical composition of the ocean, *Annu. Rev. Earth Planet. Sci.*, *24*, 191–224, doi:10.1146/annurev.earth.24.1.191.

Emmanuel, S., and B. Berkowitz (2006), An experimental analogue for convection and phase separation in hydrothermal systems, *J. Geophys. Res.*, *111*, B09103, doi:10.1029/2006JB004351.

Emmanuel, S., and B. Berkowitz (2007), Phase separation and convection in heterogeneous porous media: Implications for seafloor hydrothermal systems, *J. Geophys. Res.*, *112*, B05210, doi:10.1029/2006JB004804.

Evans, D. G., and J. P. Raffensperger (1992), On the stream function for variable-density groundwater flow, *Water Resour. Res.*, *28*(2), *141–142*, 145.

Farrar, C. D., M. L. Sorey, W. C. Evans, J. F. Howle, B. D. Kerr, B. M. Kennedy, C.-Y. King, and J. R. Southon (1995), Forest-killing diffuse CO_2 emission at Mammoth Mountain as a sign of magmatic unrest, *Nature*, *376*, 675–678, doi:10.1038/376675a0.

Faust, C. R., and J. W. Mercer (1979a), Geothermal reservoir simulation: 1. Mathematical models for liquid- and vapor-dominated hydrothermal systems, *Water Resour. Res.*, *15*, 23–30, doi:10.1029/WR015i001p00023.

Faust, C. R., and J. W. Mercer (1979b), Geothermal reservoir simulation: 2. Numerical solution techniques for liquid- and vapor-dominated hydrothermal systems, *Water Resour. Res.*, *15*, 31–46, doi:10.1029/WR015i001p00031.

Fehn, U., and L. M. Cathles (1979), Hydrothermal convection at slow-spreading mid-ocean ridges, *Tectonophysics*, *55*, 239–260, doi:10.1016/0040-1951(79)90343-3.

Fehn, U., and L. M. Cathles (1986), The influence of plate movement on the evolution of hydrothermal convection cells in the oceanic crust, *Tectonophysics*, *125*, 289–312, doi:10.1016/0040-1951(86)90167-8.

Fehn, U., K. E. Green, R. P. Von Herzen, and L. M. Cathles (1983), Numerical models for the hydrothermal field at the Galapagos Spreading Center, *J. Geophys. Res.*, *88*, 1033–1048.

Fialko, Y., Y. Khazan, and M. Simons (2001), Deformation due to a pressurized horizontal circular crack in an elastic half-space, with applications to volcano geodesy, *Geophys. J. Int.*, *146*, 181–190, doi:10.1046/j.1365-246X.2001.00452.x.

Finizola, A., A. Revil, E. Rizzo, S. Piscitelli, T. Ricci, J. Morin, B. Angeletti, L. Mocochain, and F. Sortino (2006), Hydrogeological insights at Stromboli volcano (Italy) from geoelectrical, temperature, and CO_2 soil degassing investigations, *Geophys. Res. Lett.*, *33*, L17304, doi:10.1029/2006GL026842.

Fisher, A. T. (1998), Permeability within basaltic oceanic crust, *Rev. Geophys.*, *36*, 143–182, doi:10.1029/97RG02916.

Fisher, A. T., E. E. Davis, and K. Becker (2008), Borehole-to-borehole hydrologic response across 2.4 km in the upper oceanic crust: Implications for crustal-scale properties, *J. Geophys. Res.*, *113*, B07106, doi:10.1029/2007JB005447.

Fontaine, F. J., M. Rabinowicz, and J. Boulegue (2001), Permeability changes due to mineral diagenesis in fractured crust: Implications for hydrothermal circulation at mid-ocean ridges, *Earth Planet. Sci. Lett.*, *184*, 407–425, doi:10.1016/S0012-821X(00)00332-0.

Fontaine, F. J., W. S. D. Wilcock, and D. A. Butterfield (2007), Physical controls on the salinity of mid-ocean ridge hydrothermal vents, *Earth Planet. Sci. Lett.*, *257*, 132–145, doi:10.1016/j.epsl.2007.02.027.

Fontaine, F. J., M. Cannat, and J. Escartin (2008), Hydrothermal circulation at slow-spreading mid-ocean ridges: The role of along-axis variations in axial lithospheric thickness, *Geology*, *36*, 759–762, doi:10.1130/G24885A.1.

Fontaine, F. J., W. S. D. Wilcock, D. E. Foustoukos, and D. A. Butterfield (2009), A Si-Cl geothermobarometer for the reaction zone of high-temperature, basaltic-hosted mid-ocean ridge hydrothermal systems, *Geochem. Geophys. Geosyst.*, *10*, Q05009, doi:10.1029/2009GC002407.

Fornari, D. J., T. Shank, K. L. Von Damm, T. K. P. Gregg, M. Lilley, G. Levai, A. Bray, R. M. Haymon, M. R. Perfit, and R. Lutz (1998), Time-series temperature measurements at high-temperature hydrothermal vents, East Pacific Rise 9°49′–51°N: Evidence for monitoring a crustal cracking event, *Earth Planet. Sci. Lett.*, *160*, 419–431, doi:10.1016/S0012-821X(98)00101-0.

Forsyth, P. A. (1991), A control volume finite element approach to NAPL groundwater contamination, *SIAM J. Sci. Stat. Comput.*, *12*, 1029–1057.

Fournier, R. O. (1990), Double-diffusive convection in geothermal systems: The Salton Sea, California, geothermal system as a likely candidate, *Geothermics*, *19*, 481–496, doi:10.1016/0375-6505(90)90001-R.

Fournier, R. O. (1991), The transition from hydrostatic to greater than hydrostatic fluid pressure in presently active continental hydrothermal systems in crystalline rock, *Geophys. Res. Lett.*, *18*, 955–958, doi:10.1029/91GL00966.

Fournier, R. O. (1999), Hydrothermal processes related to movement of fluid from plastic into brittle rock in the magmatic-epithermal environment, *Econ. Geol.*, *94*, 1193–1211.

Fournier, R. O., and R. W. Potter II (1982), An equation correlating the solubility of quartz in water from 25° to 900°C at pressures up to 10000 bars, *Geochim. Cosmochim. Acta*, *46*, 1969–1973, doi:10.1016/0016-7037(82)90135-1.

Foustoukos, D. I., and W. E. Seyfried Jr. (2007), Fluid phase separation processes in submarine hydrothermal systems, *Rev. Mineral. Geochem.*, *65*, 213–239, doi:10.2138/rmg.2007.65.7.

Fridleifsson, G. O., and W. A. Elders (2005), The Icelandic Deep Drilling Project: A search for deep unconventional geothermal resources, *Geothermics*, *34*, 269–285, doi:10.1016/j.geothermics.2004.11.004.

Fujimitsu, Y., S. Ehara, R. Oki, and R. Kanou (2008), Numerical model of the hydrothermal system beneath Unzen volcano, Japan, *J. Volcanol. Geotherm. Res.*, *175*, 35–44, doi:10.1016/j.jvolgeores.2008.03.032.

Furlong, K. P., R. B. Hanson, and J. R. Bowers (1991), Modeling thermal regimes. in *Contact Metamorphism*, *Rev. in Mineral.*, vol. 26, edited by D. M. Kerrick, pp. 437–505, Mineral. Soc. of Am., Washington, D. C.

Geiger, S., R. Haggerty, J. H. Dilles, M. H. Reed, and S. K. Matthäi (2002), New insights from reactive transport modeling: The formation of the sericitic vein envelopes during early hydrothermal alteration at Butte, Montana, *Geofluids*, *2*, 185–201, doi:10.1046/j.1468-8123.2002.00037.x.

Geiger, S., S. Roberts, S. K. Matthäi, C. Zoppou, and A. Burri (2004), Combining finite element and finite volume methods for efficient multiphase flow simulations in highly heterogeneous and structurally complex geologic media, *Geofluids*, *4*, 284–299, doi:10.1111/j.1468-8123.2004.00093.x.

Geiger, S., T. Driesner, C. A. Heinrich, and S. K. Matthäi (2005), On the dynamics of NaCl-H_2O fluid convection in the Earth's crust, *J. Geophys. Res.*, *110*, B07101, doi:10.1029/2004JB003362.

Geiger, S., T. Driesner, C. A. Heinrich, and S. K. Matthäi (2006a), Multiphase thermohaline convection in the Earth's crust: I. A new finite element-finite volume solution technique combined with a new equation of state for NaCl-H_2O, *Transp. Porous Media*, *63*, 399–434, doi:10.1007/s11242-005-0108-z.

Geiger, S., T. Driesner, C. A. Heinrich, and S. K. Matthäi (2006b), Multiphase thermohaline convection in the Earth's crust: II. Benchmarking and application of a finite element–finite volume solution technique with a NaCl-H_2O equation of state, *Transp. Porous Media*, *63*, 435–461, doi:10.1007/s11242-005-0109-y.

Geiger, S., Q. Huangfu, F. Reid, S. K. Matthäi, D. Coumou, M. Belayneh, C. Fricke, and K. Schmid (2009), Massively parallel sector scale discrete fracture and matrix simulations, SPE paper 118924 presented at SPE Reservoir Simulation Symposium, Soc. of Pet. Eng., The Woodlands, Tex.

Gerdes, M. L., L. P. Baumgartner, and M. Person (1995), Stochastic permeability models of fluid flow during contact metamorphism, *Geology*, *23*, 945–948, doi:10.1130/0091-7613(1995)023<0945:SPMOFF>2.3.CO;2.

German, C. R., and K. L. Von Damm (2003), Hydrothermal processes, in , *Treatise on Geochemistry*, vol. 6, *The Oceans and Marine Geochemistry*, edited by H. Elderfield, pp. 181–222, Elsevier, Amsterdam.

Germanovich, L. N., and R. P. Lowell (1992), Percolation theory, thermoelasticity, and discrete hydrothermal venting in the Earth's crust, *Science*, *255*, 1564–1567.

Germanovich, L. N., and R. P. Lowell (1995), The mechanism of phreatic eruptions, *J. Geophys. Res.*, *100*(B5), 8417–8434.

Germanovich, L. N., R. P. Lowell, and D. K. Astakhov (2000), Stress-dependent permeability and the formation of seafloor event plumes, *J. Geophys. Res.*, *105*(B4), 8341–8354.

Germanovich, L. N., R. P. Lowell, and D. K. Astakhov (2001), Temperature-dependent permeability and bifurcations in hydrothermal flow, *J. Geophys. Res.*, *106*, 473–495, doi:10.1029/2000JB900293.

Giambalvo, E. R., C. I. Steefel, A. T. Fisher, N. D. Rosenberg, and C. G. Wheat (2002), Effect of fluid-sediment reaction on hydrothermal fluxes of major elements, eastern flank of the Juan de Fuca Ridge, *Geochim. Cosmochim. Acta*, *66*, 1739–1757, doi:10.1016/S0016-7037(01)00878-X.

Giggenbach, W. F. (1984), Mass transfer in hydrothermal alteration systems—A conceptual approach, *Geochim. Cosmochim. Acta*, *48*, 2693–2711.

Gillis, K. M., and M. D. Roberts (1999), Cracking at the magma-hydrothermal transition: Evidence from the Troodos Ophiolite, Cyprus, *Earth Planet. Sci. Lett.*, *169*, 227–244, doi:10.1016/S0012-821X(99)00087-4.

Gilman, J. R., and H. Kazemi (1983), Improvements in simulation of naturally fractured reservoirs, *SPEJ Soc. Pet. Eng. J.*, *24*, 695–707.

Golden, C. E., S. C. Webb, and R. A. Sohn (2003), Hydrothermal microearthquake swarms beneath active vents at Middle Valley, northern Juan de Fuca Ridge, *J. Geophys. Res.*, *108*(B1), 2027, doi:10.1029/2001JB000226.

Gottschalk, M. (2007), Equations of state for complex fluids, in *Fluid-Fluid Interactions in the Earth's Lithosphere*, *Rev. in Mineral. and Geochem.*, vol. 65, edited by A. Liebscher and C. A. Heinrich, pp. 49–97, Mineral. Soc. of Am., Washington, D. C.

Grant, M. A., and M. L. Sorey (1979), The compressibility and hydraulic diffusivity of a water-steam flow, *Water Resour. Res.*, *15*, 684–686, doi:10.1029/WR015i003p00684.

Haar, L., J. S. Gallagher, and G. S. Kell (1984), *NBS/NRC Steam Tables Thermodynamic and Transport Properties and Computer Programs for Vapor and Liquid States of Water in SI Units*, Hemisphere, New York.

Hanson, R. B. (1992), Effects of fluid production on fluid flow during regional and contact metamorphism, *J. Metamorph. Geol.*, *10*, 87–97, doi:10.1111/j.1525-1314.1992.tb00073.x.

Hanson, R. B. (1995), The hydrodynamics of contact metamorphism, *Geol. Soc. Am. Bull.*, *107*, 595–611, doi:10.1130/0016-7606(1995)107<0595:THOCM>2.3.CO;2.

Hanson, R. B. (1996), Hydrodynamics of magmatic and meteoric fluids in the vicinity of granitic intrusions, *Trans. R. Soc. Edinburgh Earth Sci.*, *87*, 251–259.

Harris, R. N., A. T. Fisher, and D. S. Chapman (2004), Fluid flow through seamounts and implications for global mass fluxes, *Geology*, *32*, 725–728, doi:10.1130/G20387.1.

Harten, A. (1983), High resolution schemes for hyperbolic conservation laws, *J. Comput. Phys.*, *49*, 357–393, doi:10.1016/0021-9991(83)90136-5.

Hayba, D. O., and S. E. Ingebritsen (1994), The computer model HYDROTHERM, a three-dimensional finite-difference model to simulate ground-water flow and heat transport in the temperature range of 0 to 1, 200°C, *U.S. Geol. Surv. Water Resour. Invest. Rep.*, *94-4045*.

Hayba, D. O., and S. E. Ingebritsen (1997), Multiphase groundwater flow near cooling plutons, *J. Geophys. Res.*, *102*, 12,235–12,252, doi:10.1029/97JB00552.

Haymon, R. M. (1996), The response of ridge-crest hydrothermal systems to segmented, episodic magma supply, *Geol. Soc. Spec. Publ.*, *118*, 157–168.

Hedenquist, J. W., and R. W. Henley (1985), Hydrothermal eruptions in the Waiotapu geothermal system, New Zealand: Their origin, associated breccias, and relation to precious metal mineralization, *Econ. Geol.*, *80*(1), 640–641, 668.

Hedenquist, J. W., and J. L. Lowenstern (1994), The role of magmas in the formation of hydrothermal ore deposits, *Nature*, *370*, 519–527, doi:10.1038/370519a0.

Helmig, R. (1997), *Multiphase Flow and Transport Processes in the Subsurface: A Contribution to the Modeling of Hydrosystems*, Springer, New York.

Hill, D. P., et al. (1993), Seismicity remotely triggered by the magnitude 7.3 Landers, California, earthquake, *Science*, *260*, 1617–1623.

Hirth, G. H., J. Escartin, and J. Lin (1998), The rheology of the lower oceanic crust: Implications for lithosphere deformation at mid-ocean ridges, in *Faulting and Magmatism at Mid-Ocean Ridges*, *Geophys. Monogr. Ser.*, vol. 106, edited by W. R. Buck et al., pp. 291–303, AGU, Washington, D. C.

Hofmeister, A. M., M. Pertermann, and J. M. Branlund (2007), Thermal conductivity of the Earth, in , *Treatise on Geophysics*, vol. 2, edited by G. D. Price, pp. 543–578, Elsevier, Amsterdam.

Hogeweg, N., T. E. C. Keith, E. M. Colvard, and S. E. Ingebritsen (2005), Ongoing hydrothermal heat loss from the Valley of 10000 Smokes, Alaska, *J. Volcanol. Geotherm. Res.*, *143*, 279–291, doi:10.1016/j.jvolgeores.2004.12.003.

Horne, R. N., C. Satik, G. Mahiya, K. Li, W. Ambusso, R. Tovar, C. Wang, and H. Nassori (2000), Steam-water relative permeability, paper presented at World Geothermal Congress 2000, Int. Geotherm. Assoc., Beppu, Japan, 28 May to 10 June.

Hubbert, M. K. (1956), Darcy's law and the field equations of the flow of underground fluids, *Trans. Am. Inst. Min. Metall. Pet. Eng.*, *207*, 222–239.

Hurwitz, S., and M. J. S. Johnston (2003), Groundwater level changes in a deep well in response to a magma intrusion event on Kilauea Volcano, Hawai'i, *Geophys. Res. Lett.*, *30*(22), 2173, doi:10.1029/2003GL018676.

Hurwitz, S., S. E. Ingebritsen, and M. L. Sorey (2002), Episodic thermal perturbations associated with groundwater flow: An example from Kilauea Volcano, Hawaii, *J. Geophys. Res.*, *107* (B11), 2297, doi:10.1029/2001JB001654.

Hurwitz, S., K. L. Kipp, S. E. Ingebritsen, and M. E. Reid (2003), Groundwater flow, heat transport, and water table position within volcanic edifices: Implications for volcanic processes in the Cascade Range, *J. Geophys. Res.*, *108*(B12), 2557, doi:10.1029/2003JB002565.

Hurwitz, S., L. B. Christiansen, and P. A. Hsieh (2007), Hydrothermal fluid flow and deformation in large calderas: Inferences from numerical simulations, *J. Geophys. Res.*, *112*, B02206, doi:10.1029/2006JB004689.

Husen, S., R. Taylor, R. B. Smith, and H. Heasler (2004), Changes in geyser eruption behavior and remotely triggered seismicity in Yellowstone National Park produced by the 2002 M 7.9 Denali fault earthquake, Alaska, *Geology*, *32*, 537–540, doi:10.1130/G20381.1.

Hutnak, M., S. Hurwitz, S. E. Ingebritsen, and P. A. Hsieh (2009), Numerical models of caldera deformation: Effects of multiphase and multicomponent hydrothermal fluid flow, *J. Geophys. Res.*, *114*, B04411, doi:10.1029/2008JB006151.

Ingebritsen, S. E., and D. O. Hayba (1994), Fluid flow and heat transport near the critical point of H_2O, *Geophys. Res. Lett.*, *21*, 2199–2203.

Ingebritsen, S. E., and C. E. Manning (1999), Geological implications of a permeability-depth curve for the continental crust, *Geology*, *27*, 1107–1110.

Ingebritsen, S. E., and S. A. Rojstaczer (1996), Geyser periodicity and the response of geysers to deformation, *J. Geophys. Res.*, *101*, 21,891–21,905, doi:10.1029/96JB02285.

Ingebritsen, S. E., and M. L. Sorey (1988), Vapor-dominated zones within hydrothermal systems: Evolution and natural state, *J. Geophys. Res.*, *93*, 13,635–13,655, doi:10.1029/JB093iB11p13635.

Ingebritsen, S. E., W. E. Sanford, and C. E. Neuzil (2006), *Groundwater in Geologic Processes*, 2nd ed., Cambridge Univ. Press, Cambridge, U. K.

Iverson, R. M. (1997), The physics of debris flows, *Rev. Geophys.*, *35*, 245–296, doi:10.1029/97RG00426.

Johnson, H. P., M. Hutnak, R. P. Dziak, C. G. Fox, I. Urcuyo, J. P. Cowen, J. Nabelek, and C. Fisher (2000), Earthquake-induced changes in a hydrothermal system on the Juan de Fuca mid-ocean ridge, *Nature*, *407*, 174–177, doi:10.1038/35025040.

Johnson, J. W., and D. Norton (1991), Critical phenomena in hydrothermal systems: State, thermodynamic, electrostatic, and

transport properties of H_2O in the critical region, *Am. J. Sci.*, *291*, 541–648.
Jupp, T., and A. Schultz (2000), A thermodynamic explanation for black smoker temperatures, *Nature*, *403*, 880–883, doi:10.1038/35002552.
Jupp, T., and A. Schultz (2004), Physical balances in subseafloor hydrothermal convection cells, *J. Geophys. Res.*, *109*, B05101, doi:10.1029/2003JB002697.
Kawada, Y., S. Yoshida, and S. I. Watanabe (2004), Numerical simulations of mid-ocean ridge hydrothermal circulation including the phase separation of seawater, *Earth Planets Space*, *56*, 193–215.
Keating, G. N. (2005), The role of water in cooling ignimbrites, *J. Volcanol. Geotherm. Res.*, *142*, 145–171, doi:10.1016/j.jvolgeores.2004.10.019.
Keating, G. N., J. W. Geissman, and G. A. Zyvoloski (2002), Multiphase modeling of contact metamorphic systems and application to transitional geomagnetic fields, *Earth Planet. Sci. Lett.*, *198*, 429–448, doi:10.1016/S0012-821X(02)00487-9.
Kelley, D. S., and J. R. Delaney (1987), Two-phase separation and fracturing in mid-ocean ridge gabbros at temperatures greater than 700°C, *Earth Planet. Sci. Lett.*, *83*, 53–66, doi:10.1016/0012-821X(87)90050-1.
Kelley, D. S., J. A. Baross, and J. R. Delaney (2002), Volcanoes, fluids, and life at mid-ocean ridge spreading centers, *Annu. Rev. Earth Planet. Sci.*, *30*, 385–491, doi:10.1146/annurev.earth.30.091201.141331.
Kim, J., H. A. Tchelepi, and R. Juanes (2009), Stability and accuracy of sequential methods for coupled flow and geomechanics, SPE paper 1 19084 presented at SPE Reservoir Simulation Symposium, Soc. of Pet. Eng., The Woodlands, Tex.
Kipp, K. L., Jr., P. A. Hsieh, and S. R. Charlton (2008), Guide to the revised ground-water flow and heat transport simulator: HYDROTHERM–Version 3, *U.S. Geol. Surv. Tech. Methods*, 6–A25, U.S. Geol. Surv., Reston, Va.
Kiryukhin, A. V., and V. A. Yampolsky (2004), Modeling study of the Pauzhetsky geothermal field, *Geothermics*, *33*, 421–442, doi:10.1016/j.geothermics.2003.09.010.
Kiryukhin, A. V., N. P. Asaulova, and S. Finsterle (2008), Inverse modeling and forecasting for the exploitation of the Pauzhetsky geothermal field, Kamchatka, Russia, *Geothermics*, *37*, 540–562, doi:10.1016/j.geothermics.2008.04.003.
Kissling, W. M. (2005a), Transport of three-phase hyper-saline brines in porous media: Examples, *Transp. Porous Media*, *60*, 141–157, doi:10.1007/s11242-004-4795-7.
Kissling, W. M. (2005b), Transport of three-phase hyper-saline brines in porous media: Theory and code implementation, *Transp. Porous Media*, *61*, 25–44, doi:10.1007/s11242-004-3306-1.
Kissling, W. M., and G. J. Weir (2005), The spatial distribution of the geothermal fields in the Taupo Volcanic Zone, New Zealand, *J. Volcanol. Geotherm. Res.*, *145*, 136–150, doi:10.1016/j.jvolgeores.2005.01.006.
Konikow, L. F., and J. D. Bredehoeft (1992), Ground-water models cannot be validated, *Adv. Water Resour.*, *15*, 75–83, doi:10.1016/0309-1708(92)90033-X.
Kostova, B., T. Pettke, T. Driesner, P. Petrov, and C. A. Heinrich (2004), LA ICP-MS study of fluid inclusions in quartz from the Yuzhna Petrovitsa deposit, Madan ore field, Bulgaria, *Schweiz. Mineral. Petrogr. Mitt.*, *84*, 25–36.
Lachenbruch, A. H., J. H. Sass, R. J. Munroe, and T. H. Moses Jr. (1976), Geothermal setting and simple heat-conduction models for the Long Valley caldera, *J. Geophys. Res.*, *81*, 769–784, doi:10.1029/JB081i005p00769.
Larsson, A. (1992), The international projects INTRACOIN and HYDROCOIN and INTRAVAL, *Adv. Water Resour.*, *15*, 85–87, doi:10.1016/0309-1708(92)90034-Y.
Lee, S. H., P. Jenny, and H. A. Tchelepi (2002), A finite-volume method with hexahedral mulitblock grids for modeling flow in porous media, *Comput. Geosci.*, *6*, 353–379, doi:10.1023/A:1021287013566.
Lewis, K. C. (2007), Numerical modeling of two-phase flow in the sodium chloride-water system with applications to seafloor hydrothermal systems, Ph.D. thesis, Ga. Inst. of Technol., Atlanta.
Lewis, K. C., and R. P. Lowell (2009a), Numerical modeling of two-phase flow in the NaCl-H_2O system: Introduction of a numerical method and benchmarking, *J. Geophys. Res.*, *114*, B05202, doi:10.1029/2008JB006029.
Lewis, K. C., and R. P. Lowell (2009b), Numerical modeling of two-phase flow in the NaCl-H_2O system: 2. Examples, *J. Geophys. Res.*, *114*, B08204, doi:10.1029/2008JB006030.
Li, K., and R. N. Horne (2006), Comparison of methods to calculate relative permeability from capillary pressure in consolidated water-wet porous media, *Water Resour. Res.*, *42*, W06405, doi:10.1029/2005WR004482.
Li, K., and R. N. Horne (2007), Systematic study of steam-water capillary pressure, *Geothermics*, *36*, 558–574, doi:10.1016/j.geothermics.2007.08.002.
Lister, C. R. B. (1974), On the penetration of water into hot rock, *Geophys. J. R. Astron. Soc.*, *39*, 465–509.
Lister, C. R. B. (1980), Heat flow and hydrothermal circulation, *Annu. Rev. Earth Planet. Sci.*, *8*, 95–117, doi:10.1146/annurev.ea.08.050180.000523.
Lister, C. R. B. (1983), The basic physics of water penetration into hot rock, in *Hydrothermal Processes at Seafloor Spreading Centers*, edited by P. A. Rona et al., pp. 141–168, Plenum, New York.
Lopez, D. L., and L. Smith (1995), Fluid flow in fault zones: Influence of hydraulic anisotropy and heterogeneity on the fluid flow and heat transfer regime, *Water Resour. Res.*, *32*, 3227–3235.
Lopez, D. L., and S. N. Williams (1993), Catastrophic volcanic collapse: Relation to hydrothermal processes, *Science*, *260*, 1794–1796.
Lowell, R. P. (1991), Modeling continental and submarine hydrothermal systems, *Rev. Geophys.*, *29*, 457–476, doi:10.1029/91RG01080.
Lowell, R. P., and L. N. Germanovich (1994), On the temporal evolution of high-temperature hydrothermal systems at ocean ridge crests, *J. Geophys. Res.*, *99*, 565–575, doi:10.1029/93JB02568.
Lowell, R. P., and L. N. Germanovich (1995), Hydrothermal processes at mid-ocean ridges: Results from scale analysis and single-pass models, in *Mid-Ocean Ridges: Hydrothermal Interaction Between the Lithosphere and Oceans*, *Geophys. Monogr. Ser.*, vol. 148, edited by C. R. German, J. Lin, and L. M. Parson, pp. 219–244, AGU, Washington, D. C.
Lowell, R. P., and W. Xu (2000), Sub-critical two-phase seawater convection near a dike, *Earth Planet. Sci. Lett.*, *174*, 385–396, doi:10.1016/S0012-821X(99)00275-7.
Lu, X., and S. W. Kieffer (2009), Thermodynamics and mass transport in multicomponent, multiphase H_2O systems of planetary interest, *Annu. Rev. Earth Planet. Sci.*, *37*, 449–477, doi:10.1146/annurev.earth.031208.100109.
Lutz, R. A., and M. J. Kennish (1993), Ecology of deep-sea hydrothermal vent communities: A review, *Rev. Geophys.*, *31*, 211–242, doi:10.1029/93RG01280.
MacKenzie, F. T., and R. M. Garrels (1966), Chemical mass balance between rivers and oceans, *Am. J. Sci.*, *264*, 507–525.
Manning, C. E., and S. E. Ingebritsen (1999), Permeability of the continental crust: The implications of geothermal data and metamorphic systems, *Rev. Geophys.*, *37*, 127–150, doi:10.1029/1998RG900002.
Manning, C. E., S. E. Ingebritsen, and D. K. Bird (1993), Missing mineral zones in contact metamorphosed basalts, *Am. J. Sci.*, *293*, 894–938.
Mannington, W., M. J. O'Sullivan, and D. Bullivant (2004), Computer modelling of the Wairakei-Tauhara geothermal sys-

tem, New Zealand, *Geothermics*, *33*, 401–419, doi:10.1016/j.geothermics.2003.09.009.

Mastin, L. G. (1991), The roles of magma and groundwater in the phreatic eruptions at Inyo Craters, Long Valley caldera, California, *Bull. Volcanol.*, *53*, 579–596, doi:10.1007/BF00493687.

Matthäi, S. K., and M. Belayneh (2004), Fluid flow partitioning between fractures and a permeable rock matrix, *Geophys. Res. Lett.*, *31*, L07602, doi:10.1029/2003GL019027.

Matthäi, S. K., C. A. Heinrich, and T. Driesner (2004), Is the Mount Isa copper deposit the product of forced brine convection in the footwall of a major reverse fault?, *Geology*, *32*, 357–360, doi:10.1130/G20108.1.

Matthäi, S. K., et al. (2007), Numerical simulations of multiphase fluid flow in structurally complex reservoirs, in *Structurally Complex Reservoirs*, edited by S. J. Jolley et al., *Geol. Soc. Spec. Publ.*, *292*, 405–429.

Menand, T., A. Raw, and A. W. Woods (2003), Thermal inertia and reversing buoyancy in flow in porous media, *Geophys. Res. Lett.*, *30*(6), 1291, doi:10.1029/2002GL016294.

Mogi, K. (1958), Relations of the eruptions of various volcanoes and the deformation of ground surfaces around them, *Bull. Earthquake Res. Inst. Univ. Tokyo*, *36*, 94–134.

Moore, D. E., C. A. Morrow, and J. D. Byerlee (1983), Chemical reactions accompanying fluid flow through granite held in a temperature gradient, *Geochim. Cosmochim. Acta*, *47*, 445–453, doi:10.1016/0016-7037(83)90267-3.

Moore, D. E., D. A. Lockner, and J. D. Byerlee (1994), Reduction of permeability in granite at elevated temperatures, *Science*, *265*, 1558–1561.

Morrow, C., D. Lockner, D. Moore, and J. Byerlee (1981), Permeability of granite in a temperature gradient, *J. Geophys. Res.*, *86*, 3002–3008.

Morrow, C. A., D. E. Moore, and D. A. Lockner (2001), Permeability reduction in granite under hydrothermal conditions, *J. Geophys. Res.*, *106*, 30,551–30,560, doi:10.1029/2000JB000010.

Muffler, L. J. P. (Ed.) (1979), Assessment of geothermal resources of the United States–1978, *U.S. Geol. Surv. Circ.*, *790*.

Narasimhan, T. N., and P. A. Witherspoon (1976), An integrated finite difference method for analyzing fluid flow in porous media, *Water Resour. Res.*, *12*, 57–65, doi:10.1029/WR012i001p00057.

Nehlig, P. (1994), Fracture and permeability analysis in magma-hydrothermal transition zones in the Samail Ophiolite (Oman), *J. Geophys. Res.*, *99*, 589–601, doi:10.1029/93JB02569.

Neuman, S. P. (2005), Trends, prospects and challenges in quantifying flow and transport through fractured rocks, *Hydrogeol. J.*, *13*, 124–147, doi:10.1007/s10040-004-0397-2.

Neuzil, C. E. (1995), Abnormal pressures as hydrodynamic phenomena, *Am. J. Sci.*, *295*, 742–786.

Neuzil, C. E. (2003), Hydromechanical coupling in geologic processes, *Hydrogeol. J.*, *11*, 41–83.

Newhall, C. G., S. E. Albano, N. Matsumoto, and T. Sandoval (2001), Roles of groundwater in volcanic unrest, *J. Geol. Soc. Philippines*, *56*, 69–84.

Newman, A. V., T. H. Dixon, G. I. Ofoegbu, and J. E. Dixon (2001), Geodetic and seismic constraints on recent activity at Long Valley Caldera, California: Evidence for viscoelastic rheology, *J. Volcanol. Geotherm. Res.*, *105*, 183–206, doi:10.1016/S0377-0273(00)00255-9.

Nield, D. A. (1968), Onset of thermohaline convection in a porous medium, *Water Resour. Res.*, *4*, 553–560, doi:10.1029/WR004i003p00553.

Nield, D. A., and A. Bejan (1992), *Convection in Porous Media*, Springer, New York.

Norton, D. L. (1984), Theory of hydrothermal systems, *Annu. Rev. Earth Planet. Sci.*, *12*, 155–178, doi:10.1146/annurev.ea.12.050184.001103.

Norton, D., and J. Knight (1977), Transport phenomena in hydrothermal systems: Cooling plutons, *Am. J. Sci.*, *277*, 937–981.

Norton, D., and H. P. Taylor Jr. (1979), Quantitative simulation of the hydrothermal systems of crystallizing magmas on the basis of transport theory and oxygen isotope data: An analysis of the Skaergaard intrusion, *J. Petrol.*, *20*, 421–486.

Oldenburg, C. M., and K. Pruess (2000), Simulation of propagating fronts in geothermal reservoirs with the implicit Leonard total variation diminishing scheme, *Geothermics*, *29*, 1–25, doi:10.1016/S0375-6505(99)00048-6.

Oreskes, N., K. Shrader-Frechette, and K. Belitz (1994), Verification and validation of numerical models in the Earth sciences, *Science*, *84*, 85–92.

O'Sullivan, M. J., K. Pruess, and M. J. Lippmann (2001), State of the art of geothermal reservoir simulation, *Geothermics*, *30*, 395–429, doi:10.1016/S0375-6505(01)00005-0.

O'Sullivan, M. J., A. Yeh, and W. I. Mannington (2009), A history of numerical modeling of the Wairekei geothermal field, *Geothermics*, *38*, 155–168, doi:10.1016/j.geothermics.2008.12.001.

Palliser, C., and R. McKibbin (1998a), A model for deep geothermal brines. I. *T-p-X* state-space description, *Transp. Porous Media*, *33*, 65–80, doi:10.1023/A:1006537425101.

Palliser, C., and R. McKibbin (1998b), A model for deep geothermal brines. II. Thermodynamic properties—Density, *Transp. Porous Media*, *33*, 129–154, doi:10.1023/A:1006597626918.

Palliser, C., and R. McKibbin (1998c), A model for deep geothermal brines. III. Thermodynamic properties—Enthalpy and viscocity, *Transp. Porous Media*, *33*, 155–171, doi:10.1023/A:1006549810989.

Paluszny, A., S. K. Matthäi, and M. Hohmeyer (2007), Hybrid finite element-finite volume discretization of complex geologic structures and a new simulation workflow demonstrated on fractured rocks, *Geofluids*, *7*, 186–208, doi:10.1111/j.1468-8123.2007.00180.x.

Parmentier, E. M. (1981), Numerical experiments on ^{18}O depletion in igneous intrusions cooling by groundwater convection, *J. Geophys. Res.*, *86*(7), 131–137, 144.

Piquemal, J. (1994), Saturated steam relative permeabilities of unconsolidated porous media, *Transp. Porous Media*, *17*, 105–120, doi:10.1007/BF00624727.

Pirajno, F., and M. J. van Kranendonk (2005), Review of hydrothermal processes and systems on Earth and implications for Martian analogues, *Aust. J. Earth Sci.*, *52*, 329–351, doi:10.1080/08120090500134571.

Polak, A., D. Elsworth, H. Yasuhara, A. S. Grader, and P. M. Halleck (2003), Permeability reduction of a natural fracture under net dissolution by hydrothermal fluids, *Geophys. Res. Lett.*, *30*(20), 2020, doi:10.1029/2003GL017575.

Polyansky, O. P., V. V. Reverdatto, and V. G. Sverdlova (2002), Convection of two-phase fluid in a layered porous medium driven by the heat of magmatic dikes and sills, *Geochem. Int.*, *40*(suppl. 1), S69–S81.

Pruess, K. (1988), SHAFT, MULKOM, TOUGH: A set of numerical simulators for multiphase fluid and heat flow, *Rep. LBL-24430*, Lawrence Berkeley Natl. Lab., Berkeley, Calif.

Pruess, K. (1991), TOUGH2—A general-purpose numerical simulator for multiphase fluid and heat flow, *Rep. LBL-29400*, Lawrence Berkeley Natl. Lab., Berkeley, Calif.

Pruess, K. (2004), The TOUGH codes—A family of simulation tools for multiphase flow and transport processes in permeable media, *Vadose Zone J.*, *3*, 738–746, doi:10.2113/3.3.738.

Pruess, K., C. Calore, R. Celati, and Y. S. Wu (1987), An analytical solution for heat transfer at a boiling front moving through a porous medium, *Int. J. Heat Mass Transfer*, *30*, 2595–2602, doi:10.1016/0017-9310(87)90140-2.

Pruess, K., J. M. Zerzan, R. C. Schoeder, and P. A. Witherspoon (1979), Description of the three-dimensional two-phase simulator SHAFT78 for use in geothermal reservoir studies, SPE paper 7699 presented at Fifth Symposium on Reservoir Simulation, Soc. of Pet. Eng., Denver, Colo.

Pruess, K., C. Oldenburg, and G. Moridis (1999), TOUGH2 user's guide, version 2.0, *Rep. LBNL-43134*, Lawrence Berkeley Natl. Lab., Berkeley, Calif.

Pruess, K., J. Garcia, T. Kovscek, C. Oldenburg, C. I. Steefel, and T. F. Xu (2004), Code intercomparison builds confidence in numerical simulation models for geologic disposal of CO_2, *Energy*, *29*, 1431–1444.

Rabinowicz, M., J. Boulegue, and P. Genthon (1998), Two- and three-dimensional modeling of hydrothermal convection in the sedimented Middle Valley segment, Juan de Fuca Ridge, *J. Geophys. Res.*, *103*, 24,045–24,065, doi:10.1029/98JB01484.

Rabinowicz, M., J. C. Sempere, and P. Genthon (1999), Thermal convection in a vertical permeable slot: Implications for hydrothermal convection along mid-ocean ridges, *J. Geophys. Res.*, *104*, 29,275–29,292, doi:10.1029/1999JB900259.

Raffensperger, J. P. (1997), Evidence and modeling of large-scale groundwater convection in Precambrian sedimentary basins, in *Basin-Wide Diagenetic Patterns: Integrated Petrologic, Geochemical, and Hydrologic Considerations*, edited by I. P. Montañez, J. M. Gregg, and K. L. Helton, *Spec. Publ. SEPM Soc. Sediment. Geol.*, *57*, 15–26.

Reid, M. E. (2004), Massive collapse of volcano edifices triggered by hydrothermal pressurization, *Geology*, *32*, 373–376, doi:10.1130/G20300.1.

Revil, A., et al. (2008), Inner structure of La Fossa di Vulcano (Vulcano Island, southern Tyrrhenian Sea, Italy) revealed by high-resolution electric resistivity tomography coupled with self-potential, temperature, and CO_2 diffuse degassing measurements, *J. Geophys. Res.*, *113*, B07207, doi:10.1029/2007JB005394.

Rojstaczer, S. A., S. Wolf, and R. Michel (1995), Permeability enhancement in the shallow crust as a cause of earthquake-induced hydrological changes, *Nature*, *373*, 237–239, doi:10.1038/373237a0.

Rojstaczer, S. A., S. E. Ingebritsen, and D. O. Hayba (2008), Permeability of continental crust influenced by internal and external forcing, *Geofluids*, *8*, 128–139, doi:10.1111/j.1468-8123.2008.00211.x.

Rosenberg, N. D., and F. J. Spera (1992), Thermohaline convection in a porous medium heated from below, *Int. J. Heat Mass Transfer*, *35*, 1261–1273.

Rutqvist, J., Y. S. Wu, C. F. Tsang, and G. Bodvarsson (2002), A modeling approach for analysis of coupled multiphase fluid flow, heat transfer, and deformation in fractured porous rock, *Int. J. Rock Mech. Min. Sci.*, *39*, 429–442, doi:10.1016/S1365-1609(02)00022-9.

Saar, M. O., and M. Manga (2004), Depth dependence of permeability in the Oregon Cascades inferred from hydrogeologic, thermal, seismic, and magmatic modeling constraints, *J. Geophys. Res.*, *109*, B04204, doi:10.1029/2003JB002855.

Sammel, E. A., S. E. Ingebritsen, and R. H. Mariner (1988), The hydrothermal system at Newberry volcano, Oregon, *J. Geophys. Res.*, *93*, 10,149–10,162, doi:10.1029/JB093iB09p10149.

Sass, J. H., A. H. Lachenbruch, T. H. Moses Jr., and P. Morgan (1992), Heat flow from a scientific research well at Cajon Pass, California, *J. Geophys. Res.*, *97*, 5017–5030.

Schardt, C., R. Large, and J. Yang (2006), Controls on heat flow, fluid migration, and massive sulphide formation of an off-axis hydrothermal system—The Lau basin perspective, *Am. J. Sci.*, *306*, 103–134, doi:10.2475/ajs.306.2.103.

Scheidegger, A. E. (1974), *The Physics of Flow Through Porous Media*, 3rd ed., Univ. of Toronto Press, Toronto, Ont., Canada.

Schmidt, C., and R. J. Bodnar (2000), Synthetic fluid inclusions: XVI. PVTX properties in the system H_2O-NaCl-CO_2 at elevated temperatures, pressures and salinities, *Geochim. Cosmochim. Acta*, *64*, 3853–3869.

Schoofs, S., and F. J. Spera (2003), Transition to chaos and flow dynamics of thermochemical porous medium convection, *Transp. Porous Media*, *50*, 179–195, doi:10.1023/A:1020699112998.

Schoofs, S., F. J. Spera, and U. Hansen (1999), Chaotic thermohaline convection in low-porosity hydrothermal systems, *Earth Planet. Sci. Lett.*, *174*, 213–229, doi:10.1016/S0012-821X(99)00264-2.

Schultz, A., J. R. Delaney, and R. E. McDuff (1992), On the partitioning of heat flux between diffuse and point source seafloor venting, *J. Geophys. Res.*, *97*, 12,299–12,314, doi:10.1029/92JB00889.

Sclater, J. G., C. Jaupart, and D. Galson (1980), The heat flow through oceanic and continental crust and the heat loss of the Earth, *Rev. Geophys.*, *18*, 269–311, doi:10.1029/RG018i001p00269.

Seyfried, W. E., Jr. (1987), Experimental and theoretical constraints on hydrothermal alteration processes at mid-ocean ridges, *Annu. Rev. Earth Planet. Sci.*, *15*, 317–335, doi:10.1146/annurev.ea.15.050187.001533.

Shinohara, H. (2008), Excess degassing from volcanoes and its role on eruptive and intrusive activity, *Rev. Geophys.*, *46*, RG4005, doi:10.1029/2007RG000244.

Shmonov, V. M., V. M. Viviovtova, A. V. Zharikov, and A. A. Grafchikov (2003), Fluid permeability of the continental crust: Estimation from experimental data, *J. Geochem. Explor.*, *78-79*, 697–699.

Simpson, F. (2001), Fluid trapping at the brittle-ductile transition re-examined, *Geofluids*, *1*, 123–136, doi:10.1046/j.1468-8123.2001.00011.x.

Slichter, C. S. (1899), Theoretical investigations of motions of groundwater flow, *U.S. Geol. Surv. Annu. Rep., 19*, part II, pp. 295–380, U.S. Geol. Surv., Reston, Va.

Sohn, R. A. (2007), Stochastic analysis of exit fluid temperature records from the active TAG hydrothermal mound (Mid-Atlantic Ridge, 26°N): 1. Modes of variability and implications for subsurface flow, *J. Geophys. Res.*, *112*, B07101, doi:10.1029/2006JB004435.

Sohn, R. A., D. J. Fornari, K. L. Von Damm, J. A. Hildebrand, and S. C. Webb (1998), Seismic and hydrothermal evidence for a cracking event on the East Pacific rise crest at 9°50′ N, *Nature*, *396*, 159–161, doi:10.1038/24146.

Sondergeld, C. H., and D. L. Turcotte (1977), Experimental study of two-phase convection in porous medium with applications to geological problems, *J. Geophys. Res.*, *82*, 2045–2053.

Sorey, M. L., M. A. Grant, and E. Bradford (1980), Nonlinear effects in two-phase flow to wells in geothermal reservoirs, *Water Resour. Res.*, *16*, 767–777, doi:10.1029/WR016i004p00767.

Stanford Geothermal Program (1980), Proceedings of special panel on geothermal model intercomparison study at the 6th Workshop on Geothermal Reservoir Engineering, Stanford University, Stanford, California, December 17, 1980, *Stanford Geotherm. Program Rep.*, *SGP-TR-42*, Stanford Univ., Stanford, Calif.

Steefel, C. I., and A. C. Lasaga (1994), A coupled model for transport of multiple chemical species and kinetic precipitation/dissolution reactions with application to reactive flow in single phase hydrothermal systems, *Am. J. Sci.*, *294*, 529–592.

Stein, C. A., and S. Stein (1994), Constraints on hydrothermal heat flux through the oceanic lithosphere from global heat flow, *J. Geophys. Res.*, *99*, 3081–3095.

Stephansson, O., and K.-B. Min (2004), Thermo-hydro-mechanical (THM) coupled processes for performance and safety assessments of nuclear waste repository: Lessons learnt from EC BENCHPAR project, paper presented at Euradwaste '04, Eur. Comm., Luxembourg, 29–31 March. (Available at http://www.cordis.lu/fp6-euratom/ev_euradwaste04_proceedings.htm)

Stober, I., and K. Bucher (2007), Hydraulic properties of the crystalline basement, *Hydrogeol. J.*, *15*, 213–224, doi:10.1007/s10040-006-0094-4.

Straus, J. M., and G. Schubert (1981), One-dimensional model of vapor-dominated geothermal systems, *J. Geophys. Res.*, *86*, 9433–9438.

Stüben, K. (2001), A review of algebraic multigrid, *J. Comput. Appl. Math.*, *128*, 281–309, doi:10.1016/S0377-0427(00)00516-1.

Summers, R., K. Winkler, and J. Byerlee (1978), Permeability changes during the flow of water through Westerly Granite at temperatures of 100°–400°C, *J. Geophys. Res.*, *83*, 339–344, doi:10.1029/JB083iB01p00339.

Sweby, P. K. (1984), High resolution schemes using flux limiters for hyperbolic conservation laws, *SIAM J. Numer. Anal.*, *21*, 995–1011.

Symonds, R. B., T. M. Gerlach, and M. H. Reed (2001), Magmatic gas scrubbing: Implications for volcano monitoring, *J. Volcanol. Geotherm. Res.*, *108*, 303–341, doi:10.1016/S0377-0273(00)00292-4.

Talwani, P., L. Chen, and K. Gahalaut (2007), Seismogenic permeability, k_s, *J. Geophys. Res.*, *112*, B07309, doi:10.1029/2006JB004665.

Tanger, J. C., IV, and K. S. Pitzer (1989), Thermodynamics of NaCl-H_2O: A new equation of state for the near-critical region and comparisons with other equations for adjoining regions, *Geochim. Cosmochim. Acta*, *53*, 973–987, doi:10.1016/0016-7037(89)90203-2.

Taylor, H. P., Jr. (1971), Oxygen isotope evidence for large-scale interaction between meteoric groundwaters and Tertiary granodiorite intrusions, Western Cascade Range, Oregon, *J. Geophys. Res.*, *76*(7), 7855–7874.

Thiery, R., and L. Mercury (2009), Explosive properties of water in volcanic and hydrothermal systems, *J. Geophys. Res.*, *114*, B05205, doi:10.1029/2008JB005742.

Titley, S. R. (1990), Evolution and style of fracture permeability in intrusion-centered hydrothermal systems, in *The Role of Fluids in Crustal Processes*, edited by J. D. Bredehoeft and D. L. Norton, pp. 50–63, Natl. Acad., Washington, D. C.

Todaka, N., C. Akasaka, T. Xu, and K. Pruess (2004), Reactive geothermal transport simulations to study the formation mechanism of an impermeable barrier between acidic and neutral fluid zones in the Onikobe Geothermal Field, Japan, *J. Geophys. Res.*, *109*, B05209, doi:10.1029/2003JB002792.

Todesco, M. (2009), Signals from the Campi Flegrei hydrothermal system: Role of a "magmatic" source of fluids, *J. Geophys. Res.*, *114*, B05201, doi:10.1029/2008JB006134.

Todesco, M., J. Rutqvist, G. Chiodini, K. Pruess, and C. M. Oldenburg (2004), Modeling of recent volcanic episodes at Phlegrean Fields (Italy), *Geothermics*, *33*, 531–547, doi:10.1016/j.geothermics.2003.08.014.

Tsypkin, G. G., and C. Calore (2003), Role of capillary forces in vapour extraction from low-permeability, water-saturated geothermal reservoirs, *Geothermics*, *32*, 219–237, doi:10.1016/S0375-6505(03)00018-X.

Udell, K. S. (1985), Heat transfer in porous media: Considering phase change and capillarity—The heat pipe effect, *Int. J. Heat Mass Transfer*, *28*, 485–495, doi:10.1016/0017-9310(85)90082-1.

Urabe, T., et al. (1995), The effect of magmatic activity on hydrothermal venting along the superfast-spreading East Pacific Rise, *Science*, *269*, 1092–1095.

Urmeneta, N. A., S. Fitzgerald, and R. N. Horne (1998), The role of capillary forces in the natural state of fractured geothermal reservoirs, in *Proceedings of the 23rd Workshop on Geothermal Reservoir Engineering*, vol. 26, pp. 100–109, Stanford Univ., Stanford, Calif.

Vaughan, P. J., D. E. Moore, C. A. Morrow, and J. D. Byerlee (1986), Role of cracks in progressive permeability reduction during flow of heated aqueous fluids through granite, *J. Geophys. Res.*, *91*, 7517–7530.

Vennard, J. K., and R. L. Street (1975), *Elementary Fluid Mechanics*, John Wiley, New York.

Verma, A. K. (1990), Effects of phase transformation on steam-water relative permeabilities, Ph.D. thesis, Univ. of Calif., Berkeley.

Von Damm, K. L. (1990), Seafloor hydrothermal activity: Black smoker chemistry and chimneys, *Annu. Rev. Earth Planet. Sci.*, *18*, 173–204, doi:10.1146/annurev.ea.18.050190.001133.

Von Damm, K. L. (1995), Temporal and compositional diversity in seafloor hydrothermal fluids, *Rev. Geophys.*, *33*, 1297–1305.

Von Damm, K. L., M. D. Lilley, W. C. Shanks, M. Brockington, A. M. Bray, K. M. O'Grady, E. Olson, A. Graham, and G. Proskurowski (2003), Extraordinary phase separation and segregation in vent fluids from the southern East Pacific Rise, *Earth Planet. Sci. Lett.*, *206*, 365–378, doi:10.1016/S0012-821X(02)01081-6.

Vosteen, H.-D., and R. Schellschmidt (2003), Influence of temperature on thermal conductivity, thermal capacity and thermal diffusivity for different types of rock, *Phys. Chem. Earth*, *28*, 499–509.

Walker, J. J., J. R. Spear, and N. R. Pace (2005), Geobiology of a microbial endolithic community in the Yellowstone geothermal environment, *Nature*, *434*, 1011–1014.

Wang, C. T., and R. N. Horne (2000), Boiling flow in a horizontal fracture, *Geothermics*, *29*, 759–772, doi:10.1016/S0375-6505(00)00029-8.

Wang, K. (2004), Applying fundamental principles and mathematical models to understand processes and estimate parameters, in *Hydrogeology of the Oceanic Lithosphere*, edited by E. E. Davis and H. Elderfield, pp. 376–413, Cambridge Univ. Press, Cambridge, U. K.

Ward, J. D. (1964), Turbulent flow in porous media, *Proc. Am. Soc. Civ. Eng.*, *90*, 1–12.

Wilcock, W. S. D. (1998), Cellular convection models of mid-ocean ridge hydrothermal convection and the temperatures of black smoker fluids, *J. Geophys. Res.*, *103*, 2585–2596.

Wilcock, W. S. D., and A. T. Fisher (2004), Geophysical constraints on the subseafloor environment near mid-ocean ridges, in *The Subsurface Biosphere at Mid-Ocean Ridges*, *Geophys. Monogr. Ser.*, vol. 114, edited by W. S. D. Wilcock et al., pp. 51–74, AGU, Washington, D. C.

Williams, D. L., and R. P. Von Herzen (1974), Heat loss from the Earth: New estimate, *Geology*, *2*, 327–328, doi:10.1130/0091-7613(1974)2<327:HLFTEN>2.0.CO;2.

Williams-Jones, A. E., and C. A. Heinrich (2005), Vapor transport of metals and the formation of magmatic hydrothermal ore deposits, *Econ. Geol.*, *100*, 1287–1312.

Windman, T., N. Zolotova, F. Schwandner, and E. L. Shock (2007), Formate as an energy source for microbial metabolism in chemosynthetic zones of hydrothermal ecosystems, *Astrobiology*, *7*, 873–890, doi:10.1089/ast.2007.0127.

Wooding, R. A. (1957), Steady state free thermal convection of liquid in a saturated permeable medium, *J. Fluid Mech.*, *2*, 273–285, doi:10.1017/S0022112057000129.

Woods, A. W. (1999), Liquid and vapor flow in superheated rock, *Annu. Rev. Fluid Mech.*, *31*, 171–199, doi:10.1146/annurev.fluid.31.1.171.

Wu, C. C., and G. J. Hwang (1998), Flow and heat transfer characteristics inside packed and fluidized beds, *J. Heat Transfer*, *120*, 667–673, doi:10.1115/1.2824335.

Wu, Y.-S., K. Zhang, C. Ding, K. Pruess, E. Elmroth, and G. S. Bodvarsson (2002), An efficient parallel-computing method for modeling nonisothermal multiphase flow and multicomponent transport in fractured porous media, *Adv. Water Resour.*, *25*, 243–261, doi:10.1016/S0309-1708(02)00006-4.

Xu, T., and K. Pruess (2001), On fluid flow and mineral alteration in fractured caprock of magmatic hydrothermal systems, *J. Geophys. Res.*, *106*(B2), 2121–2138, doi:10.1029/2000JB900356.

Xu, T., E. Sonnenthal, N. Spycher, K. Pruess, G. Brimhall, and J. Apps (2001), Modeling multiphase non-isothermal fluid flow and reactive geochemical transport in variably saturated fractured rocks. 2. Applications to supergene copper enrichment and hydrothermal flows, *Am. J. Sci.*, *301*, 34–59, doi:10.2475/ajs.301.1.34.

Xu, T., Y. Ontoy, P. Molling, N. Spycher, M. Parini, and K. Pruess (2004a), Reactive transport modeling of injection well scaling and acidizing at Tiwi field, Philippines, *Geothermics*, *33*, 477–491, doi:10.1016/j.geothermics.2003.09.012.

Xu, T., E. Sonnenthal, N. Spycher, and K. Pruess (2004b), TOUGHREACT user's guide: A simulation program for non-isothermal multiphase reactive geochemical transport in variable saturated geologic media, *Pap. LBNL-55460*, Lawrence Berkeley Natl. Lab., Berkeley, Calif.

Yasuhara, H., A. Polak, Y. Mitani, A. S. Grader, P. M. Halleck, and D. Elsworth (2006), Evolution of fracture permeability through fluid-rock reaction under hydrothermal conditions, *Earth Planet. Sci. Lett.*, *244*, 186–200, doi:10.1016/j.epsl.2006.01.046.

Zhang, K., Y.-S. Wu, and K. Pruess (2008), User's guide for TOUGH2-MP—A massively parallel version of the TOUGH2 code, Lawrence Berkeley Natl. Lab., Berkeley, Calif. (Available at http://www.tough2.com/index.html)

Zyvoloski, G. A. (1983), Finite element methods for geothermal reservoir simulation, *Int. J. Numer. Anal. Methods Geomech.*, *7*, 75–86, doi:10.1002/nag.1610070108.

Zyvoloski, G. A., and M. J. O'Sullivan (1980), Simulation of a gas-dominated, two-phase geothermal reservoir, *SPEJ Soc. Pet. Eng. J.*, *20*, 52–58.

Zyvoloski, G. A., Z. V. Dash, and S. Kelkar (1988), FEHM: Finite element heat and mass transfer code, *Rep. LA-11224-MS*, Los Alamos, Natl. Lab., Los Alamos, N. M.

Zyvoloski, G. A., B. A. Robinson, Z. D. Dash, and L. L. Trease (1997), Summary of models and methods for the FEHM application—A finite-element heat- and mass-transfer code, *Rep. LA-13307-MS*, Los Alamos, Natl. Lab., Los Alamos, N. M.

T. Driesner, Institute of Isotope Geochemistry and Mineral Resources, ETH Zurich, NW F81.3, Clausiusstr. 25, CH-8092 Zurich, Switzerland.

S. Geiger, Institute of Petroleum Engineering, Heriot-Watt University, Edinburgh EH14 4AS, UK.

S. Hurwitz and S. E. Ingebritsen, U.S. Geological Survey, 345 Middlefield Rd., Menlo Park, CA 94025, USA. (seingebr@usgs.gov)